Wave energy dissipation by a viscous surface layer: Effects on the shear diffusion of a mineral oil slick

M.A. (Ties) Kuijpers

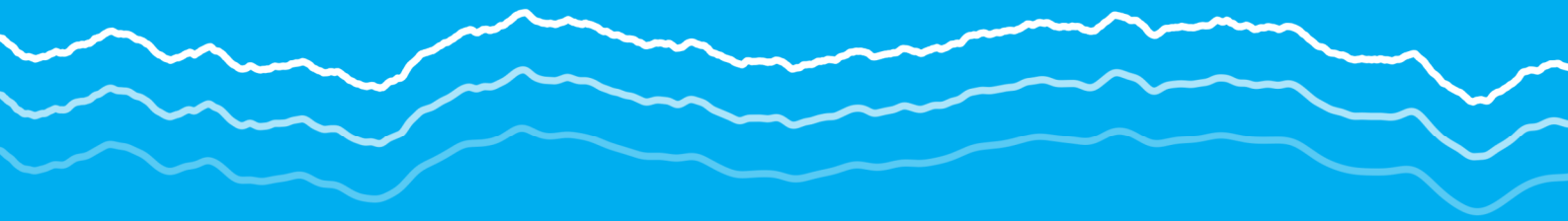

TU Delft

Witteveen + Bos

Wave energy dissipation by a viscous surface layer: Effects on the shear diffusion of a mineral oil slick

M.A. (Ties) Kuijpers

Date
20 November 2019

Student number
4236998

Thesis committee
prof. dr. ir. A.J.H.M. Reniers, TU Delft
prof. dr. ir. W.S.J. Uijttewaal, TU Delft
dr. ir. M. Zijlema, TU Delft
dr. W. Ridderinkhof, Witteveen+Bos

TU Delft

Witteveen + Bos

Wave energy dissipation by a viscous surface layer: Effects on the shear diffusion of a mineral oil slick

by

M.A. (Ties) Kuijpers

to obtain the degree of Master of Science
at the Delft University of Technology
to be defended publicly on Wednesday 20 November 2019 at 3.30 p.m.

Student number
4236998

Thesis committee

prof. dr. ir. A.J.H.M. Reniers (chair)
TU Delft; Civil Engineering and Geosciences; Environmental Fluid Mechanics

prof. dr. ir. W.S.J. Uijttewaal
TU Delft; Civil Engineering and Geosciences; Rivers, Ports, Waterways and Dredging Engineering

dr. ir. M. Zijlema, TU Delft
TU Delft; Civil Engineering and Geosciences; Environmental Fluid Mechanics

dr. W. Ridderinkhof
Witteveen+Bos

An electronic version of this thesis is available at http://repository.tudelft.nl/

Preface

This thesis reports on my graduation work within the MSc Civil Engineering at TU Delft, of which I completed the Hydraulic Engineering track. The document you're reading right now, is the result of a project that has occupied my mind for one year. The project, in my experience, has been all about balancing the scientific and the engineering sides to an interesting and inexhaustive research field. When answering questions raises new questions, there is a risk of getting lost. Luckily, a helpful team guided me.

People that have spent a serious amount of their valuable time on this thesis are the members of my graduation committee, Ad Reniers, Wim Uijttewaal, and Marcel Zijlema, whom I am grateful to for our discussions. I also liked receiving papers from you, that often brought confusion at first, but in the end did help in the convergence process.

At Witteveen+Bos, Wim Ridderinkhof, I very much appreciate that you offered me the opportunity to write my thesis in the Hydrodynamics and Morphology group. I like your critical thinking, and your way of life heading into *het grote niks*, which then mostly turns out to be quite a full agenda. All of the colleagues, a big thank you for aiding me when I encountered problems of various kind, like compiling my own version of SWAN on the Linux cluster and skiing downhill in Zoetermeer. Anne, thank you for drawing my attention to the H&M group when I was looking for a graduation internship.

Marieke, your PhD thesis has inspired me to dive into oil spill science. I like to thank you for reading my manuscript occasionally. I would also like to thank Gert for reviewing my work.

The biggest thank you in number probably has to go to all kind people I stumbled upon while studying in Delft. You demonstrated that student life encompasses much more than the curriculum one is ought to complete. Every single one of you should know I am sincerely grateful for the memories we share (luckily, they are all unrelated to oil spills). Dennis, I enjoyed the *cappu* meetings at OD54, where we discussed our graduation 'troubles' and shared our preference for Rachmaninoff piano concertos.

I of course must not forget thanking my parents for their continuous support (not the least financially) during the seven years I spent in Delft. My mother actually dared taking on the challenge of reading my drafts every now and then. Many thanks to both of you.

Last but not least, Janneke, I cannot express how much I appreciate your understanding for me being occupied and/or tired at times. You cheered me up every day of the graduation process.

This thesis marks the end of my time as a student. I've had a great time, so saying goodbye isn't easy. Yet, I'm convinced that it is time for a new phase to start and that great experiences will come along the way. For now, I hope you enjoy reading my thesis. Please don't hesitate to contact me if you want to discuss it.

Ties Kuijpers
Delft, November 2019

Abstract

Mineral oil spills at sea can have many negative consequences. For both preventive and responsive purposes, it is essential to accurately forecast oil spill evolution. Shear diffusion (in this context, i.e. the combined effect of vertical mixing and differentiated horizontal advection of mass) determines for a significant part the evolution of an oil spill. These processes are partially forced by waves.

A viscous fluid layer attenuates the waves throughout the area the layer covers. In this thesis, surface oil slicks are modeled as a continuous viscous fluid layer. It is investigated to what extent the wave-forced shear diffusion of the oil is affected by the oil-induced attenuation of the waves.

For this purpose, the spectral wave model SWAN is extended with a module for energy dissipation due to a viscous fluid layer. The stationary, 1D wave energy balance is solved for uniformly forced waves in deep water. A high cutoff frequency (5 Hz) is employed to include the wave frequencies at which the dissipation is active. Also, special attention is paid to the choice of the wind and whitecapping formulation. Simulations are performed in full factorial setup, varying wind speed, oil layer thickness and oil viscosity. The results are compared to a no-oil case. Based on the difference, functions are fitted for the reduction of two key wave properties: the whitecapping dissipation rate and the surface Stokes drift velocity.

The reduction functions are included in the oil spill module of the particle tracking model OpenDrift, which is subsequently used to calculate oil spill evolution due to shear diffusion for 2DV cases. The results of oil spill simulations with and without the implemented reduction functions are compared. Idealized cases (only wave-forced) show that for sufficiently thick layers ($h_+ \geq \mathcal{O}\{10^{-3}\}$ m) of sufficiently viscous ($\nu_+ \geq \mathcal{O}\{10^{-3}\}$ m^2/s) oil, the Stokes drift reduction can significantly affect the wave-driven evolution of an oil spill in two ways: the average forward transport is reduced and the skewness of the oil mass distribution is increased to 'less negative' or even positive values. If simple sheared wind drift and ambient vertical turbulence are added, however, the relative importance of these effects becomes smaller. In none of the cases, a difference is found for the distribution of the oil mass between surface and subsurface, which implies that the whitecapping reduction hardly affects the results.

It is recommended that further effort is put into obtaining a detailed understanding of the (differentiated) forward transport of the surface and near-surface oil, so that wave and wind effects can be distinguished, and modeled independently, more accurately.

Keywords: oil spill, mineral oil, shear diffusion, oil dispersion, Stokes drift, viscous wave attenuation, SWAN, OpenDrift

Table of contents

Abbreviations

2DV	two-dimensional, width-averaged
LE	Lagrangian element
OSM	oil spill model
PM	Pierson-Moskowitz
PTM	particle tracking method
SWAN	Simulating WAves Nearshore
SWM	spectral wave model

Symbols and notation

The used symbols are explained below. The symbol is printed bold if it represents a vector.

Symbol	Parameter	Unit
a	wave amplitude	m
c_g	wave group velocity	m/s
C	concentration	kg/m^2
d	droplet diameter	m
E	wave energy	m^2
f	wave frequency (linear)	s^{-1}
F	sea surface agitation rate	s^{-1}
g	gravitational acceleration	m/s^2
h	depth/thickness	m
H	wave height	m
k	wave number	rad/m
K	mass diffusivity	m^2/s
L	length	m
m	mass	kg
m_n	n-th order spectral moment	m^2/s^n
M	mass flux (per unit area)	kg/(m^{2}s)
n	number / sample size	-
N	complex wave frequency (angular)	rad/s
Oh	Ohnesorge number	-
Re	Reynolds number	-
S	wave energy source/sink	m^2/s
t	time	s
T	wave period	s
u, v, w	flow velocity (in x, y and z-direction, respectively)	m/s
U_{10}	wind speed at 10 meter height	m/s
$\mathcal{Y}$	complex decay rate amplification factor	-
We	Weber number	-
x, y, z	Cartesian coordinates (z positive upward)	m
α	spatial wave amplitude decay rate	m^{-1}
β	temporal wave amplitude decay rate	s^{-1}
γ	surface/interface tension	N/m
η	sea surface elevation	m
θ	direction (with respect to x-axis, counter-clockwise)	rad
Θ	temperature	K
λ	fractional oil entrainment rate	s^{-1}
ν	kinematic viscosity	m^2/s
ρ	mass density	kg/m^3
φ	wave phase	rad
χ	surface/interface elasticity	N/m
ψ	surface/interface viscosity	Ns/m
ω	wave frequency (angular)	rad/s

Probabilistic notation and definitions

Symbol	Parameter	Definition (density function)
p	probability density	
P	probability	
$\mathcal{N}(\mu, \sigma^2)$	normal distribution	$p(Z) = \frac{1}{\sqrt{2\pi\sigma^2}} \exp\left(-\frac{(Z-\mu)^2}{2\sigma^2}\right)$
$\mathcal{U}(a, b)$	uniform distribution	$p(Z) = \begin{cases} \frac{1}{b-a}, & \text{for } a \leq Z \leq b \\ 0, & \text{otherwise} \end{cases}$

Statistical notation and definitions

Symbol	Parameter	Definition (for sample of size n)
μ	mean	$\mu_Z = \frac{1}{n}\sum_{j=1}^{n} Z_j$
σ^2	variance	$\sigma_Z^2 = \frac{1}{n-1}\sum_{j=1}^{n}(Z_j - \mu_Z)^2$
γ_1	skewness	$\gamma_{1,Z} = \frac{\sqrt{n(n-1)}}{n-2} \frac{\frac{1}{n}\sum_{j=1}^{n}(Z_j - \mu_Z)^3}{\left(\frac{1}{n}\sum_{j=1}^{n}(Z_j - \mu_Z)^2\right)^{3/2}}$

Mathematical notation

Symbol	Definition
$\mathcal{D}$	relative reduction
$\mathcal{O}\{\cdot\}$	a term of order
i	imaginary unit
$\Re\{\cdot\}$	real part of a complex number
$\Im\{\cdot\}$	imaginary part of a complex number

1. Introduction

1

In this chapter, the research topic of this thesis is introduced. First, the context of the subject is given (§ 1.1) and the relevant processes are described (§ 1.2). Then, the research problem and the thesis objective are stated (§ 1.3). Finally, the build-up of the report is explained (§ 1.4).

1.1. Context

Every once in a while, mineral oil spills at sea occur. Prominent examples are the blow-out at the *Deepwater Horizon* drilling rig in 2010 and the grounding of the *Exxon Valdez* oil tanker in 1989. In a marine environment, the oil is subject to multiple transport processes, which move it, and weathering processes, which change its physical and chemical properties (Fingas, 2016). The evolution of an oil spill is the consequence of a complex and chaotic interplay between various transport and weathering processes[1].

Oil spills often have negative consequences, like fouling of beaches and animals, and toxic effects (Fingas, 2016). Therefore, it is essential that the evolution of an oil spill can be forecasted for preventive or responsive purposes. Oil spill models (OSMs) are used to forecast the oil spill evolution through time. They do so by calculating the combined effect of the various transport and weathering processes for many small time steps. Various meteo-hydrodynamical data, such as current, wave and wind data serve as input for OSMs. The output of OSM simulations contains the trajectory of the oil through time.

1.2. Concepts

Waves are a driving force for oil mass transport, so the presence of waves affects the oil. On the other hand, the presence of oil affects the waves. These effects are explained in this paragraph, as they together lead to the feedback mechanism that is investigated in this thesis.

Waves drive oil transport

Breaking waves cause vertical mixing of the upper layer of the sea, as shown in Figure 1. If a surface oil layer is present, breaking waves cause entrainment (submergence) of the surface oil and subsequent breakup into small droplets. This process is called oil dispersion[2] (Delvigne and Sweeney, 1988). After entrainment, the oil droplets tend to resurface due to buoyancy. Dependent on the droplet size diameter, resurfacing typically takes between hours and days, but the smallest droplets may not resurface at all due to oceanic turbulence (Röhrs et al., 2018). As a consequence, the oil is spread vertically over the water column.

Propagating waves cause forward motion of the fluid, as shown in Figure 2. This process is called Stokes drift (Stokes, 1847). The resulting flow is sheared. It is maximal at the sea surface and it decays downward. As a consequence, an oil droplet at some depth will travel at a lower speed than the oil slick at the surface.

The combination of the described processes, vertical mixing and sheared flow, causes so-called shear diffusion. As a consequence, a mineral oil slick at sea elongates in the direction of waves and wind, while the oil slick is thicker at the downwind side than at the upwind side. This is explained further in Chapter 2.

[1] In the remainder of this thesis, only transport processes are considered. The possible effects of weathering processes are not taken into account.

[2] Please do not confuse with wave dispersion.

An oil layer affects waves

Waves are affected by the presence of pollution at the sea surface. Attenuation of surface waves by organic oil layers has already been recognized in ancient times (Alpers and Hühnerfuss, 1989). The effect was rediscovered by Franklin (1774), who found that small waves in a lake were attenuated if a small amount of olive oil was released onto the water, and he accounted of seamen who confirmed observing similar effects at sea, implying that the effects also play a role on large scales. It is even claimed that storm-caught ships were saved due to the release of oil onto the water, which reduced the number of breaking waves. In the mentioned cases, most likely organic oils were used. It is thought that surface tension gradients are responsible for the observed effect. This is called Marangoni damping (Alpers and Hühnerfuss, 1989). An organic oil layer with the thickness of only several molecules is sufficient to obtain such a damping effect.

Marangoni damping could also arise in a mineral oil spill. However, it is hypothesized that for the typical layer thicknesses and viscosities seen in mineral oil spills, a different type of damping may be more relevant: energy dissipation due to viscous effects. This is explained further in Chapter 3. Regardless of the exact damping mechanism at play, the consequences of the wave attenuation may be the same: the aforementioned vertical mixing and Stokes drift may be reduced.

Figure 1. *Breaking of waves causes a white spray to be formed, commonly called a whitecap. Vertical mixing is accelerated in the vicinity of the breaking wave.*[3]

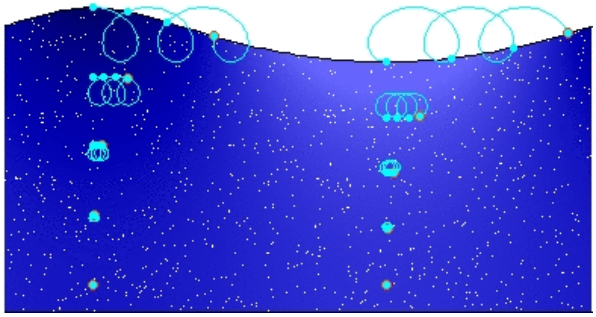

Figure 2. *Trajectories of selected particles that are subjected to orbital wave motion. The location of the particles is indicated for zero, one, two and three wave periods after start. A net forward transport is the result. Note that the particles near the surface move forward faster than particles at depth.*[4]

[3] Image by Archangel12, retrieved from https://commons.wikimedia.org/wiki/File:Breaking_waves_(13286850323).jpg

[4] Image by Kraaiennest, retrieved from https://commons.wikimedia.org/wiki/File:Deep_water_wave_after_three_periods.png

1.3. Problem description and objective

Waves are a driving force for oil spill evolution. Therefore, in their forecasting calculations, OSMs use wave data (often originating from wave models) and empirical equations that link wave properties to oil transport processes.

The combination of the two previously described concepts, waves driving oil transport and an oil layer affecting waves, leads to a feedback between oil and waves, so that oil presence affects oil transport. This feedback is currently not taken into account, because wave models do not address the presence of the oil slick. As a consequence, the wave data that OSMs rely on may be inaccurate for the oil-covered area. Inaccurate wave data may cause inaccurate model results, which in turn may lead to suboptimal oil spill prevention and response (Fingas, 2016). Furthermore, the algorithms used in OSMs may be inaccurate in the first place, if they were calibrated based on inaccurate wave data. Including more aspects of the physics into a model, allows for a more accurate calibration of the model and the underlying equations. Concluding, the accuracy of OSMs may be improved if the oil-induced wave attenuation effect is taken into account.

The impact of the viscous energy dissipation on the evolution of oil spills is still uncertain. The uncertainty can be attributed to two unknowns: (i) the effect of viscous energy dissipation on integral wave properties, and (ii) the effect of the consequential variation of wave properties throughout an oil slick on the oil spill evolution.

This thesis aims to study the viscous oil effect on the waves and the subsequent effect on the wave-driven oil spill evolution. To reach the objective, the following research question is formulated:

How is the wave-driven evolution of a marine mineral oil spill affected by oil-induced viscous wave attenuation?

Before answering the above research question, answers to the following sub-questions are required.

I. By which mechanisms and at what rate is an oil slick transported by the waves?
II. What is the effect of an oil slick on the wave properties that determine the oil slick transport?
III. What is the difference between oil spill evolution with and without taking into account the effect of oil on the waves?

1.4. Thesis outline

The approach to answering these research questions is shown graphically below.

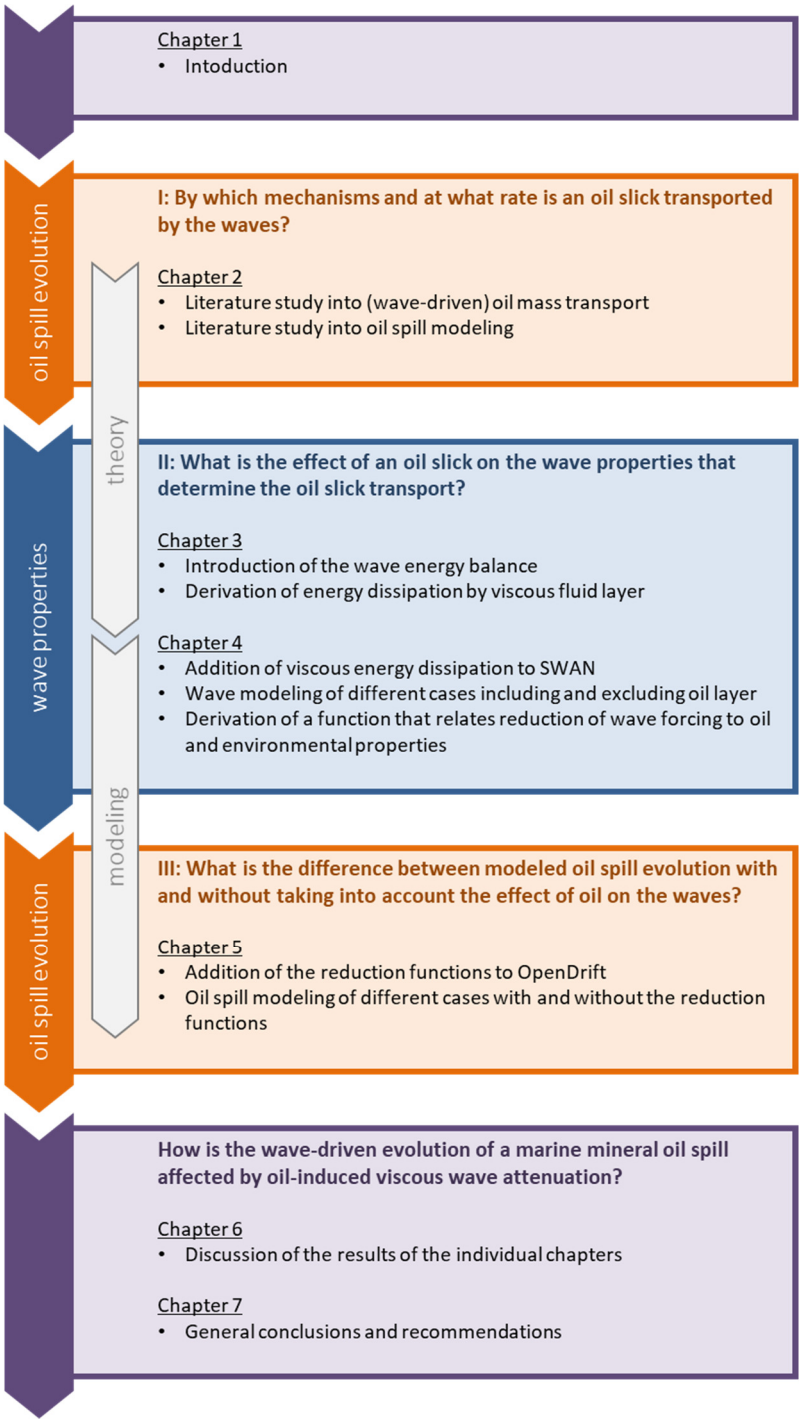

2. Theory of oil spill evolution

In this chapter, oil mass transport processes are discussed, including how they lead to shear diffusion (§ 2.1). Then, for the wave processes that are relevant to shear diffusion of oil, the equations that describe those processes are presented (§ 2.2). Finally, it is explained how oil spill evolution is modeled by combining the equations into an oil spill model (§ 2.3).

2.1. Shear diffusion as a consequence of wave processes

Elliott, Hurford, and Penn (1986) observed that a mineral oil slick at sea elongates in the direction of waves and wind, and that the oil slick is thicker at the downwind side than at the upwind side. They attributed this effect to shear diffusion, which is the consequence of vertical mixing of oil in combination with differentiated horizontal advection. The shear diffusion process consists of three steps, which are explained more thoroughly in this paragraph. Also, the role of waves in the process is clarified.

Shear diffusion step by step

The first step of the shear diffusion process is the dispersion of oil. Oil dispersion comprises of entrainment (submergence) of surface oil and the subsequent breakup of the oil into small droplets, caused by breaking waves (Figure 3b). This causes the oil to spread over the vertical. The dispersion process is characterized by the entrainment rate λ, the entrainment depth z_e, and the droplet size d.

The second step is advection: the transport of mass, caused by an ambient flow. Oil mass at sea is advected by waves, wind and currents. Because of wave and wind forcing, the flow velocity at sea is not uniform over the vertical. Therefore, a particle near the surface moves forward faster than a particle at depth (Figure 3c). The advection process is characterized by the forward velocity u.

Because crude oil and many of its refined products have a lower mass density than water, the submerged oil droplets that are created during the breaking wave impact, resurface afterwards and become part of the surface slick again (Figure 3d). This is the third step of the shear diffusion process. The resurfacing process is characterized by the buoyant rise velocity w_B.

Processes driving shear diffusion

Breaking waves are the main driver for the dispersion of oil, the first step of the shear diffusion process. Wave and wind forcing cause the sheared near-surface flow, which transport the dispersed oil droplets in the second step of the shear diffusion process. The resurfacing of the dispersed oil droplets is a consequence of competition between buoyancy (caused by the mass density difference between oil and water) and ambient turbulence.

In this thesis, only the wave-induced part of the shear diffusion is researched. This means that, for the advection step of the shear diffusion process, wind (and current) effects are neglected. It must be noted that it is a hard task to separate the different advection processes in practice. In addition to that, although the presence of ambient turbulence is caused by amongst others waves and wind, the buoyant rise step of the shear diffusion process is considered to be independent of wave and wind forcing.

(a) *an oil slick floats on the sea surface*

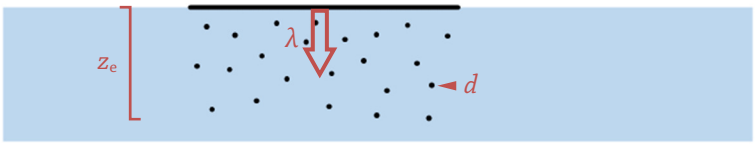

(b) *part of the oil is dispersed by breaking waves*

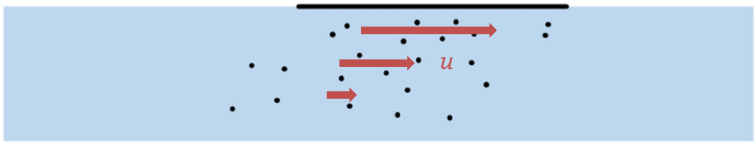

(c) *the oil is advected at different speeds by sheared flow*

(d) *the submerged oil resurfaces due to buoyancy*

Figure 3. *The individual steps of the shear diffusion process. Side view of the upper part of the water column, not to scale.*

Analytical framework to describe shear diffusion

Elliott (1986) presented an analytical expression for the shear diffusion of a neutrally buoyant tracer that is instantaneously released in a fluid with sheared flow along the x-axis. If ambient horizontal diffusion processes (e.g., molecular and turbulent diffusion) are neglected, the following mass spreading along the x-axis is the result, expressed in terms of variance,

$$\sigma_x^2 = \frac{2}{3} K_\mathrm{v} \left(\frac{\partial u}{\partial z}\right)^2 t^3 ,$$

where K_v is the vertical mass diffusivity, u is the flow velocity in x-direction, z is the vertical coordinate, and t is the time from release. Although this equation for shear diffusion only holds for neutrally buoyant tracers, and for spatially uniform K_v and $\partial u/\partial z$, in absence of boundaries (such as the sea surface), it gives an impression of the processes at play.

Within this framework, the action of waves can be interpreted as follows. As waves break, they enhance vertical mixing in the fluid, causing higher K_v, albeit only locally. Furthermore, waves shear the near-surface flow, causing higher $\partial u/\partial z$. The fact that the vertical mixing of an oil spill determines for a large part its horizontal evolution, is confirmed by Röhrs et al. (2018), using an OSM that accounts for oil dispersion and advection, and comparing the results to experimental field data.

For positively buoyant particles, like oil droplets, the mass spreading in both the vertical and horizontal plane is smaller than for neutrally buoyant particles. In addition, positively buoyant particles move forward faster than neutrally buoyant particles. This is due to the fact that positively buoyant particles collect near the water surface (Boufadel, Bechtel, and Weaver, 2006). Hence, for positively buoyant particles, the previous equation provides only an upper bound,

$$\sigma_x^2 \leq \frac{2}{3} K_\mathrm{v} \left(\frac{\partial u}{\partial z}\right)^2 t^3 .$$

2.2. Descriptive equations

Different mass transport processes together lead to shear diffusion. In this paragraph, the equations that describe the individual processes are collected. Because the oil spill model OpenDrift is used in this thesis, the equations that are used in that model are described here.

Dimensionless numbers

Several dimensionless numbers arise in the equations. They are collected here. The Weber number *We*, Ohnesorge number *Oh*, and Reynolds number *Re* are defined as follows, respectively,

$$We = \frac{\rho_- g \mathcal{H} \mathcal{L}}{\gamma_{ow}}, \qquad Oh = \nu_+ \sqrt{\frac{\rho_+}{\gamma_{ow} \mathcal{L}}}, \qquad Re = \frac{\rho_- \sqrt{g\mathcal{H}}\, \mathcal{L}}{\nu_+ \rho_+},$$

where ν_+ is the kinematic viscosity of oil, ρ_+ is the mass density of oil, ρ_- is the mass density of water, γ_{ow} is the oil-water interfacial tension, g is the gravitational acceleration, $\mathcal{H}$ is a wave height scale, and $\mathcal{L}$ is a length scale. The wave height scale $\mathcal{H}$ and length scale $\mathcal{L}$ are defined per equation.

Entrainment rate (λ)

Li, Spaulding, and French-McCay (2017) define the fractional entrainment rate as

$$\lambda = \frac{M}{\rho_+ h_+},$$

where M is the surface-to-subsurface oil mass flux per unit area, ρ_+ is the mass density of oil, and h_+ is the oil layer thickness. Using dimensional analysis and performing a fit to experimental data, the authors found

$$\lambda = 4.604 \cdot 10^{-10} \cdot We^{1.805} \cdot Oh^{-1.023} \cdot F,$$

where F is the sea surface agitation rate. They use

$$\mathcal{H} = H_s, \qquad \mathcal{L} = d_{RT} = 4\sqrt{\frac{\gamma_{ow}}{(\rho_- - \rho_+) g}},$$

as scales for wave height and for length, where H_s is the significant wave height, and d_{RT} is the Rayleigh-Taylor instability maximum diameter.

Entrainment depth (z_e)

Delvigne and Sweeney (1988) experimentally found that the entrained oil after a wave-breaking event is uniformly mixed over the upper fluid layer, which is approximately as thick as 1.5 times the height of the breaking wave. Hence, the entrainment depths of oil droplets after entrainment are described by a uniform distribution, as follows,

$$z_{\mathrm{e}} \sim \mathcal{U}(-1.5\, H_{\mathrm{b}}\,, 0)\,,$$

where H_{b} is the breaking wave height.

Droplet size (d)

Several equations are derived to describe the droplet size distribution that develops after a wave breaking event, like the ones by Johansen, Reed, and Bodsberg (2015); Li, Spaulding, French-McCay, Crowley, and Payne (2017); Zeinstra-Helfrich, Koops, and Murk (2016). In this thesis, the equation by Johansen et al. (2015) will be used, because it is implemented in OpenDrift and it includes a dependency on oil layer thickness.

The droplet size distribution after entrainment fits well to a lognormal distribution (Reed, Leirvik, Johansen, and Brørs, 2009). Using dimensional analysis and performing a fit to experimental data, Johansen et al. (2015) found that the number-mean droplet diameter equals

$$d_{50}^{\mathrm{N}} = (2.251\, We^{-0.6} + 0.060\, Re^{-0.6})\, \mathcal{L}\,,$$

They use

$$\mathcal{H} = H_{\mathrm{p}}\,, \qquad \mathcal{L} = h_{+}\,,$$

as scales for wave height and for length, where H_{p} is the plunge wave height, and h_{+} is the oil layer thickness. Additionally, they found the base-10 logarithm of the droplet size standard deviation to equal 0.38. Röhrs et al. (2018) implemented the equation in OpenDrift after transformation of the number-based droplet size distribution into a volume-based droplet size distribution, finally yielding

$$\ln(d) \sim \mathcal{N}\left(d_{50}^{\mathrm{V}}, (0.38 \ln(10))^2\right),$$

with

$$\ln\left(d_{50}^{\mathrm{V}}\right) = \ln\left(d_{50}^{\mathrm{N}}\right) + 3(0.38 \ln(10))^2\,,$$

where d is the droplet diameter, d_{50}^{V} is the volume-median (or mass-median) droplet diameter, and d_{50}^{N} is the number-median droplet diameter.

Stokes drift (u_S)

Waves contribute to the mass transport in the form of Stokes drift. In a Eulerian frame of reference, Stokes drift expresses the difference between the Eulerian and the Lagrangian movement of particles,

$$\boldsymbol{U}_{\mathrm{L}} = \boldsymbol{U}_{\mathrm{E}} + \boldsymbol{U}_{\mathrm{S}} ,$$

where $\boldsymbol{U}_{\mathrm{L}}$ is the vector of Lagrangian velocity, $\boldsymbol{U}_{\mathrm{E}}$ is the vector of Eulerian velocity, and $\boldsymbol{U}_{\mathrm{S}}$ is the vector of Stokes drift velocity, often simply called Stokes drift.

Although high frequency waves (in this context defined as waves with a frequency higher than 0.55 Hz) contribute only little (approximately 3%) to the *total* Stokes mass transport in the ocean, they contribute about one third to the *surface* Stokes drift velocity (Breivik, Janssen, and Bidlot, 2014). This is the case because the orbital motion decays with depth faster for high frequency waves than for low frequency waves. Since the majority of the oil mass in an oil spill floats at the sea surface, Stokes drift is an important mass transport process for oil spills.

In case of monochromatic, unidirectional (in x-direction), deep water gravity waves, the Stokes drift velocity is equal to

$$u_{\mathrm{S}} = \omega k a^2 \exp(2kz) ,$$

where ω is the angular wave frequency, k is the wave number, a is the wave amplitude, and z is the vertical location in the water column. Note that z is defined positive upward and the origin is put at the still water level. The components of the Stokes drift in the direction perpendicular to the wave propagation and in the vertical direction are zero.

In case of irregular waves, the Stokes drift can be calculated by taking the linear superposition of the Stokes drift contributions of each individual Fourier component (assuming auto-interactions at a frequency are dominant and neglecting the effect of interactions between different frequencies). At the sea surface, it holds that

$$u_{\mathrm{S},0} = \int_0^\infty \omega k a_\omega^2 \, \mathrm{d}\omega = 4\pi \int_0^\infty f k E_f \, \mathrm{d}f = \frac{16\pi^3}{g} \int_0^\infty f^3 E_f \, \mathrm{d}f = \frac{16\pi^3}{g} \, m_3 ,$$

where m_3 is the third order spectral moment (see § 3.1).

Integration of the full wave spectrum is the most accurate way to obtain the full Stokes drift profile with depth, but often it is not available. Breivik, Bidlot, and Janssen (2016) propose an approximation that is dependent on the surface Stokes drift $u_{\mathrm{S},0}$ and the peak wave number k_{p}, which are often easier accessible. They derived that

$$u_{\mathrm{S}}(z) \approx u_{\mathrm{S},0} \left(\exp(2k_{\mathrm{p}} z) - \alpha \sqrt{-2k_{\mathrm{p}}\pi z} \; \mathrm{erfc}\left(\sqrt{-2k_{\mathrm{p}} z} \right) \right) ,$$

where erfc is the complementary error function, $u_{\mathrm{S},0}$ is the surface Stokes drift, k_{p} is the peak wave number, and α is a fitted shape factor (β in the original paper). In the case of a Pierson-Moskowitz (PM) spectrum, α = 1.05, and in the case of a JONSWAP spectrum (with a peak enhancement factor of 3.3), α = 0.96.

Buoyant rise velocity (w_B)

Tkalich and Chan (2002) suggest the following equation for the buoyant rise velocity, where the rise velocity is determined using Stokes law in the case of laminar flow, and using an empirical expression in the case of turbulent flow,

$$w_B = \begin{cases} \frac{g}{18\,\nu_-}\left(1-\frac{\rho_+}{\rho_-}\right)d^2, & \text{for } Re \leq 50 \\ \sqrt{\frac{8}{3}\left(1-\frac{\rho_+}{\rho_-}\right)gd}, & \text{for } Re > 50 \end{cases}$$

2.3. Modeling aspects

OSMs forecast the transport and weathering of spilled oil, using amongst others the equations collected in § 2.2. An OSM itself does not calculate the dynamics of the fluid. Current, wave and wind data are usually obtained from (operational) models or from measurements. An overview of some frequently used OSMs is shown in Appendix A.

All OSMs that are shown in Appendix A employ a particle tracking method (PTM) and discrete time integration to calculate where the oil is going. In a PTM-based model, the trajectories of so-called Lagrangian elements (LE), are followed in time. Each LE represents a small lump of oil mass with certain properties, like its location, mass, viscosity and density. In an OSM, all LEs together are thought of as representative for the entire spilt oil mass. The advantages of a PTM are that each LE can be assigned its own individual properties and that the numerical integration does not suffer from artificial diffusion (Elliott, 1986).

Numerical treatment of oil dispersion

During an amount of time, whitecapping takes place on various places within the oil slick and surface oil is entrained (see § 2.1). As a logical consequence, the surface LEs in the model must show entrainment behavior. As there is only a discrete number of LEs in the model, a choice must be made for each individual LE whether it is moved from the surface to the subsurface (assuming the PTM does not produce, split nor merge LEs). This can be done based on the probability of the LE being entrained (Röhrs et al., 2018),

$$P = 1 - \exp(-\lambda \Delta t) \approx \lambda \Delta t\,,$$

where λ is the dimensionless surface-to-subsurface oil entrainment rate, and Δt is the OSM time step. The approximation at the right hand side of the equation is a Taylor expansion to first order, which holds if the product $\lambda \Delta t$ is small.

An LE that is moved to the subsurface, is thought of as being hit by a breaking wave. In reality, that agitated oil mass will split into droplets with a wide range of sizes and entrainment depths. It is not possible to reproduce this behavior if the PTM does not produce, split or merge LEs. This problem can be overcome by assigning a representative droplet diameter and entrainment depth to each LE, so that the total mass transport is represented best. This can be done by choosing a droplet size from the lognormal probability distribution function of oil droplet sizes, and an intrusion depth from the uniform probability distribution function of entrainment depths. The advective transport and the buoyant rise of the submerged LE is further taken care of by the advection algorithm.

Numerical treatment of advection

The location of a fluid parcel can be determined by means of time integration of its velocity components, as follows,

$$\boldsymbol{X}(t_0 + \Delta t) = \boldsymbol{X}(t_0) + \int_{t_0}^{t_0+\Delta t} \Sigma \boldsymbol{U}(\boldsymbol{X}, t)\, \mathrm{d}t\,,$$

where in the case of an LE representing a lump of oil, $\Sigma\boldsymbol{U}$ is the velocity vector summing the ambient (subscript 'E' for Eulerian), wave ('S' for Stokes), wind ('W'), and buoyant ('B') transport velocity components,

$$\Sigma \boldsymbol{U} = \begin{bmatrix} u_\mathrm{E} + u_\mathrm{S} + u_\mathrm{W} + 0 \\ v_\mathrm{E} + v_\mathrm{S} + v_\mathrm{W} + 0 \\ w_\mathrm{E} + 0 + 0 + w_\mathrm{B} \end{bmatrix}.$$

Since OSMs employ a particle tracking method and discrete time integration, a numerical integration scheme has to be used, for which many options exist. If an LE reaches the sea surface because of upward advection, it becomes part of the surface slick again. Its vertical location is then fixed to the sea surface until the LE is dispersed again.

As discussed in § 2.1, it is hard to describe the near-surface flow, and to separate the wave-induced part (Stokes drift) from wind-induced part. Different wind speed parametrizations are found amongst different OSMs (see Appendix A). What is especially confusing, is that sometimes the wind drift in OSMs is implicitly assumed to (partially) cover the wave-driven transport processes. This practice is indicative of the fact that the near-surface transport processes still suffer from a lack of a physical understanding. Röhrs et al. (2018) suggest that the wind drift processes as employed in OSMs might actually represent sheared flow due to streaming effects (Laxague et al., 2018) or wave-current interaction (Christensen and Terrile, 2009).

In the remainder of this thesis, the ambient and wind terms of the advective transport ($\boldsymbol{U}_\mathrm{E}$ and $\boldsymbol{U}_\mathrm{W}$) will be set to zero, so that a purely wave-forced system is considered. This facilitates the comparison of the wave-related processes in different cases.

Converting between discrete and continuous properties

The thickness of an oil slick is hard to describe in the Lagrangian frame of reference that PTMs use, simply because it is the consequence of a Eulerian mass balance. Slick thickness is not a property of an LE that travels along with it, rather it is determined by the amount of mass that is present in a certain area. This poses a problem, because a dependency on oil layer thickness exists for some of the equations which are implemented in OpenDrift. Moreover, this thesis aims to include the oil-induced wave attenuation in the modeling of oil spill evolution. For this purpose, too, the oil layer thickness must be known.

Different methods exist to convert the oil mass from LEs into a continuous spatial distribution, by application of e.g. (regular) gridding, a kernel method, or triangulation. Basic illustrations of the different methods are shown in Figure 4.

With the regular gridding method, a the spatial model domain is overlain by a (regular) grid. Within each grid cell, the amount of oil mass is summed up, and subsequently divided by the grid cell area. Using the mass density, the average oil layer thickness within the grid cell is calculated. All LEs that are located within a certain grid cell, are given an oil layer thickness property equal to the average oil slick thickness of the considered grid cell.

Kernel methods obtain the value of a property at a certain point by weighing the contributions of surrounding discrete elements by distance. For this, kernel functions of varying complexity can be used.

A Voronoi diagram shows the areas in space that are closest to a certain 'cell center'. In the case of a PTM, cell centers are the LEs. Thus, by making a Voronoi diagram for a certain spatial configuration of the LEs, the area of the cell corresponding to each LE can be used to calculate the oil layer thickness by dividing the oil volume of the LE by the area of the corresponding Voronoi cell.

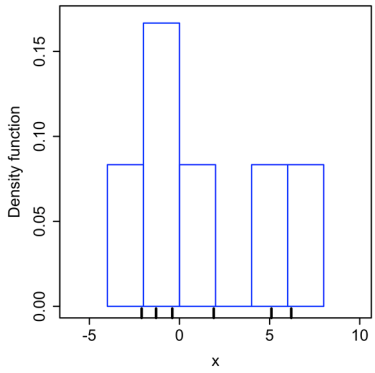

(a) *gridding method*[5]

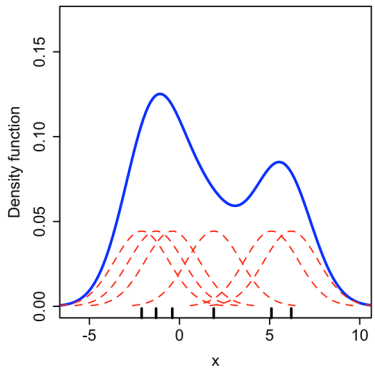

(b) *kernel method*[5]

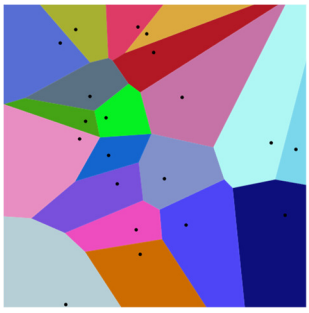

(c) *Voronoi method*[6]

Figure 4. *Methods for transforming discrete mass distribution to continuous mass distribution.*

[5] Image by Drleft, retrieved from
https://commons.wikimedia.org/wiki/File:Comparison_of_1D_histogram_and_KDE.png
[6] Image by Balu Ertl, retrieved from
https://commons.wikimedia.org/wiki/File:Euclidean_Voronoi_diagram.svg

2.4. Conclusions

The interaction between two wave-forced mass transport processes, dispersion and advection, leads to shear diffusion of an oil slick.

The oil dispersion process can be divided into three steps: entrainment, droplet formation, and buoyant rise. The first two of these three steps are dependent on wave height H and the sea surface agitation rate F. The definition of the used wave height varies throughout literature: significant wave height H_s, breaking wave height H_b and plunge wave height H_p are used. However, these wave height definitions are usually simply related to each other by a linear factor.

The full wave spectrum E needs to be known to calculate the advection process (Stokes drift). Since the full wave spectrum is often unknown, OSMs usually follow a simpler approach, where the wave spectrum is assumed to be similar to a standard wave spectrum, like the Pierson-Moskowitz spectrum. Then, Stokes drift profile can be calculated using surface Stokes drift $u_{S,0}$ and the peak wave number k_p. Wave height, sea surface agitation rate, surface Stokes drift, and peak wave frequency will be called the 'key' wave properties from now on.

From the literature review into oil spill modeling of these processes, it can be concluded that most OSMs use a particle tracking method. The oil masses in the model (LEs) each carry their own mass, viscosity and density. Oil layer thickness is not carried with the LEs, but must be recalculated regularly based on the distribution of LEs over space. For the wave processes to properly affect the LEs, the local wave properties need to be known each LE location at each model timestep. (Operational) wave models are not coupled to oil spill models, the change of the wave properties throughout an oil slick is not accounted for in model calculations so far.

Concluding, it must be investigated by how much the key wave properties change throughout an oil-polluted area. If that is known, the oil spill model can correct for the oil-induced wave attenuation.

3. Theory of viscous wave attenuation

In this chapter, the viscous energy dissipation due to the presence of a viscous fluid layer is quantified. First, the wave spectrum and the wave energy balance are introduced so that a proper theoretical framework for the description and calculation of waves is established (§ 3.1). Next, an equation for wave energy dissipation due to a viscous surface layer is given (§ 3.2), that is part of the wave energy balance. Finally, it is discussed which other effects, next to viscous dissipation, an oil slick may have on the wave energy balance (§ 3.3).

3.1. Framework for description and calculation of waves

In this paragraph, a basic theoretical framework for the description and calculation of waves is introduced, based on Holthuijsen (2007).

Description of waves: the wave spectrum

The interface of a unidirectional, monochromatic wave propagating in the x-direction can be described as

$$\eta(x,t) = a\,\Re\{\exp(i\varphi)\}\,,$$

$$\varphi = kx - \omega t + \varphi_0\,,$$

where η is the sea surface elevation, a is the wave amplitude, φ is the wave phase angle, which is dependent on the wave number k, the angular wave frequency ω, and the wave phase shift φ_0. The symbol i denotes the imaginary unit, and the operator $\Re$ indicates that the real part of a complex number is taken. The wave number and the wave frequency cannot be chosen independently. They are related through the wave dispersion relation, which for deep water gravity waves is given by

$$\omega = \sqrt{gk}\,.$$

Actual waves at sea are irregular. They can be modeled as a superposition of (infinitely) many wave components, each one having its own wave amplitude, number, frequency, and phase shift. This leads to a description of the sea surface level by

$$\eta(x,t) = \sum_{j=1}^{n} a_j\,\Re\{\exp(i\varphi_j)\}\,.$$

To show the distribution of the components that make up a wave signal, an energy spectrum (for discrete frequencies) or an energy density spectrum (for a continuous range of frequencies) can be made. The energy content of the monochromatic wave, integrated over depth and per unit sea surface area, is equal to[7]

$$E = \frac{1}{2}a^2\,.$$

The definition of energy density is the wave energy for the limit of a small frequency or direction range, as follows,

$$E_f = \lim_{\Delta f \to 0} \frac{a(f)^2}{2\Delta f}\,,$$

where f is the linear wave frequency. The energy (density) spectrum is simply referred to as 'wave spectrum' from now on. Examples of wave spectra are shown in Figure 5.

[7] It is common to leave the mass of the fluid (ρg) out of this equation, but still refer to it as energy.

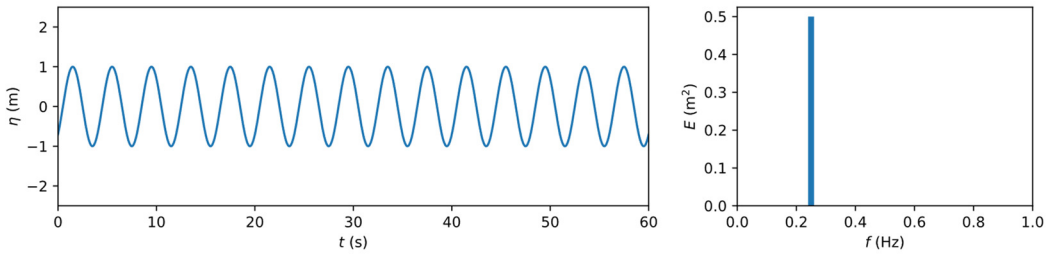

(a) *monochromatic wave*

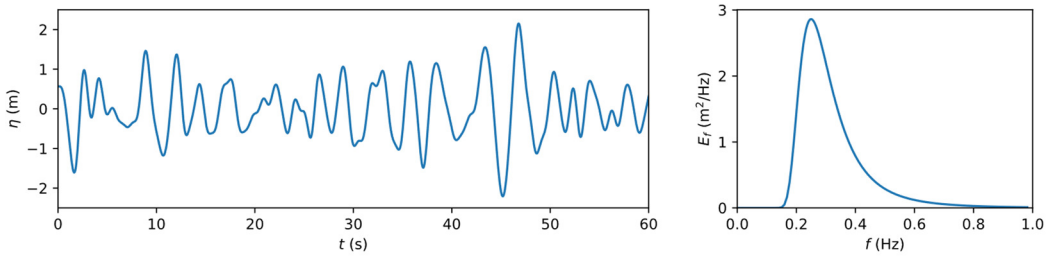

(b) *irregular wave*

Figure 5. *Two different waves, that have the same peak frequency and contain the same amount of wave energy. [left] Sea surface elevation at a fixed point in space. [right] The associated wave spectrum.*

The wave spectrum is an abstract concept, but it turns out to be very useful. Amongst others, it can be used to derive so-called integral wave properties, using the weighted moments of the wave spectrum,

$$m_n = \int_0^\infty f^n E_f(f)\,\mathrm{d}f\,,$$

where m_n is the n-th order spectral moment.

Calculation of waves: the wave energy balance

In order to calculate wave transformation, for instance by the presence of an oil slick, the wave energy balance should be studied. The wave energy balance for deep water without an ambient current is given by

$$\frac{\partial E_f}{\partial t} + \nabla \cdot \left(\boldsymbol{c}_\mathrm{g} E_f\right) = \sum S_f\,,$$

where E is the wave energy, $\boldsymbol{c}_\mathrm{g}$ is the wave group velocity vector, and S is a source of wave energy (or a sink of wave energy, which will be called a 'source term' too from now on). The subscript 'f' indicates that energy density is considered, and the operator $\nabla \cdot$ indicates that the divergence of the vector field is taken.

S can stem from energy input, energy dissipation, or energy redistribution. The latter means extraction of energy from one frequency range and input of that energy into another frequency range. The main source terms are shown in the following table.

Category	Symbol	Description
input	S_w	energy input by wind
dissipation	S_vi	energy dissipation by viscous effects
	S_wh	energy dissipation by steepness-induced wave breaking
	S_br	energy dissipation by depth-induced wave breaking
	S_bf	energy dissipation by bottom friction
redistribution	S_3	energy redistribution by triad wave-wave interaction
	S_4	energy redistribution by quadruplet wave-wave interaction

In this research, only deep water situations are considered, so depth-induced wave breaking (S_br), bottom friction (S_bf), and wave triads (S_3) are assumed to be absent. In principle, an oil layer may affect any of the remaining terms of the wave energy balance. In this research, only the effect of oil on the term S_vi of the energy balance is considered (see § 3.2). A short description of the possible effect of the oil layer on the other terms of the wave energy balance is discussed in § 3.3.

3.2. Energy dissipation by a surface oil slick

Linear wave theory assumes that the considered fluid is inviscid. Hence, there can be no wave attenuation due to viscous effects. For most purposes involving sea waves, this is a reasonable assumption. Oil, however, has a kinematic viscosity that can be orders of magnitude larger than that of water (see Appendix B), so viscous effects will be more relevant if oil is present.

In this paragraph, it is described at what rate the wave energy is dissipated due to viscous effects. First, the case of a uniform fluid with a 'clean' surface is discussed. Then, the theory for wave attenuation by a viscous fluid layer on top of an infinitely deep fluid is described.

Clean surface

Wave attenuation can be described by adding an imaginary term to the wave frequency,

$$N = \omega + i\beta \,,$$

where β represents the temporal amplitude decay rate. It is defined such that

$$\frac{\partial a}{\partial t} = -\beta a \,.$$

For monochromatic waves in clean, deep water, the temporal amplitude decay rate by viscous effects equals

$$\beta_{\mathrm{cl}} = 2\nu_{-}k^2 = 2\frac{\nu_{-}\omega^4}{g^2},$$

where ν_{-} is the kinematic viscosity of the water, k is the wave number, ω is the angular wave frequency, and g is the gravitational acceleration (Behroozi, 2004; Lamb, 1932). The subscript 'cl' indicates clean surface.

It is not evident whether molecular or turbulent kinematic viscosity should be used in the decay rate equation. For waves of 3 to 8 Hz, the wave motion probably takes place within the viscous boundary layer, so there is no effect of turbulence on the viscous dissipation (Milgram, 1998). Note that there may be turbulent energy dissipation, apart from the viscous energy dissipation. At the other end of the spectrum, Weber (1987) researched attenuation of waves of frequencies around 0.1 Hz, stating that turbulent kinematic viscosity should be used.

In this research, the wave attenuation is expected to be dominant for waves with frequencies around 2-3 Hz. The assumption is made that the associated wave motion is not affected by turbulence. Therefore, the molecular kinematic viscosity of sea water is used in this research.

Viscous surface layer

Various works are dedicated to the wave damping effect of surface layers, like surfactant films, oil layers and ice floes (Alpers and Hühnerfuss, 1989; De Carolis and Desiderio, 2002; Ermakov, Sergievskaya, and Gushchin, 2012; Jenkins and Dysthe, 1997; Jenkins and Jacobs, 1997; Sergievskaya and Ermakov, 2017; Sutherland, Halsne, Rabault, and Jensen, 2017; Weber, 1987).

Jenkins and Jacobs (1997) derived a wave dispersion relation that unifies the damping by interfacial and viscous properties, for a viscous fluid layer on top of an infinitely deep fluid. The full wave dispersion relation is given in Appendix C. There, it is also shown that, for mineral oil slicks, interfacial properties can be neglected with respect to viscous properties. A simplified wave dispersion relation is obtained, which yields a the wave amplitude decay rate equal to

$$\beta_{\mathrm{vi}} = \beta_{\mathrm{cl}}\, \Re\{\mathcal{Y}\}\,,$$

with

$$\mathcal{Y} = \frac{1 + Y + \dfrac{\sqrt{\nu_-^*}}{\nu_+^* \sqrt{i}} Y^2}{1 + \left(4\sqrt{i}\sqrt{\nu_-^*} + \dfrac{\sqrt{\nu_-^*}}{\nu_+^* \sqrt{i}} \right) Y},$$

$$Y = \frac{\rho_+ \nu_+}{\rho_- \nu_-} k h_+\,,$$

$$\nu_\pm^* = \sqrt{\frac{k^3}{g}}\, \nu_\pm\,,$$

where ν is the kinematic viscosity, ρ is the mass density, h is the layer thickness, k is the wave number, g is the gravitational acceleration, the minus index indicates lower layer properties (water), the plus index indicates upper layer properties (oil), and the subscript 'vi' indicates the presence of a viscous surface layer. The symbol i denotes the imaginary unit, and the operator $\Re$ indicates that the real part of a complex number is taken.

The real part of the parameter $\mathcal{Y}$ can be interpreted as an amplification factor for the decay rate of the clean surface case. Figure 6 shows the decay rate amplification for various combinations of oil layer thickness and oil viscosity. Figure 7 shows the decay rate for monochromatic waves of different frequencies.

No matter whether molecular kinematic viscosity (of order 10^{-6} m^2/s) or turbulent kinematic viscosity (of order 10^{-4} m^2/s) is used, very small decay rates are found for common wind waves (with frequencies of 0.1 to 1.0 Hz). This justifies the assumption to neglect viscous effects in common oceanic wave modeling. However, enhanced attenuation is found for the short gravity waves with frequencies above approximately 1.0 Hz when a viscous surface layer is present.

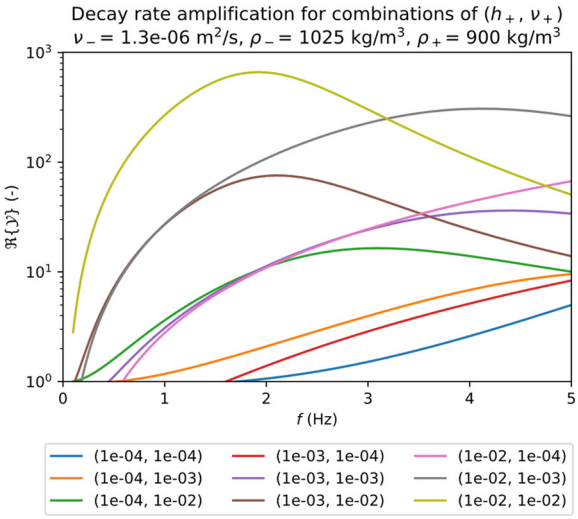

Figure 6. *The decay rate amplification for various combinations of surface layer thickness h_+ (m) and surface layer kinematic viscosity ν_+ (m^2/s), as a function of linear wave frequency f. Note the logarithmic vertical scale.*

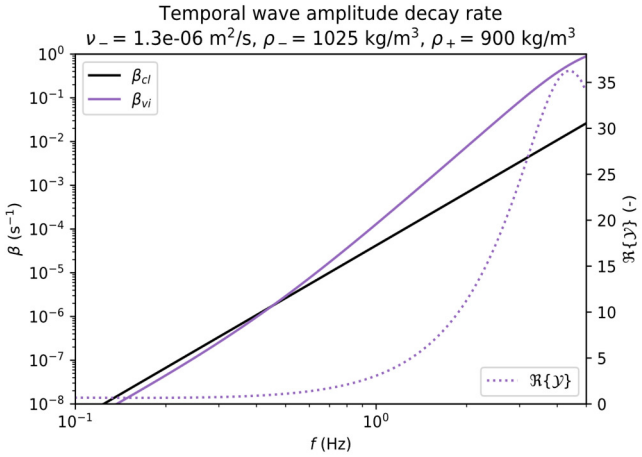

Figure 7. *The temporal amplitude decay rate β for monochromatic deep water waves caused by viscous effects, as a function of linear wave frequency f. The case of a clean surface (black drawn line, left-hand ordinate) and an example case with a surface layer thickness of 10^{-3} m with a kinematic viscosity of 10^{-3} m^2/s (colored drawn line, left-hand ordinate) are shown. The ratio between the two cases is represented by $\Re\{\mathcal{Y}\}$ (colored dashed line, right-hand ordinate).*

Wave attenuation in terms of energy

The magnitude of the term S_{vi} can be calculated using the fact that wave energy is proportional to the square of the wave amplitude. Hence, the reduction of wave energy is related quadratically to the reduction of the wave amplitude,

$$S_{vi} = \frac{\partial E}{\partial t} = \frac{\partial E}{\partial a}\frac{\partial a}{\partial t} = a(-\beta a) = -\beta a^2 = -2\beta E \, .$$

This equation can be used for irregular waves too, if E and S are replaced by their respective 'per unit frequency' properties E_f and S_f. This approach implies that the wave energy dissipation 'caused' by waves of a certain frequency actually drains wave energy from that specific frequency. Support for this approach is found by Alpers and Hühnerfuss (1989), who found a distinct dip in the wave spectrum where maximum damping was expected from theory (see Figure 8). Further support for this approach is found in the fact that energy dissipation by fluid mud is implemented in SWAN in the same manner.

3.3. Other contributions of a surface oil slick

In the previous paragraph only the effect of an oil layer on the viscous energy dissipation term of the wave energy balance was discussed. However, an oil layer may well influence the other source terms, either explicitly (the process is changed due to the oil layer) or implicitly (the viscous dissipation alters the wave spectrum, so a new balance between the source terms is created). In this paragraph, these possible effects are discussed.

In order to be able to draw conclusions about the oil effect on the waves by the viscous dissipation alone, the explicit effects of the oil on the other source terms of the wave energy balance are not included in the subsequent modeling. Implicit effects will be part of the modeling, since they are simply the consequence of the changing spectrum due to the viscous wave damping.

Input by wind (S_w)

The energy transfer from wind to waves is a source of energy in the wave energy balance. Different empirical functional forms exist for this source term S_w. Barring the onset of waves (Phillips mechanism), wind wave growth is an exponential process (Miles mechanism) where the rate of energy input grows with growing waves, i.e. a more rough sea surface. If oil attenuates waves, this consequently would lead to smaller wind input.

Also, the wind input term grows with growing friction velocity U^*, which expresses the amount of drag that exits between air and water. The presence of an oil layer at the sea surface may adapt the air-water interaction. According to Alpers and Hühnerfuss (1989), the presence of a surface layer of (organic) oil can be modeled by reducing the friction velocity U^* in a wind input equation that otherwise has the same functional form as for the clean surface case. A reduction of about 20% was found experimentally for surfactant monolayers.

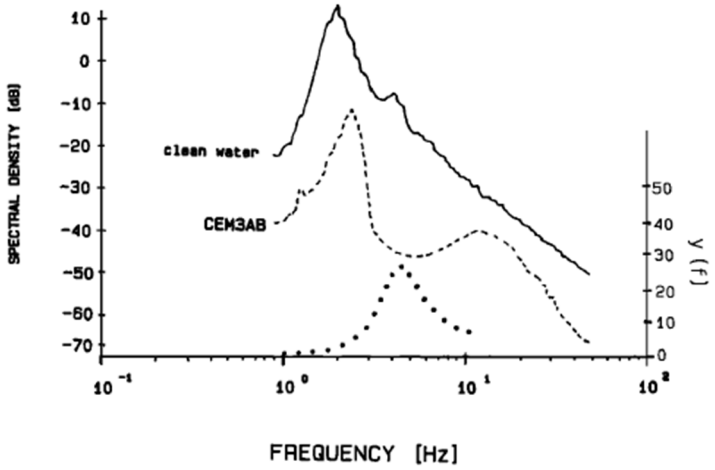

Figure 8. *Wave spectrum for the case of a clean surface (solid line, 'clean water', left-hand ordinate) and for a surface covered with a hexadecyl-tri-methyl ammonium bromide slick (dashed line, 'CEM3AB', left-hand ordinate). Also, the theoretical decay rate amplification factor γ is shown (dotted line, right-hand ordinate).*[8]

[8] Image retrieved from: (Hühnerfuss, Walter, Lange, and Alpers, 1987), their Figure 3.

Regarding the onset of wind waves, Paquier, Moisy, and Rabaud (2016) found a dependency on fluid viscosity. They identified three wave regimes in their experiments: wrinkles, regular waves and solitary waves. The wrinkle regime exists for low wind speeds. The wrinkles turn into regular waves for wind speeds higher than the critical friction velocity, which scales to fluid kinematic viscosity by the relation $U_c^* \propto \nu^{0.20}$. For a kinematic viscosity of $1.0 \cdot 10^{-6}$ m^2/s, this is found to correspond to a wind speed of about 3.6 m/s. For a kinematic viscosity of $85 \cdot 10^{-6}$ m^2/s, it relates to a wind speed of about 8.0 m/s. For fluids with kinematic viscosity over about 10^{-4} m^2/s, periodic solitary waves are generated instead of regular waves. It is not clear how these findings apply in when a less viscous fluid is overlain by a more viscous fluid, like in the case of sea water with an oil layer at the surface.

Benetazzo et al. (2019) show in an experiment that the onset of waves from a still surface is hindered by the presence of a surface organic oil layer. However, when initial waves are present (relatively long waves, generated by a paddle), those waves do grow, and they do so similarly in the clean surface and viscous surface layer cases.

Concluding, the energy input into the waves has a dependency on the friction velocity (that expresses the drag that exists between air and water), the amount of wave energy (that expresses the roughness of the sea). Also, the onset of waves is found to be dependent on fluid viscosity (at least in case of a uniform fluid) and on the presence of a surface layer.

In the remainder of this thesis, it is assumed that the wind input formulations do not change as a consequence of the presence of an oil layer. Hence, the possible effects of the altered drag relationship and wave onset inhibition are not taken into account, since they are explicit effects. The exponential growth effect is taken into account in this study, since the energy content of the wave spectrum may change as a consequence of the newly introduced viscous dissipation term in SWAN. This is thus an implicit effect.

Dissipation by whitecapping (S_{wh})

Wave breaking is a consequence of waves becoming too steep. The theoretical maximum steepness of an individual wave is 0.14 (Miche, 1944). However, observations show that waves at open sea break at a smaller steepness, and breaking waves are on average only slightly steeper than other waves: the average steepness of breaking waves is 0.042, versus a steepness of 0.036 for non-breaking waves (Holthuijsen and Herbers, 1986).

The presence of an oil layer may affect the wave breaking process at the small scale of the wave crest. Unfortunately, there is no theoretical understanding of the breaking process (Holthuijsen, 2007) and it is unknown how oil affects the breaking process locally (Tkalich and Chan, 2002). Therefore, in this thesis, local alteration of the wave breaking process is not taken into account, since it is an explicit effect. The wave breaking dependency on wave steepness and on wave energy is automatically taken into account in this study, since it is an implicit effect as it is part of the whitecapping sink term equations in SWAN.

Redistribution by quadruplets (S_4)

Quadruplet wave-wave interactions are due to the non-linearity of the equations of motion. The quadruplet source/sink term transfers wave energy from certain frequencies to certain other frequencies. The integrated effect of the quadruplets is zero, i.e. no energy is added to or extracted from the spectrum by the quadruplets. Energy is only redistributed.

Assuming that the viscous surface layer causes attenuation but has no effect on wave length, there is no explicit effect on the non-linear transfer, since the quadruplet pairs will stay the same. It must be noted that if the presence of an oil layer does affect wave length, the quadruplet pairs will change, an thus an explicit effect is introduced. Apart from that, as the viscous energy dissipation causes a change of spectral shape, the quadruplet action will adjust implicitly. Enhanced energy dissipation from a certain frequency range will cause a dip in the wave spectrum, which will be balanced by non-linear transfer from the remaining part of the spectrum. This concept is used by Alpers and Hühnerfuss (1989) to explain the attenuation of waves outside of the frequency range where damping effects were expected. Restricted by the computer power and memory of their time, they were not able to perform reliable numerical calculations on this effect. In this thesis, numerical simulation of the wave spectrum including quadruplet contributions is performed.

3.4. Conclusions

Theory shows that the presence of a surface fluid layer with viscous or interfacial properties causes wave energy dissipation. For the parameter domain common to oil spill modeling, the interfacial properties are negligible with respect to the viscous properties. The associated dissipation amplification is largest in the range of short gravity waves (with frequencies higher than approximately 1 Hz).

For monochromatic waves, the viscous layer dissipation (S_{vi}) alone leads to an exponential decay of the wave amplitude. The full wave energy balance must be solved to determine the net effect of the viscous surface layer for real deep water cases, where energy is added to the waves by wind (S_w), energy is dissipated from the waves by whitecapping (S_{wh}), and energy is exchanged between waves of different frequency by quadruplet interactions (S_4). Implicit effects of the oil layer presence are expected, such as increased energy redistribution by quadruplets and decreased wave whitecapping.

4. Modeling of viscous wave attenuation

In this chapter, the spectral wave model SWAN[9] is used to solve the deep-water wave energy balance with and without the contribution of a surface oil slick, so the effect of oil on the key wave parameters can be determined.

First, it is explained how the key wave parameters are calculated from the model output (§ 4.1). Then, the model is adapted, so wave energy dissipation due to a viscous fluid layer can be included (§ 4.2). As the oil effect is mainly present in the high-frequency range of the wave spectrum, special model settings are necessary regarding the frequency domain and the numerical solving procedure (§ 4.3). Special attention is paid to the choice of wind input and whitecapping dissipation formulations, so that a valid reference spectrum is obtained for further simulations (§ 4.4). Afterwards, the change of key wave parameters is derived from model simulations in which part of the domain is covered with oil. Functions are fitted that relate the reduction of the whitecapping dissipation rate and of the surface Stokes drift to wind speed, oil layer thickness and oil viscosity (§ 4.5).

[9] Simulating WAves Nearshore; for a description of the model, see (The SWAN team, 2019a, 2019b).

4.1. Modeling approach

As concluded in Chapter 2, the wave height H (which reflects the potential energy release in a wave breaking event) and the sea surface agitation rate F (which reflects the wave breaking rate) are the key wave parameters for the oil dispersion process. The oil advection is caused by the Stokes drift, which is described by the key wave parameters surface Stokes drift $u_{S,0}$ and the peak wave number k_p. In this chapter, using SWAN, the change of these parameters in an oil-covered area is investigated. In this paragraph, it is described how the key wave properties are calculated from the SWAN output.

The wave spectrum plays a main role for determining many wave properties. Spectral moments (see § 3.1) are convenient for doing so. A common way to determine wave height H is to use the definition for significant wave height based on the zeroth order spectral moment (Holthuijsen, 2007),

$$H_s = 4\sqrt{m_0}\,.$$

For surface Stokes drift velocity $u_{S,0}$, the third order spectral moment can be used (see § 2.2),

$$u_{S,0} = \frac{16\pi^3}{g} m_3\,.$$

A correction for the directional spreading of the waves will be applied. The peak wave number k_p is easy to derive from spectral output, because it is located at the frequency bin with the highest energy density.

The final wave property that a measure has to be found for is sea surface agitation rate F. This cannot easily be derived from the wave spectrum. It is not calculated by SWAN, either. Yet, another measure for it can be found: the whitecapping dissipation rate S_{wh}. As will be explained later, it is simply assumed that

$$F \propto S_{wh}\,.$$

where S_{wh} is the whitecapping energy dissipation.

4.2. SWAN model adaptation

To simulate waves in the presence of an oil layer, the dissipative contribution of the oil layer to the wave energy balance should be included in the model. As explained in § 3.2, this dissipative contribution can be expressed in terms of the imaginary wave number. In this respect, great similarity is found with theory on fluid mud that is already included in SWAN (Ng, 2000).

The source code of SWAN version 41.20AB was downloaded from the SWAN homepage[10]. In the subroutine that handles the fluid mud dissipation, the imaginary wave number is replaced. The fluid mud subroutine also incorporates a change of the real wave number. In this research, this effect is neglected (see Appendix C), so that part of the subroutine is deactivated. After adaptation, a new SWAN executable is compiled.

4.3. General model settings

Various wave simulations are performed in this chapter. In this paragraph, the general assumptions and model settings which are generic throughout all simulations are discussed.

Domain and discretization

Only stationary cases are considered. Ergo, it is assumed that $\partial/\partial t = 0$. Even though it does not often occur in reality that waves are in equilibrium, this assumption provides a simple and unambiguous starting point for this research. To further constrain the number of variables that influence the results, only the case of fully developed waves is looked into, i.e. the waves are not time-limited, nor fetch-limited, nor depth-limited. As a consequence of this choice, the Pierson-Moskowitz spectrum will serve as the general reference spectrum. Furhermore, there are assumed to be no gradients perpendicular to the wave propagation direction, which is chosen to coincide with the x-axis, i.e. $\partial/\partial y = 0$. Hence, the spatial domain can be considered to be one-dimensional.

The lower boundary of the frequency domain is set at 0.04 Hz, as is SWAN standard. A value of 5 Hz is chosen for the cutoff frequency, i.e. the upper boundary of the frequency domain. This choice is based on the expectation that the oil-induced attenuation is present mainly in the frequency range of short gravity waves (above approximately 1 Hz). Frequencies higher than 5 Hz are not considered relevant, because the energy in the spectrum diminishes rapidly with frequency. Moreover, capillary effects start to play a role for such short waves, which SWAN does not solve. The frequency domain is divided into 100 logarithmically distributed frequency bins.

The directional domain covers all directions and it is distributed in 30 bins of equal size, so each directional bin covers 12°.

[10] swanmodel.sf.net, last accessed 23 February 2019.

According to The SWAN team (2019a), for accurate calculation of the quadruplet interactions, the recommended increment factor for the frequency domain discretization is 1.07 (these simulations: 1.05) and the recommended directional resolution is 10° (these simulations: 12°). The frequency and direction discretization of these simulations are thus considered sufficient.

Numerical solving procedure

As quadruplet interactions are important for the detailed shape of the equilibrium wave spectrum, it is decided to use the XNL algorithm, which is exact, rather than the DIA algorithm, which is an approximation. A major disadvantage of the XNL method is that it significantly slows down the calculations.

The results of some preliminary simulations showed spurious oscillations in the high frequency part of the spectrum. These instabilities appear to be caused by the quadruplet source term, which is highly sensitive to small changes in the high frequency part of the spectrum. To suppress the spurious oscillations, the SWAN option of frequency-dependent under-relaxation is enabled (The SWAN team, 2019a). Frequency-dependent under-relaxation causes smaller updates to be made to higher frequency waves during the convergence process. It is found that the spurious oscillations disappear if a sufficient amount of under-relaxation is applied. There are two general disadvantages to the under-relaxation method. First, the 'sufficient' amount of under-relaxation has to be found empirically for every simulation. In this research, it is found by trial-and-error, where in general it is aimed for a low value in order to reduce the amount of numerical 'enhancing' applied. No further attention will be paid to this procedure in the remainder of this report, as the general assumption with the under-relaxation method is that it does not affect the final, stationary result. Second, more iterations are needed to converge to the stationary solution.

Because of the use of the computationally expensive XNL algorithm, and because of the high number of iterations needed due to the under-relaxation, the model calculations take a long time. It is decided to initiate the models by means of a hotstart, using a hotfile that contains the directional wave spectrum for every grid point in the domain. In this way, the initial condition of the model is equal to the boundary condition. Using the hotstart, somewhat faster convergence is yielded with respect to the standard initiation method that SWAN uses, i.e. a stationary run in second generation mode.

In the postprocessing phase, convergence is checked using an automated script that checks the relative change of energy density over one iteration, for all frequencies (directionally integrated) at selected gridpoints. Less than 10% of the entries show relative changes of more than 0.1% per iteration. Maximum relative changes are found in the order of 1% per iteration. This is considered acceptable.

4.4. Reference wave spectra

Modeling viscous wave damping requires a larger prognostic frequency domain than usual. A frequency domain between 0.04 and 5 Hz is chosen. In this paragraph, it is investigated which wind/whitecap formulations yield a realistic equilibrium wave spectrum when such a large frequency domain is used. For this, a basic deep water case with uniform wind forcing is simulated. Viscous dissipation for the clean surface case is activated, but the effects of oil are not yet considered. The rationale behind this step is that, if a certain model setup produces a realistic equilibrium spectrum for a clean surface reference scenario, then the same setup can be expected to produce a realistic equilibrium result, too, if the dissipation of a viscous surface layer is added.

Necessity of comparison of wind/whitecap formulations

As explained in § 3.1, four source terms contribute to the deep-water wave energy balance. These different source terms are known with different certainties. Dissipation by viscous effects (S_{vi}) and redistribution by quadruplets (S_4) are derived from the physics underlying the waves. One can thus exactly calculate their magnitude. Input by wind (S_w) and dissipation by whitecapping (S_{wh}), however, are based on empirical formulations, which are validated for specific cases only. It is necessary to compare the performance of the different wind/whitecap formulations, because two aspects of the wave modeling in this thesis are special.

First, in this research the high-frequency range (tail) of the spectrum is solved prognostically. Usually, for the intended engineering purposes of spectral wave models (SWMs), integral wave parameters like the significant wave height or the peak wave period are of interest, and the tail of the spectrum is hardly relevant, since it contains a limited amount of energy. Therefore, in SWMs, the frequency domain is discretized up to a certain maximum frequency (usually around 1 Hz), called the cutoff frequency. Waves with frequencies higher than the cutoff frequency are represented by a diagnostic tail of a fixed shape that is added to the spectrum. In this research, however, the tail of the spectrum is actually of interest and its shape is unknown beforehand. Therefore, the cutoff frequency is set at a higher value of 5 Hz. The effect of extending the prognostic part of the wave spectrum on the numerical solution should be investigated.

Second, this research aims to simulate a steady-state situation. Wind/whitecap formulations are usually calibrated for correctly reproducing a measured growth curve of the wave energy. There is no guarantee that the formulations give good results for steady-state situations, too. It should therefore be checked which steady-state solution is obtained with the different wind/whitecap formulations.

Criteria for a well-performing wind/whitecap formulation

It is impossible to obtain the 'true' wave spectrum using a numerical model. A model is always based on assumptions and dependent on empiricism. For a numerical model, also the discretization and the numerical solving procedure affect the result. While the PM spectrum (see Appendix D) is generally considered to be the equilibrium wave spectrum for fully developed sea waves, this will not necessarily be reproduced by a numerical wave model. In this thesis, a numerically modeled reference wave spectrum that is 'close enough' to the PM spectrum is sought for so that at least the qualitative oil effect on the key wave properties can be investigated. Quantitative conclusions can be drawn, as long as one is aware that the

calculations have been made on the assumption of a certain spectrum (which is close to, but not exactly equal to, the wave spectrum found at sea).

Having noted the limitations of a numerical model, an equilibrium spectrum is sought that is as close as reasonably possible the PM spectrum. Three criteria are defined for rating the performance of the different wind/whitecap formulations. First, the total energy content of the resulting wave spectrum should be close to the energy content of the PM spectrum. Second, the wave spectrum should show fair resemblance to the PM spectral shape. Since the damping processes of interest take place at relatively high frequencies (approximately 1 to 5 Hz), especially the spectral tail should be of correct shape. The scientific community has not reached full agreement on the exact shape of the spectrum tail, but consensus is that it should be of a shape in between f^{-4} and f^{-5} (Holthuijsen, 2007). Third, the wave spectrum and the source term contributions to the energy balance should not be dependent on the choice of cutoff frequency.

The different wind/whitecap formulations

SWAN has different options for wind/whitecap formulations, each having a different background. Each of the options consists of a wind input formulation and a whitecap dissipation formulation, which usually contain multiple calibration parameters. Four variants are available, which are named '*Komen*' (Komen, Hasselmann, and Hasselmann, 1984), '*Janssen*' (Janssen, 1989, 1991), '*Westhuysen*' (van der Westhuysen, Zijlema, and Battjes, 2007), and '*ST6*' (Rogers, Babanin, and Wang, 2012). Some relevant features of these formulations are explained below, with a focus on the whitecapping part. For a more complete description of these formulations, see the references mentioned above, and (The SWAN team, 2019a).

The *Komen* and *Janssen* whitecap formulations are quite similar. They are based on a coefficient that is dependent on the average wave steepness. The energy that is calculated to be dissipated by whitecapping is assigned to the spectral frequencies proportionally to the distribution of energy density over the spectral frequencies. Waves of some frequency will thus lose energy to whitecapping, dependent on the steepness of the spectrum as a whole. It is said that the whitecap formulation is dependent on 'integral' spectral properties. In SWAN, the whitecap formulation of *Janssen* can be used with the wind formulation by *Komen*, and vice versa.

The *Westhuysen* whitecap formulation is different, since its coefficient is not dependent on the average wave steepness, but on the amount of spectral saturation at each frequency. Waves of some frequency will lose energy to whitecapping based on the amount of energy oversaturation at that specific frequency. It is said that the whitecap formulation is dependent on 'local' spectral properties.

The *ST6* wind/whitecap formulation is the most recent. Its whitecap formulation depends on both integral and local spectral properties. Waves of a certain frequency will not lose energy to whitecapping if the spectrum at that frequency is not saturated. Furthermore, the amount of whitecapping is proportional to the spectral steepness of the spectrum from the low frequencies up to the frequency of consideration. With this approach it is achieved that for waves of a certain frequency, only longer waves count for determining spectral steepness. This matches the observation that shorter waves sometimes break by breaking of longer waves or modulation by longer waves.

Simulation setup

Next, actual numerical wave modeling with the different wind/whitecap formulations is performed. This is done in two steps. First, it is investigated which wind/whitecap formulations are suitable for modeling the steady-state situation (equilibrium wave spectrum), while employing a frequency domain running up to 5 Hz. Second, for the wind/whitecap formulations that are considered suitable, the reference equilibrium spectrum is determined in detail. These spectra are then used as initial/boundary condition in the next paragraph.

A spatial domain of 50 km is chosen with a grid size of 500 m, as illustrated in Figure 11. One additional grid cell is added to the end of the domain, to prevent spurious boundary effects. As boundary and initial conditions, PM spectra are used. The waves are given the SWAN standard value for directional spreading, 31.5°. Output of the spectrum and of the source/sink terms is requested along the domain at 0.0, 0.5, 5.0 and 50 km. All four wind/whitecap formulations are modeled.

Simulation results

The development of the wave spectra along the domain is shown in Figure 9. The source terms that belong with the wave spectrum at 50 km are shown in Figure 10.

With the *Komen* and the *Janssen* formulations, significant under- and overestimation of reasonable spectral tail levels is found. Combining the one wind input formulation with the other whitecapping formulation and vice versa, or adjusting the calibration parameter, does not improve the result. This behavior is attributed to the fact that the *Komen* and the *Janssen* whitecapping formulations are dependent on integral wave parameters only. Because the spectral shape criterion is not be fulfilled by the *Komen* and *Janssen* formulations, no further modeling is performed with these formulations.

An overview of the performance of the *Westhuysen* and *ST6* formulations is given in the following table.

Criterion	**Westhuysen**	**ST6**
(1) energy content	Slight increase w.r.t. PM spectrum.	Very slight increase w.r.t. PM spectrum.
(2) spectral shape	Straight tail of shape f^{-4}. Peak in accordance with PM spectrum.	Tail roughly between f^{-4} and f^{-5}. Higher peak w.r.t. PM spectrum.
(3) cutoff sensitivity	Source terms reach beyond 5 Hz.	Source hardly contribute around 5 Hz.

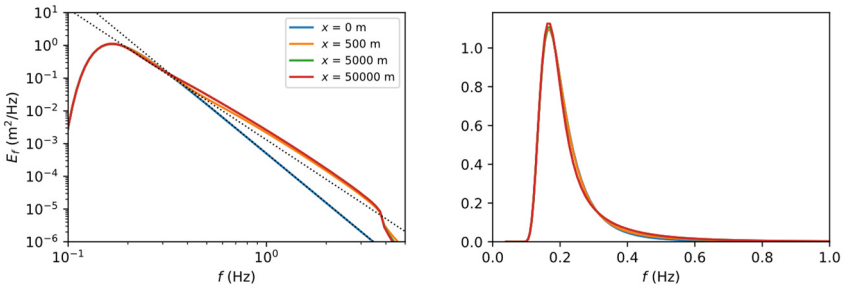

(a) *Komen*

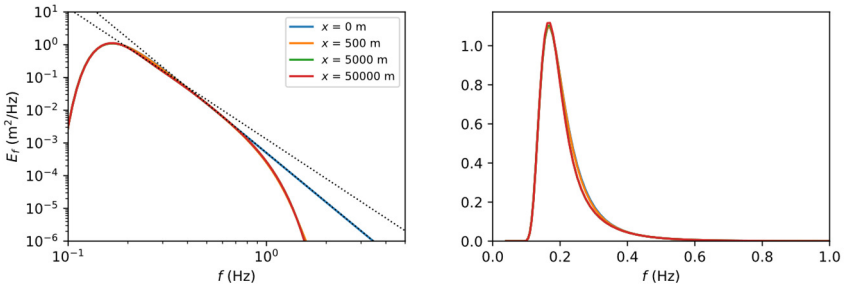

(b) *Janssen*

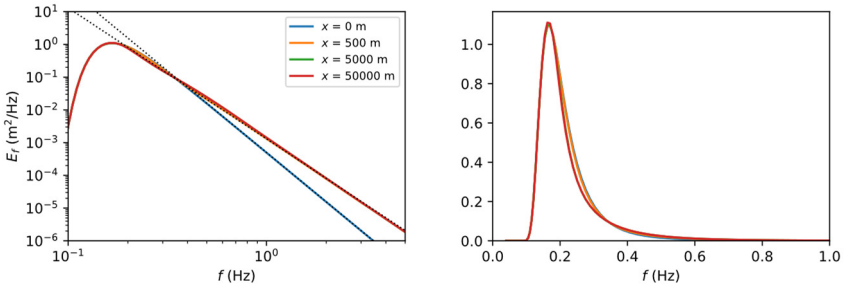

(c) *Westhuysen*

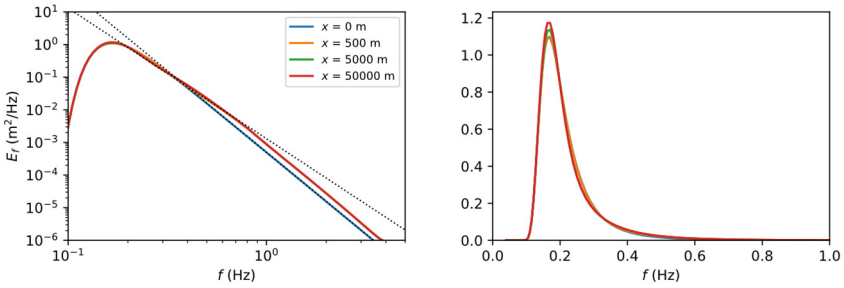

(d) *ST6*

Figure 9. *Wave spectra at four different locations along the domain, on logarithmic and on linear scales. The initial spectrum (at x = 0 km) equals a PM spectrum. Reference lines indicating a f^{-4} and f^{-5} tail shape are added to the logarithmic plots.*

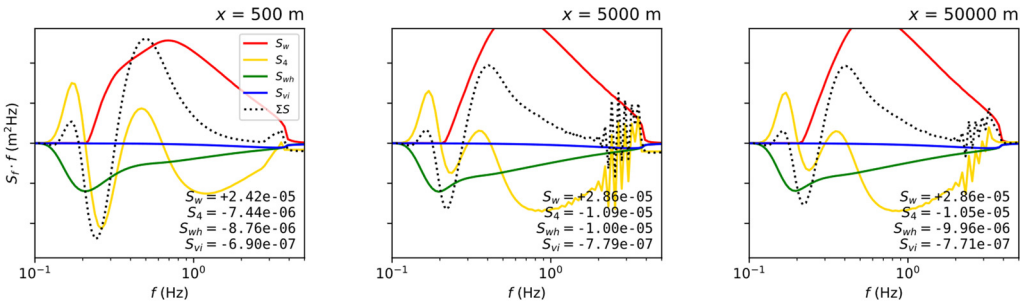

(a) *Komen*

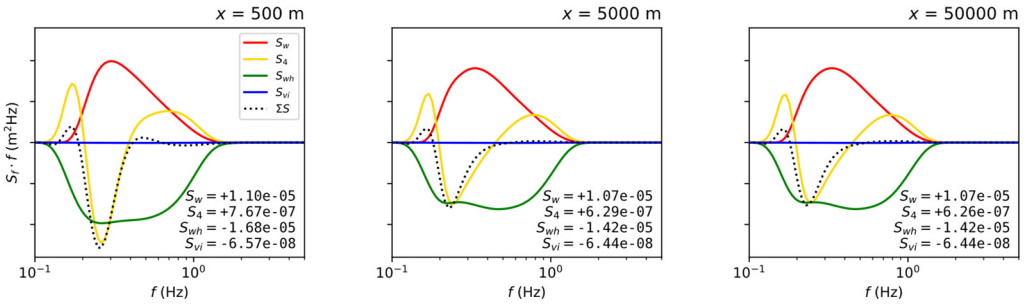

(b) *Janssen*

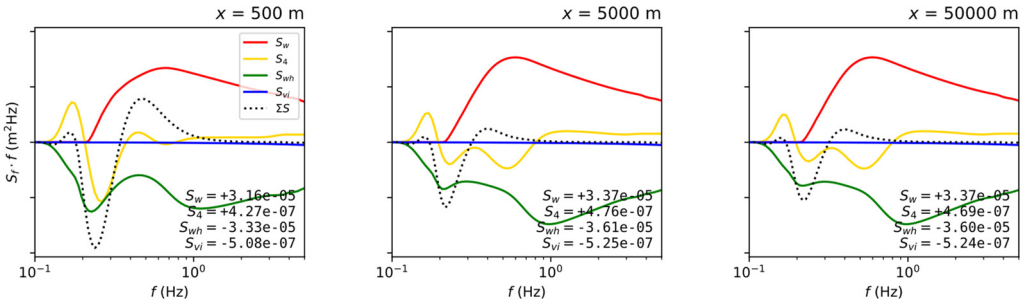

(c) *Westhuysen*

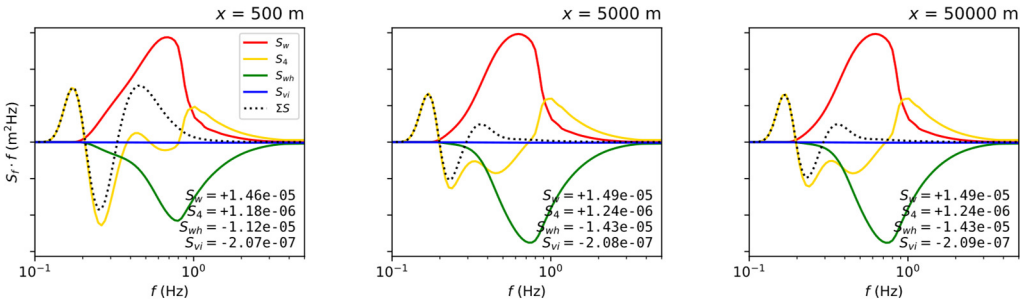

(d) *ST6*

Figure 10. *Source terms at three different locations along the domain, including their integrated contribution (in m²). Please note the logarithmic x-axis and the associated area-preserving transformation of the y-axis by multiplication with f.*

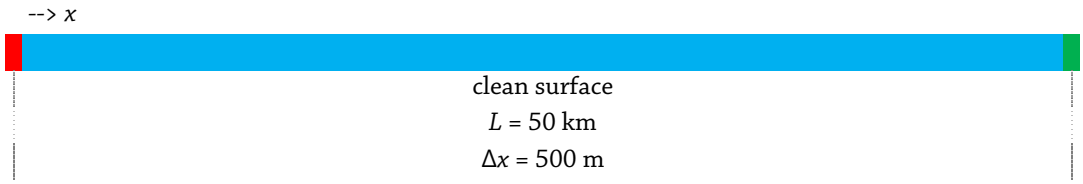

Figure 11. *Top view of the modeled spatial domain for the comparison of the wind/whitecap formulations. The red line indicates the location of the wave boundary condition. The green line indicates the location where the equilibrium wave spectrum is taken.*

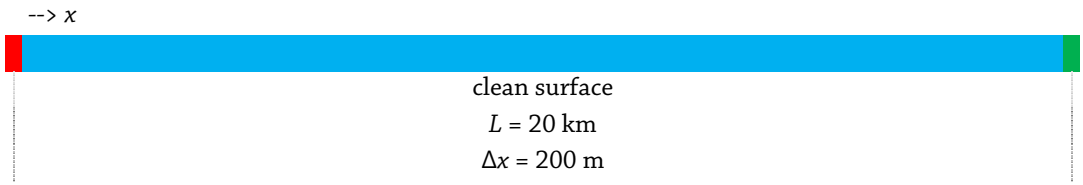

Figure 12. *Top view of the modeled spatial domain for simulation of reference wave spectra. The red line indicates the location of the wave boundary condition. The green line indicates the location where the equilibrium wave spectrum is taken.*

Figure 13. *Top view of the modeled spatial domain for the simulation of wave attenuation by an oil slick. The red line indicates the location of the wave boundary condition. The hatched part of the domain is used in the results section.*

Final reference wave spectra

Due to their overall fair, but mixed, performances, it is decided that both the *Westhuysen* and the *ST6* formulations are used in the next step: determining the wave attenuation by an oil slick.

As a last step before that, the reference equilibrium wave spectra should be determined in detail for the three wind speeds at which oil spill modeling will be performed. Simulations are executed for wind speeds of 5.0, 7.5 and 10.0 m/s. A PM spectrum is used as boundary and initial condition. The following significant wave height H_s and peak wave period T_p correspond to the three wind speeds. The waves are given the SWAN standard value for directional spreading of wind waves, 31.5°.

U_{10} (m/s)	H_s (m)	T_p (s)
5.0	0.61	3.9
7.5	1.38	5.9
10.0	2.45	7.8

For the modeling of the reference equilibrium wave spectra, a domain length of 20 km is chosen, with a smaller grid size than before. One additional grid cell is added to the end of the domain, to prevent spurious boundary effects. The spatial domain is shown in Figure 12. The total domain length appears long enough for the spectra to obtain the specific shape that belongs with the used wind/whitecap formulation, whereas the smaller grid size (200 m) improves the connection with the smaller grid size that which will be used in the subsequent modeling (25 m).

Some directional asymmetry in the spectrum is found at the coordinate of 20.0 km, despite the extra grid cell at the end of the domain. Therefore, the wave spectra at the coordinate of 19.8 km are taken. The resulting wave spectra are shown in Figure 14. Although it is recognized that the wave spectra are not in full equilibrium yet, they are close to it. This is determined on the basis of the source terms (see Figure 10). The sum of the source terms is practically equal to zero in the short gravity wave range (above approximately 1 Hz). There is some contribution to the waves of lower frequencies, which is not possible to avoid completely. At least the source terms are stable between 5 and 50 km, whereas still some difference can be found between 0.5 and 5 km. Concluding, no full equilibrium is reached in the domain of 20 kilometer, but it is sufficiently long to obtain the necessary spectral characteristics. Also, the change of spectrum over distance is small enough so it will not be disturbing the subsequent simulations.

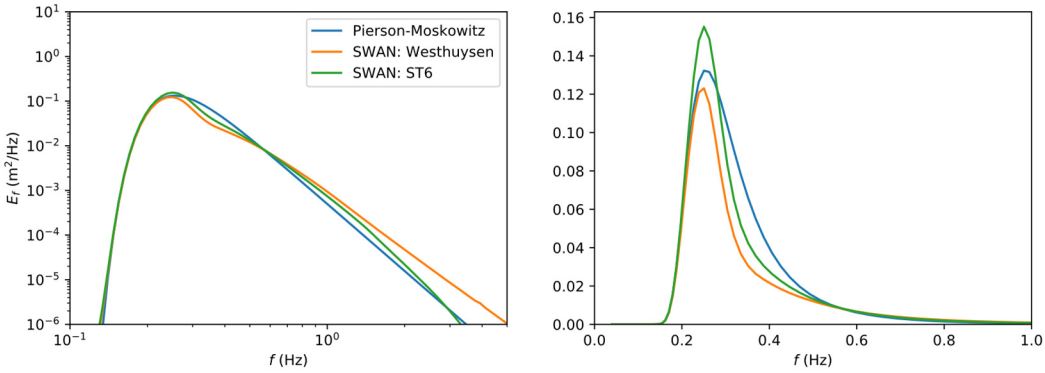

(a) U_{10} = 5.0 m/s

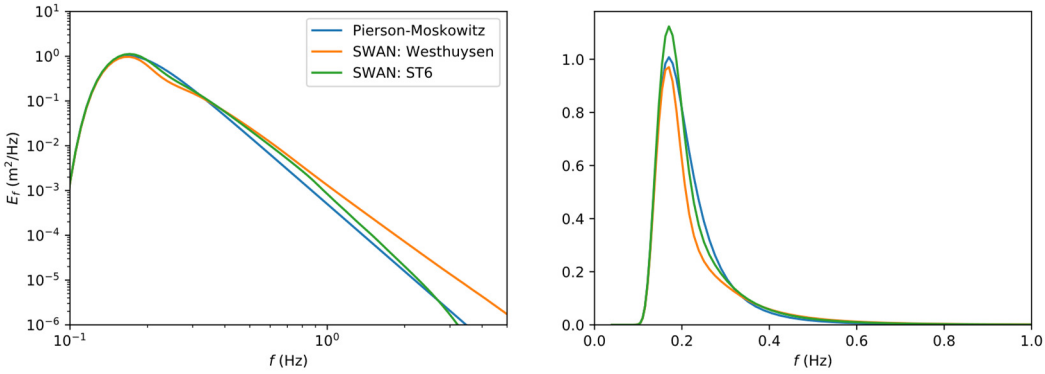

(b) U_{10} = 7.5 m/s

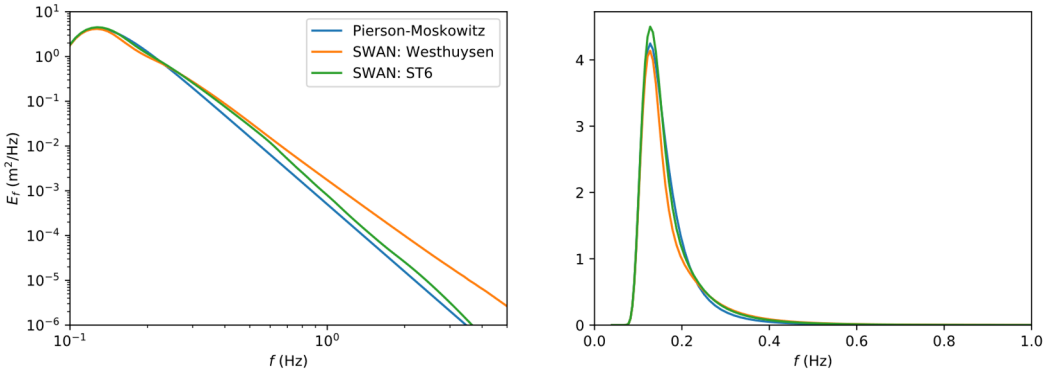

(c) U_{10} = 10.0 m/s

Figure 14. *Resulting reference wave spectra, taken at x = 20 km, on logarithmic and on linear scales.*

4.5. Simulating wave attenuation by an oil slick

In this paragraph, model simulations are executed that include an oil slick over part of the spatial domain. The *Westhuysen* and *ST6* wind/whitecap formulations are used, accompanied by the reference wave spectra obtained in the previous paragraph. The oil effect on the two key wave properties (whitecapping dissipation rate and surface Stokes drift velocity) is quantified from the results, to which a function is fitted.

Simulation setup

A spatial domain of 5 km is chosen with a grid size of 25 m. An oil layer is present in the fourth kilometer of the domain. The spatial domain is shown in Figure 13. As boundary and initial condition, the equilibrium spectra are used that were derived in § 4.4. Detailed spectral output is requested along the domain between x = 2000 m and x = 5000 m.

A full factorial setup is chosen. Three independent parameters are varied: wind speed, oil layer thickness and oil viscosity. For wind speed U_{10}, three values are chosen, that cover the range of wind speeds where oil spill modeling is used most often. For lower wind speeds, wave action is limited. For higher wind speeds, even heavy mineral oil slicks are dispersed very rapidly (Zeinstra-Helfrich, Koops, and Murk, 2017).

For oil layer thickness and oil viscosity, 25 combinations are chosen, and a no-oil case. Oil density ρ_+ is taken at a fixed value of 900 kg/m^3 for the wave modeling, because it is desirable to keep the number of independent variables limited. Moreover, the result is hardly sensitive to the exact value of the oil density (Zhang, Zhang, Wang, Meng, and Zhang, 2015).

The chosen parameter values are shown in the table below. They cover the parameter domain of interest, as defined in Appendix B.

U_{10} (m/s)	h_+ (m)	ν_+ (m^2/s)
	no-oil case	
	all combinations of:	
5.0	$10^{-4.0}$	$10^{-4.0}$
7.5	$10^{-3.5}$	$10^{-3.5}$
10.0	$10^{-3.0}$	$10^{-3.0}$
	$10^{-2.5}$	$10^{-2.5}$
	$10^{-2.0}$	$10^{-2.0}$

The 78 combinations that result are executed twice. Once for the *Westhuysen* and once for the *ST6* wind/whitecap formulation. The total count of SWM simulations thus comes at 156.

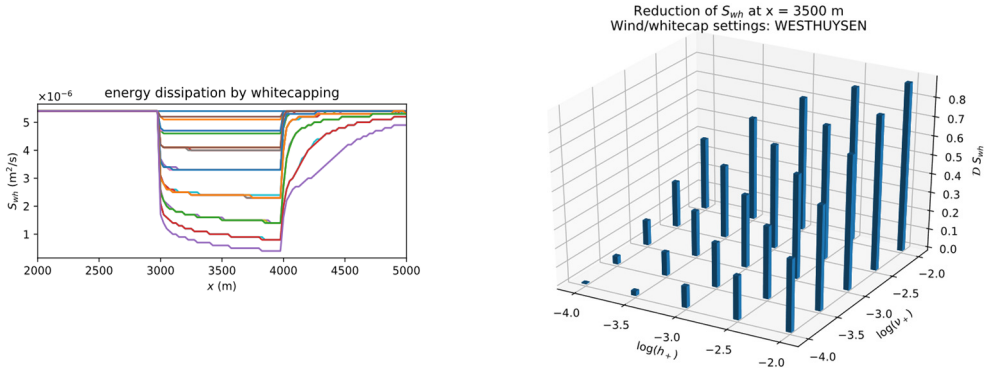

(a) U_{10} = 5.0 m/s

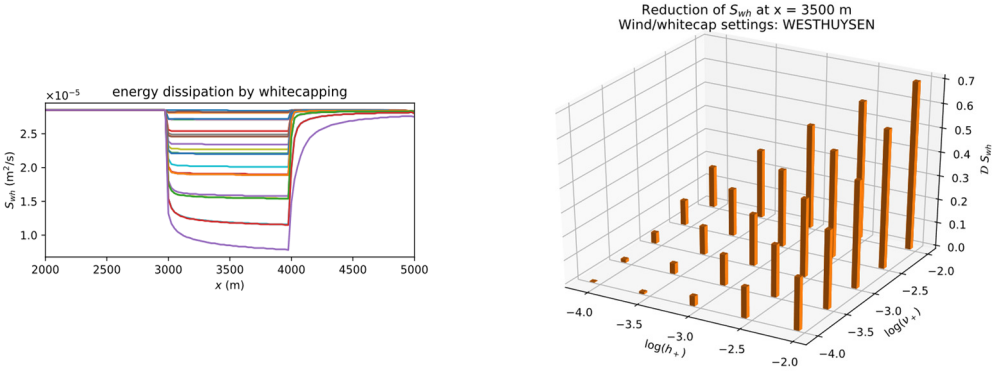

(b) U_{10} = 7.5 m/s

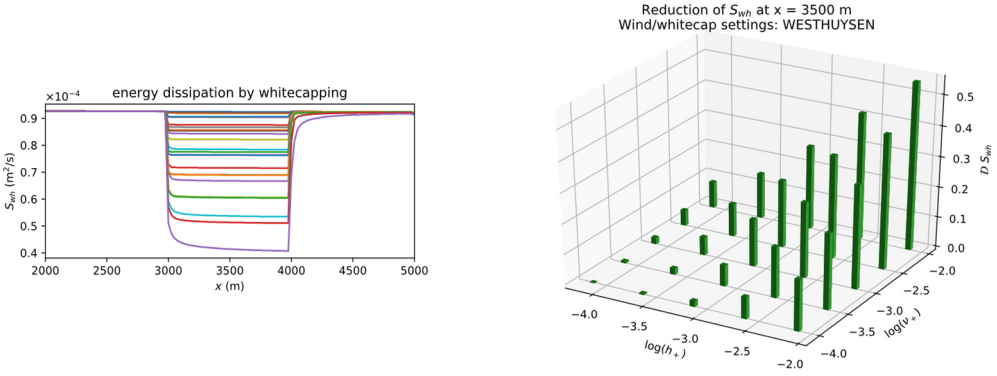

(c) U_{10} = 10.0 m/s

Figure 15. *SWM results for energy dissipation by whitecapping, for the Westhuysen wind/whitecap formulation. Note the different vertical scales.* [left] *Value of S_{wh} along the domain for various simulations.* [right] *Relative reduction of S_{wh} for the various oil properties (red bars for negative values, i.e. an increase in S_{wh}).*

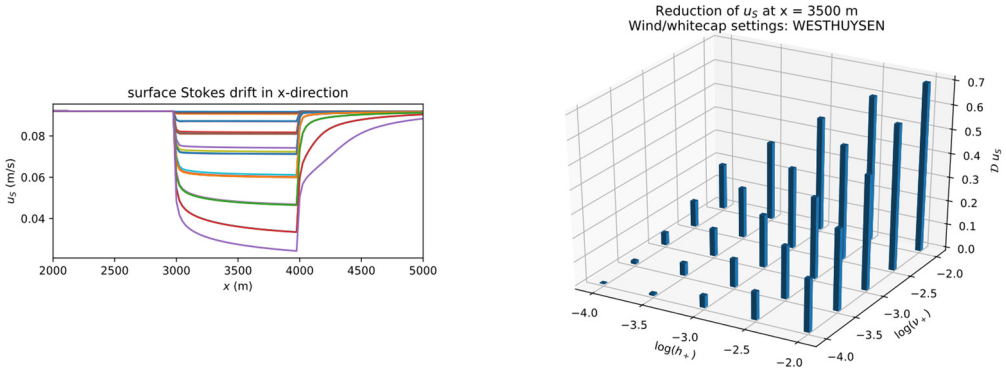

(a) U_{10} = 5.0 m/s

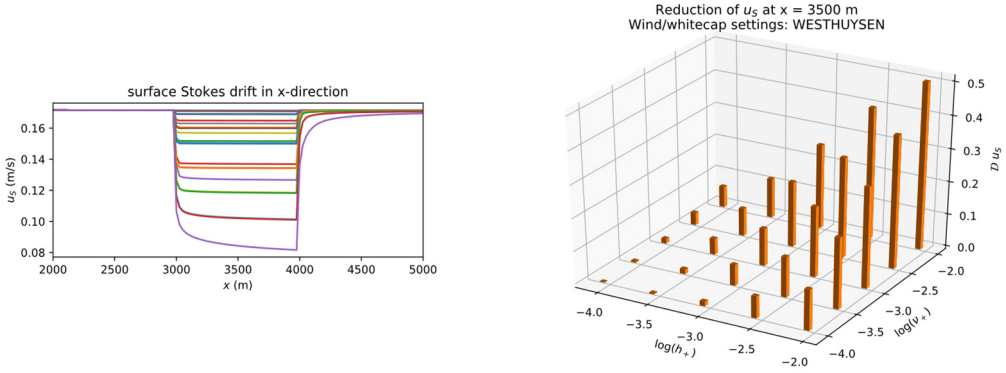

(b) U_{10} = 7.5 m/s

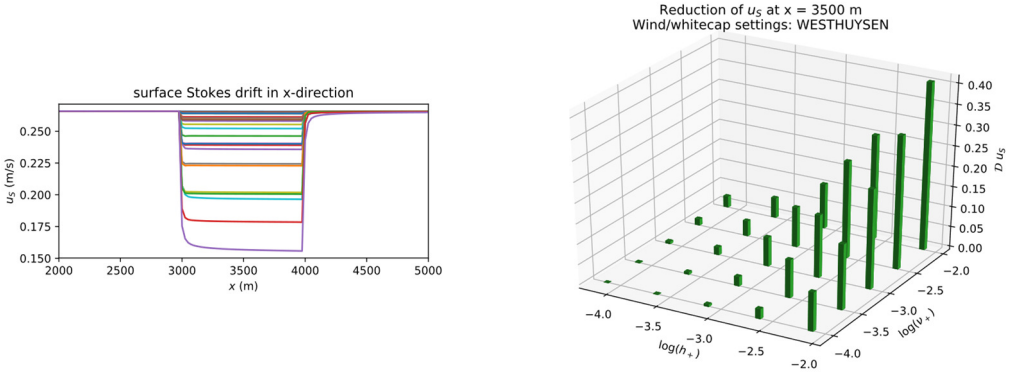

(c) U_{10} = 10.0 m/s

Figure 16. *SWM results for surface Stokes drift in x-direction, for the Westhuysen wind/whitecap formulation. Note the different vertical scales.* [left] *Value of $u_{S,0}$ along the domain for various simulations.* [right] *Relative reduction of $u_{S,0}$ for the various oil properties.*

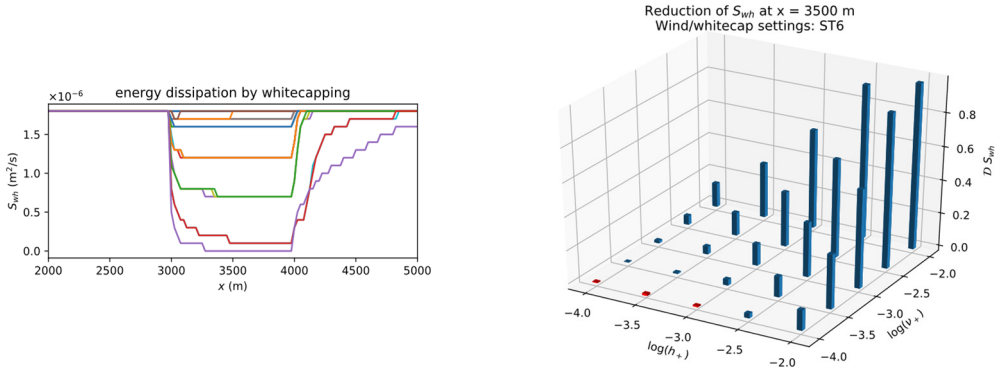

(a) U_{10} = 5.0 m/s

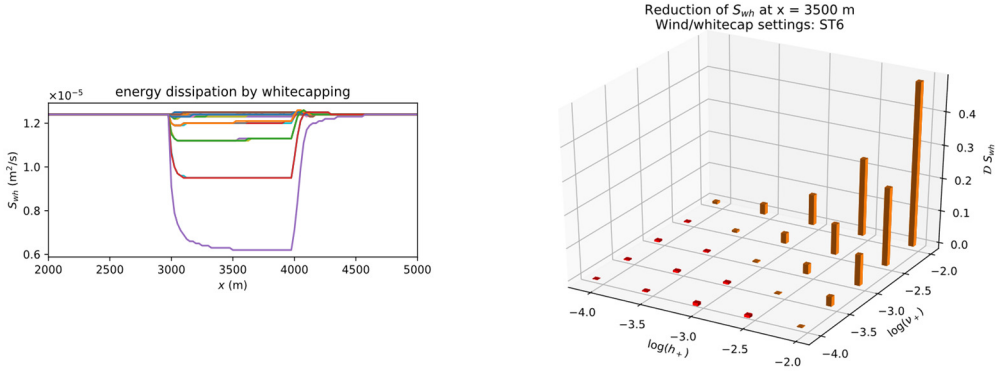

(b) U_{10} = 7.5 m/s

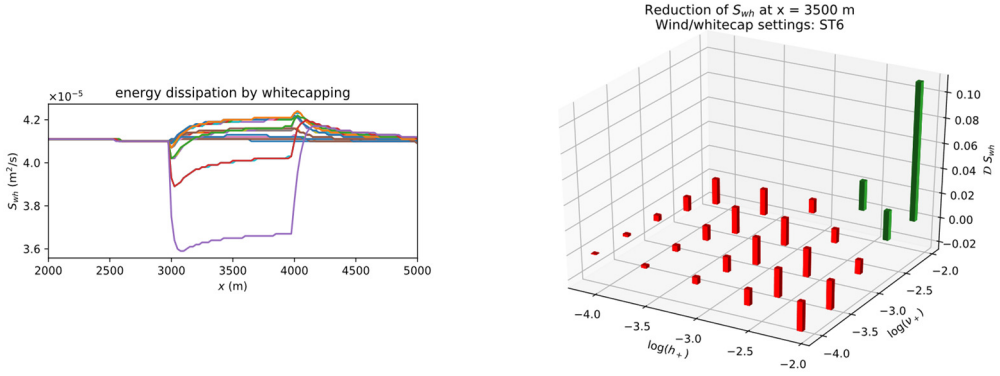

(c) U_{10} = 10.0 m/s

Figure 17. *SWM results for energy dissipation by whitecapping, for the ST6 wind/whitecap formulation. Note the different vertical scales.* [left] *Value of S_{wh} along the domain for various simulations.* [right] *Relative reduction of S_{wh} for the various oil properties (red bars for negative values, i.e. an increase in S_{wh}).*

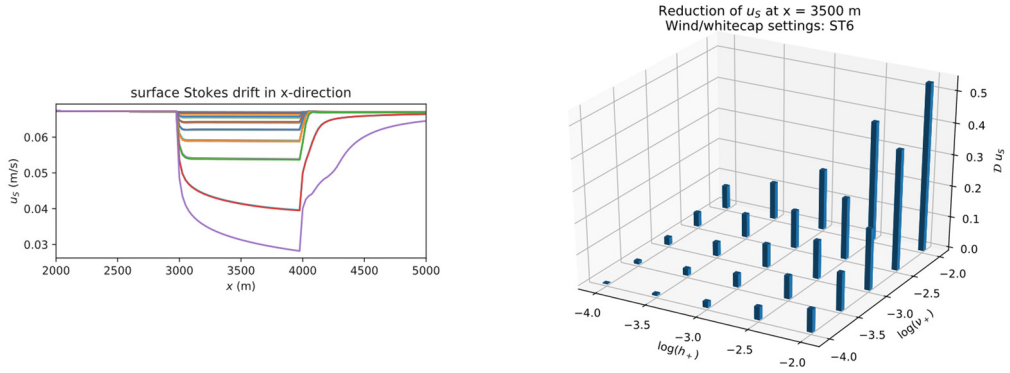

(a) U_{10} = 5.0 m/s

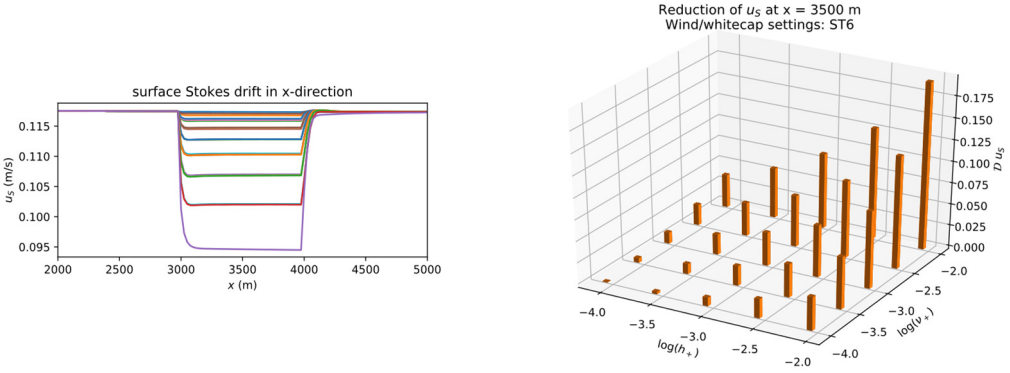

(b) U_{10} = 7.5 m/s

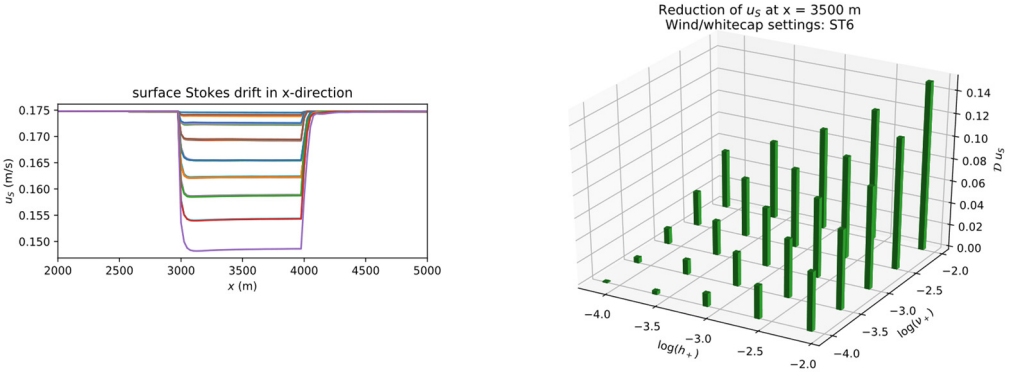

(c) U_{10} = 10.0 m/s

Figure 18. *SWM results for surface Stokes drift in x-direction, for the ST6 wind/whitecap formulation. Note the different vertical scales.* [left] *Value of $u_{S,0}$ along the domain for various simulations.* [right] *Relative reduction of $u_{S,0}$ for the various oil properties.*

Simulation results

In Figure 15 and Figure 16 (for *Westhuysen*), and Figure 17 and Figure 18 (for *ST6*), graphs of the key wave properties S_{wh} and $u_{S,0}$ along the spatial domain are shown. For the *ST6* wind/whitecap formulation, deep water wave energy dissipation consists not only of a whitecapping part (S_{wh}), but also of a swell dissipation part (S_{sw}). The latter represents wave energy loss to turbulence. Although swell dissipation is quite different from whitecapping dissipation, they are taken together in this thesis. In this way, the results for *Westhuysen* and *ST6* can be compared more easily, since the *Westhuysen* wind/whitecap formulation does not distinguish between S_{wh} and S_{sw}. Also, the relative contribution of S_{sw} is small in comparison to S_{wh}. The key wave properties H_s and k_p are found not to change significantly in any of the simulations.

The results show that the waves reach their new equilibrium within a relatively short distance after entering or exiting the oil slick, except for some cases where the oil layer is both relatively thick and relatively viscous. Assuming an 'instantaneous' new equilibrium means that the wave properties are independent of 'oil fetch', i.e. the distance the waves have travelled through the oil-covered area. This makes it possible to express the wave attenuation independent of location, which will at a later stage enable a decoupling of the wave model from the oil model. Due to the variation, albeit little, of the wave properties over the length of the oil slick, a reference location has to be chosen for performing calculations. The x-coordinate of 3500 m is chosen for this purpose.

To express the attenuation of a certain wave property, the relative reduction operator is introduced, which is defined as follows,

$$\mathcal{D} = \frac{[\cdot]_{cl} - [\cdot]_{vi}}{[\cdot]_{cl}},$$

where the index 'vi' indicates the presence of a viscous surface layer (oil layer), and the index 'cl' indicates a clean surface (no oil). The reduction factor, by definition, takes the value 0 if there is no effect, and the value 1 if the property of interest is reduced to zero. The relative reduction value $\mathcal{D}$ can be used to obtain the wave properties for a case with a viscous layer from the wave properties for a case with a clean surface, as follows,

$$[\cdot]_{vi} = (1 - \mathcal{D})[\cdot]_{cl}.$$

Reduction functions

Reduction functions are obtained by regressing a function to the data points obtained from the SWM simulations. An influence of the following form is proposed,

$$[\cdot]_{vi} = \frac{[\cdot]_{cl}}{1 + \mathcal{F}},$$

so that $\mathcal{D}$ is related to $\mathcal{F}$ as follows, and varies between 0 and 1,

$$\mathcal{D} = \frac{\mathcal{F}}{1 + \mathcal{F}}.$$

The Buckingham Π theorem states that if a meaningful relation exists between n physical variables, having a total of m physical dimensions, then that relation can be written in the form of an equation of $n–m$ dimensionless numbers. In this case, the following physical variables are taken into account: wind speed U_{10} (m/s), oil layer thickness h_+ (m), oil kinematic viscosity ν_+ (m^2/s), and gravitational acceleration g (m/s^2). Four variables and two dimensions (length and time) can be distinguished, so two dimensionless variables can be formed. The following ones are chosen,

$$\Pi_1 = \frac{g}{U_{10}^2} h_+ ,$$

$$\Pi_2 = \frac{g}{U_{10}^3} \nu_+ .$$

Hence, $\mathcal{F}$ can be expressed as

$$\mathcal{F} = \mathcal{p}\, \Pi_1^q\, \Pi_2^r = \mathcal{p} \left(\frac{g}{U_{10}^2} h_+\right)^q \left(\frac{g}{U_{10}^3} \nu_+\right)^r = \mathcal{p}\, h_+^q\, \nu_+^r\, g^{q+r}\, U_{10}^{-2q-3r} .$$

The fitting is performed using the non-linear least squares method with the Levenberg-Marquardt algorithm. The fitted parameter values are shown in the table below, including two measures for the quality of the fit: the mean of the absolute error, $\mu_{|\epsilon|}$, and the maximum absolute error, $\max|\epsilon|$. The fitted curves are visualized in Figure 19 (for *Westhuysen*) and Figure 20 (for *ST6*).

Variable	ST6	WESTHUYSEN
S_{wh} (incl. S_{sw})	$\mathcal{p} = 8.8 \cdot 10^7$ $q = 1.16$ $r = 1.24$	$\mathcal{p} = 5.5 \cdot 10^3$ $q = 0.54$ $r = 0.50$
	$\mu_{\|\epsilon\|} = 2.7 \cdot 10^{-2}$ $\max\|\epsilon\| = 1.5 \cdot 10^{-1}$	$\mu_{\|\epsilon\|} = 2.3 \cdot 10^{-2}$ $\max\|\epsilon\| = 8.0 \cdot 10^{-2}$
$u_{S,0}$	$\mathcal{p} = 5.3 \cdot 10^2$ $q = 0.51$ $r = 0.49$	$\mathcal{p} = 1.2 \cdot 10^3$ $q = 0.53$ $r = 0.43$
	$\mu_{\|\epsilon\|} = 1.7 \cdot 10^{-2}$ $\max\|\epsilon\| = 5.9 \cdot 10^{-2}$	$\mu_{\|\epsilon\|} = 2.5 \cdot 10^{-2}$ $\max\|\epsilon\| = 8.6 \cdot 10^{-2}$

The general fit of the function to the data is quite good, with a mean error that is relatively small with respect to the function values. A minor dependence of the error on the independent parameters was found, which implies that possibly some dependence exists that is not covered by the fitted functional form.

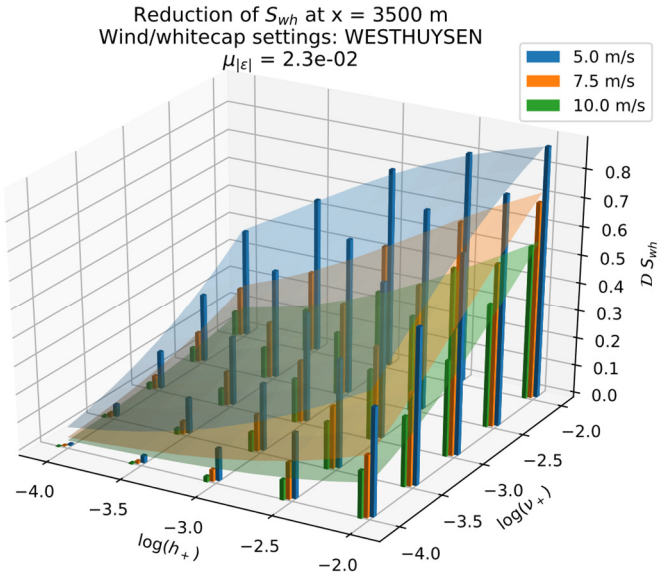

(a) $\mathcal{D}S_{\mathrm{wh}}$

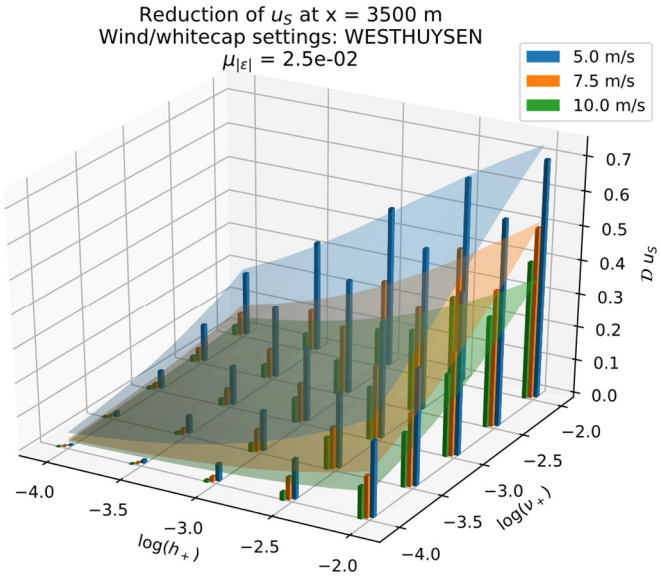

(b) $\mathcal{D}u_{\mathrm{S},0}$

Figure 19. *Relative reduction of key wave properties (colored bars) and the fitted reduction function (colored planes), for the Westhuysen wind/whitecap formulation.*

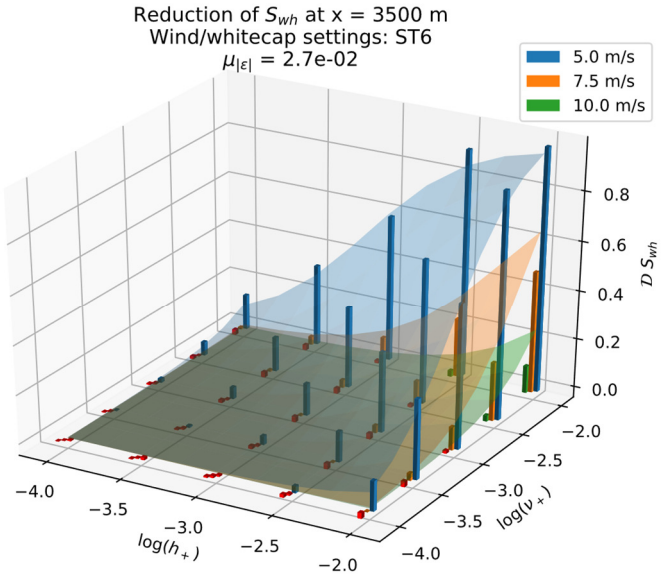

(a) $\mathcal{D}S_{\mathrm{wh}}$

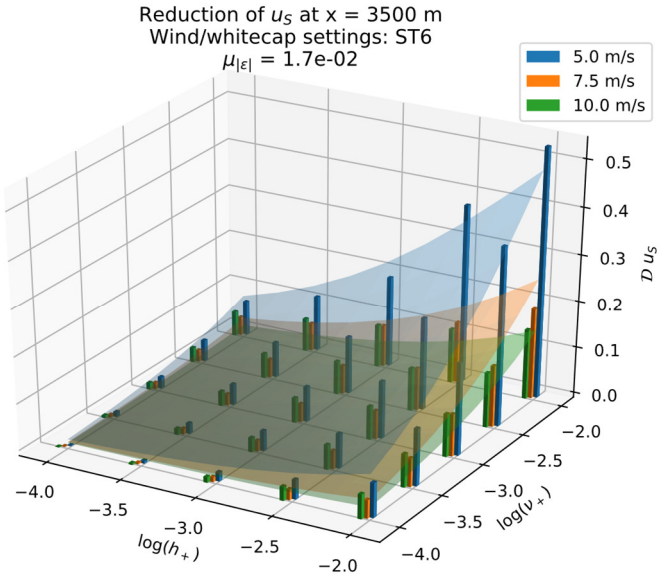

(b) $\mathcal{D}u_{\mathrm{S},0}$

Figure 20. *Relative reduction of key wave properties (colored bars) and the fitted reduction function (colored planes), for the ST6 wind/whitecap formulation.*

4.6. Conclusions

The SWAN model was used to simulate a steady-state situation for an unprecedented large prognostic frequency range. Therefore, specific model settings were required. Under-relaxation was activated to achieve numerical stability, a hotstart was employed, and the quadruplets were solved using an exact algorithm (XNL) instead of an approximate algorithm (DIA).

A comparison between the different wind/whitecap formulations in SWAN showed that, for the purposes of this thesis, the *Westhuysen* and *ST6* formulations produce better equilibrium wave spectra than the *Komen* and *Janssen* formulations. Criteria for total energy content, spectral shape and cutoff sensitivity were used. The difference is attributed to the dependence of whitecapping dissipation on wave steepness and saturation of the spectral tail. In the *Komen* and *Janssen* formulations, whitecapping can drain all energy from the tail or leave all energy in. In the Westhuysen and ST6 formulations, whitecapping in the tail is dependent on the spectral saturation of the tail.

The simulation results show oil-induced viscous energy dissipation qualitatively in accordance with theory. The results furthermore show that the waves obtain a new equilibrium within the oil slick relatively quickly. In the new 'oil slick' equilibrium, a dip exists in the wave spectrum at the frequency range where the viscous damping is active. The whitecapping dissipation decreases for nearly all cases. Though, a slight increase in whitecapping dissipation is seen at 10 m/s wind speed for the *ST6* formulation. Overall, the response of the other source/sink terms is in accordance with expectation.

Similar reduction effects appear for the different wind/whitecap formulations. But, the *Westhuysen* formulation leads to larger reductions than the *ST6* formulation. The difference is not attributed to the fact that the wind/whitecap formulations are based on different assumptions for what the equilibrium wave spectral tail should look like, which is f^{-4} for the former and approximately f^{-5} for the latter. This difference causes dissimilarity in the total amount of wave energy that is present in the spectral tail, which is key to the differences that are found for whitecapping energy dissipation and surface Stokes drift velocity between the two wind/whitecap formulations.

Functions are fitted to the SWM results, which relate wind speed, oil layer thickness and oil viscosity to the reduction of whitecapping energy dissipation and surface Stokes drift. The average error of the fitted functions is 2 to 3 percent point in terms of the relative reduction. Whitecapping reduction is, roughly speaking, somewhat more than linearly dependent on oil layer thickness (power of 1.16) and oil viscosity (power of 1.24) if the *ST6* formulation is used, and square-root dependent if the *Westhuysen* formulation is used (power of 0.54 and 0.50, respectively). Surface Stokes drift reduction is approximately square-root dependent on oil layer thickness and oil viscosity if either the *ST6* (0.51 and 0.49) or the *Westhuysen* (0.53 and 0.43) formulation is used. In general, the attenuation appears to be slightly less dependent on oil viscosity than on oil layer thickness. This effect is most pronounced when the *Westhuysen* formulation is used.

5. Modeling of oil spill evolution

In this chapter, the generic particle tracking model OpenDrift[11] is used to execute a comparative study to obtain insight in the effects of oil-induced wave attenuation on the wave-driven evolution of an oil spill.

First, the model is adapted by including the previously found reduction functions, so that in an oil spill simulation each Lagrangian element is assigned the dispersion and advection rate considering the attenuated wave forcing that it experiences, based on oil layer thickness, oil viscosity and wind speed (§ 5.1). Then, general modeling choices are made (§ 5.2). Afterwards, model simulations are executed. From the model output, the differences in evolution between various cases are determined in terms of center of mass, standard deviation and skewness of the oil mass distribution along the propagation direction, and in terms of the oil mass distribution between surface and subsurface oil (§ 5.3).

5

[11] For a description of the model, see (Dagestad et al., 2018; Röhrs et al., 2018).

5.1. OpenDrift model adaptation

In Chapter 4 it was shown that the whitecapping energy dissipation and the surface Stokes drift are affected by an oil layer. To include these findings in the calculation of wind-driven oil spill evolution, the PTM OpenDrift is adapted. The source code of OpenDrift version 1.0.7 was downloaded from the OpenDrift homepage[12]. Changes are made to the model for two different reasons: some calculation methods can be improved and the reduction functions are implemented. These changes together are discussed per parameter of interest: (i) oil layer thickness h_+, (ii) sea surface agitation rate F, and (iii) Stokes drift velocity u_S.

For the reduction functions, it is decided to implement only the results belonging to the *ST6* simulations, and not those belonging to the *Westhuysen* simulations. This is done because, with each wind/whitecap simulation belongs not only a reduction function, but also a reference scenario. This poses a challenge for the *Westhuysen* case, since due to its f^{-4} spectral tail the calculation of the Stokes drift profile has to be done quite differently from the *ST6* case. The aim of this chapter is to investigate the effect of the oil-induced wave attenuation qualitatively. It is expected that, in that sense, there will be no major differences between the *ST6* and the *Westhuysen* cases.

Oil layer thickness

Calculation of the oil layer thickness is an important part of the OSM simulations in this thesis, because the feedback effect of oil layer thickness on oil slick transport is investigated (see § 2.3). Therefore, extra attention is paid to the calculation method for oil layer thickness.

The native method of OpenDrift for calculation of the oil layer thickness is by overlaying the area spanned by the surface LEs with a grid of 20 by 20 cells. This gridding method is not too demanding in terms of required computational power, but a disadvantage of the method is it produces aliasing effects in some cases, if the LEs are arranged in a certain (regular) manner. Also, the grid is redrawn at every timestep, which causes the grid to 'jump' and the resolution to change significantly at time steps when a lagging LE is entrained or resurfaces (far) behind the main slick. These disadvantages of using a grid method can be evaded by using a meshfree method.

A Voronoi method could be used as a replacing meshfree method. However, this method has the disadvantage that a single LE disappearing from or reappearing to the surface (due to dispersion and buoyancy) can lead to a large impact on the Voronoi areas of the surrounding LEs. Taking into consideration that a single LE, when submerged, actually represents a spray of oil droplets which will resurface somewhat spread out, this behavior is deemed unrealistic.

Therefore, a kernel method is implemented. A rectangular kernel window is chosen for this research, which simply means that the contribution of all elements within a certain distance from the point of interest weigh equally. In this sense, the proposed method can be interpreted as applying the grid method (with a fixed cell size, where each LE in that cell counts equally) at every LE location individually. As a disadvantage, the method requires more memory than the native grid method, if the number of LEs is large. In general, if the number of LEs is n, the implemented kernel method is of order n^2 in terms of memory.

[12] github.com/OpenDrift/opendrift, last accessed 20 June 2019.

Sea surface agitation rate

In OpenDrift, the sea surface agitation rate is calculated using an empirical equation from Delvigne and Sweeney (1988), based on the results of Holthuijsen and Herbers (1986), which is dependent on the wind speed and the peak wave period. It equals

$$F = 0.032 \frac{U_{10} - 5}{T_{\mathrm{p}}},$$

Where U_{10} is the wind speed, and T_{p} is the peak wave period. For fully developed sea states, using T_{p} as defined in Appendix D, the equation yields

$$F = 0.040 \frac{U_{10} - 5}{U_{10}}.$$

This empirical equation is not deemed fully adequate for this research, because it does not produce any whitecapping for wind speeds below 5 m/s. Yet, some whitecapping energy dissipation was calculated for such wind speeds in the preceding wave modeling. Therefore, it is desirable that some whitecapping is also reproduced by OpenDrift for low wind speeds.

A newer equation by Salisbury, Anguelova, and Brooks (2013, 2014), based on global remote sensing data, is therefore added to the model for low wind speeds. The authors found that their expression is hardly dependent on the development of the waves. Assuming that the duration of a wave breaking event is 1 second (Zeinstra-Helfrich et al., 2017), the following expression is found,

$$F = 4.6 \cdot 10^{-5} \, U_{10}^{2.26} \, .$$

The maximum value of the two empirical equations is used, so that the full equation becomes

$$F = \max\left(0.032 \frac{U_{10} - 5}{T_{\mathrm{p}}} \; ; \; 4.6 \cdot 10^{-5} \, U_{10}^{2.26} \right).$$

The equations are compared in Figure 21, under the assumption of a fully developed sea.

As concluded in Chapter 2, the wave height H (which reflects the potential energy release in a wave breaking event) and the sea surface agitation rate F (which reflects the wave breaking rate) are the key wave parameters that affect the oil dispersion processes. As concluded in Chapter 4, the presence of a surface oil layer affects the whitecapping dissipation rate S_{wh}, whereas the significant wave height H_{s} is hardly affected. Thus, a breaking wave within the oil slick is potentially as energetic as a breaking wave outside the oil slick. Thus, in order for the whitecapping dissipation rate to reduce, the rate of whitecapping events must reduce. This is in consonance with a common explanation for wave whitecapping: short wave breaking events are influenced by longer waves, either by breaking of the longer waves or by modulation by the longer waves (Rogers et al., 2012). If there are less short waves (they are attenuated by the oil), less overtaking of short waves by long waves occurs, and thus less wave breaking events will take place. It can be concluded that it is logical to adapt the wave breaking frequency via the sea surface agitation rate F rather than the wave breaking energy via the wave height H.

Consequently, it is necessary to adapt the calculation of the sea surface agitation rate in OpenDrift so it incorporates the reflects the reduction of wave breaking. For this, the reduction of S_{wh} is used. Hence,

$$F_{\mathrm{vi}} = (1 - \mathcal{D}S_{\mathrm{wh}})\, F_{\mathrm{cl}}\,,$$

where F is the sea surface agitation rate, $\mathcal{D}S_{\mathrm{wh}}$ is the relative reduction of the whitecapping energy dissipation, the subscript 'cl' indicates clean surface, and the subscript 'vi' indicates viscous layer. The result is shown in Figure 22.

Note that, for the oil entrainment rate, there will be only a slight difference between reducing the breaking wave energy or the wave breaking frequency. The entrainment rate equation (Li, Spaulding, French-McCay, et al., 2017) depends on wave breaking frequency and wave energy in the following manner:

$$\lambda \propto F^1 We^{1.8} \propto F^1 H^{1.8} \propto F^1 E^{0.9}\,.$$

Hence, applying the reduction factor to F or to $\mathcal{E}$ has nearly the same effect. However, this applies to the entrainment rate only, not to the oil droplet size distribution and the oil vertical distribution.

Stokes drift velocity

OpenDrift normally calculates the Stokes drift profile under the assumption of a Phillips spectrum and using exponential decay with depth. This method is adapted, such that the decay with depth is instead calculated in accordance with Breivik et al. (2016), using the surface Stokes drift velocity $u_{\mathrm{S},0}$, the significant wave height H_{m0} and the mean wave period T_{m02} (see § 2.2). It is shown in Figure 23.

The simulations as performed in Chapter 4 did not exactly yield Phillips wave spectra, but attention was paid to obtaining a fair resemblance. A reduction factor is applied to the Stokes drift profile to account for the presence of an oil slick. High frequency waves mainly affect the Stokes drift near the surface. Hardly any contribution of the high-frequency waves is noticed at depth. As oil will be mainly present at the sea surface, and the submerged oil will only reside for short times in the zone near the surface during buoyant rise, it is sufficient to implement the Stokes drift reduction factor for the surface LEs only. However, it would be unrealistic if submerged LEs could overtake surface LEs. Hence,

$$u_{\mathrm{S,vi}} = \begin{cases} u_{\mathrm{S,0,cl}}\left(1 - \mathcal{D}u_{\mathrm{S,0}}\right), & \text{if } z = 0 \\ \min\left\{u_{\mathrm{S,cl}}\,;\; u_{\mathrm{S,0,cl}}\left(1 - \mathcal{D}u_{\mathrm{S,0}}\right)\right\}, & \text{if } z < 0 \end{cases}$$

where u_{S} is the Stokes drift, $u_{\mathrm{S,0}}$ is the surface Stokes drift, $\mathcal{D}u_{\mathrm{S,0}}$ is the relative reduction of the surface Stokes drift, the subscript 'cl' indicates clean surface, and the subscript 'vi' indicates viscous layer. The result is shown in Figure 24.

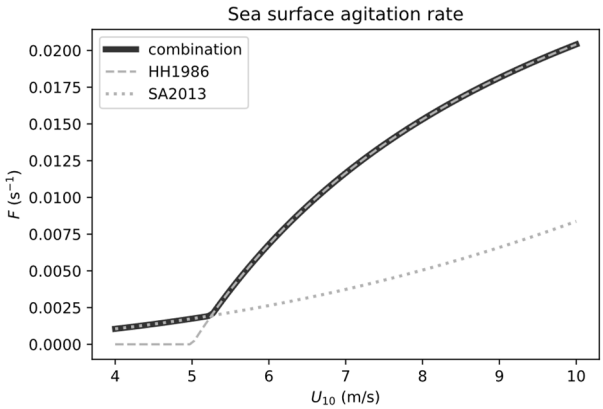

Figure 21. *Sea surface agitation rate, based on two different empirical equations. The dashed graph (HH1986) shows the formulation based on data by Holthuijsen and Herbers (1986), and it is natively implemented in OpenDrift. The dotted graph (SA2013) shows the formulation by Salisbury et al. (2013), and it is added to OpenDrift in this research to offer a solution for the cases of weak wind. The maximum of both is used.*

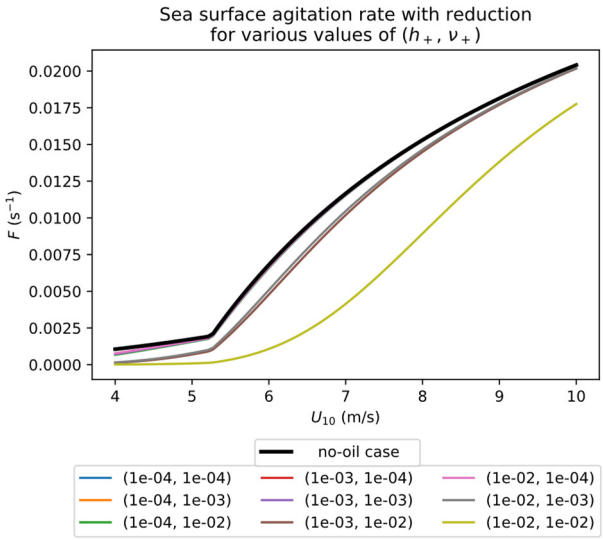

Figure 22. *Sea surface agitation rate as in Figure 21, with correction for oil layer presence for various combinations of layer thickness h_+ (m) and kinematic viscosity ν_+ (m^2/s).*

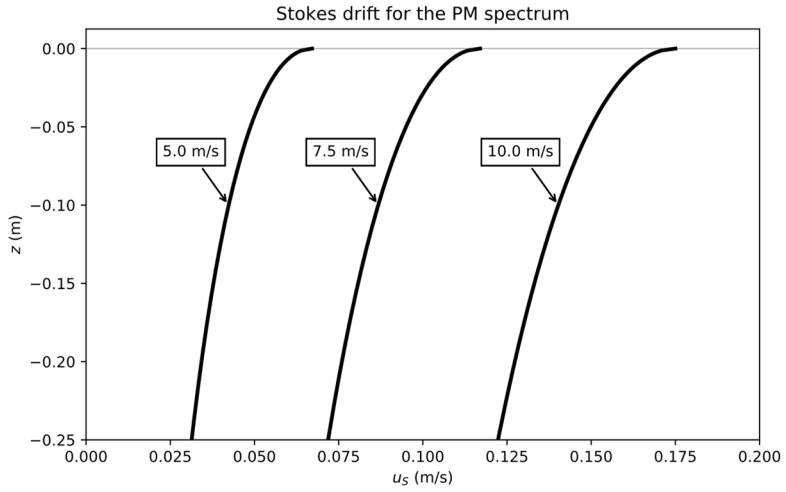

Figure 23. *Stokes drift profiles belonging to the PM spectrum, based on the formulation by Breivik et al. (2016). For surface Stokes drift, the third spectral moment m_3 of the PM spectrum is used. A directional spreading of 31.5° is assumed. Profiles are shown for three different wind speeds U_{10}.*

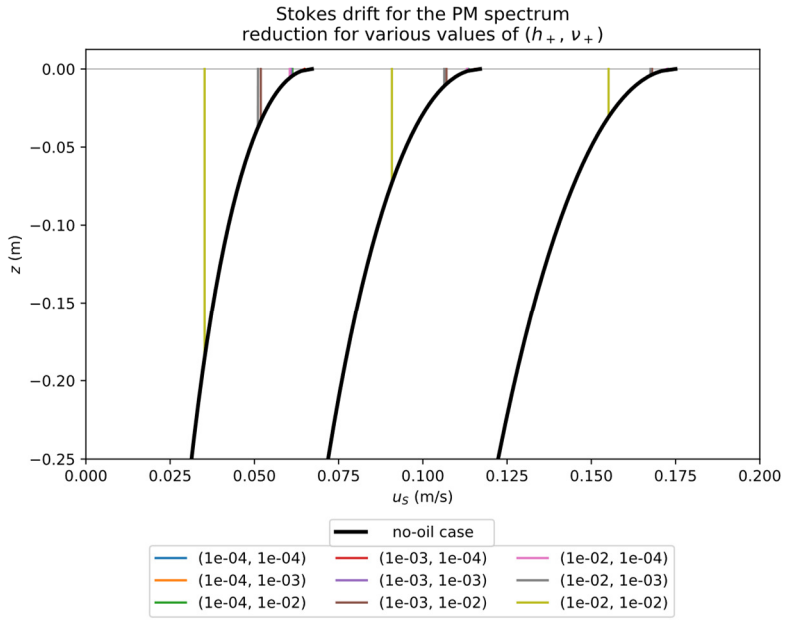

Figure 24. *Stokes drift profiles as in Figure 23, with correction for oil layer presence for various combinations of layer thickness h_+ (m) and kinematic viscosity ν_+ (m^2/s).*

5.2. General model settings

The modeled cases are based on the simulations by Zeinstra-Helfrich et al. (2017). As few additional assumptions as possible are made on the remaining environmental properties and oil properties. OpenDrift standard values are used where needed. This for instance true for the oil-water interfacial tension γ_{ow}, which is set at 0.03 N/m.

Domain and discretization

Because OpenDrift is a particle tracking model, there is no defined spatial domain nor a grid size. An oil slick of length 250 meter is initiated. Formally, the simulation is 3D, but the oil slick is initiated only one LE wide, and the LEs are given 'per meter width' properties. Furthermore, no transport processes (such as currents or diffusion) perpendicular to the oil slick are activated, so the simulation can be interpreted to be 2DV.

Simulations are given a length of 24 hours. The time step is set at 2 minutes, and a 1 minute sub-timestep is employed in the vertical mixing scheme (Visser, 1997).

5.3. Simulating oil spill evolution

Using the adapted model that includes the reduction functions, model simulations are performed that account for the viscous wave attenuation where oil is present. In this way, the oil effect on the oil spill evolution is determined.

Simulation setup

The spatial domain is shown in Figure 25. Approximately the same factorial setup as for the wave attenuation simulations will be used (see § 4.5), yielding 27 combinations of initial oil slick properties, shown in the table below. Whereas for the wave modeling, oil mass density was fixed at 900 kg/m^3, three different values are used for the oil spill modeling, because also realistic buoyancy behavior must be modeled.

U_{10} (m/s)	h_+ (m)	ν_+ (m^2/s) / ρ_+ (kg/m^3)
all combinations of:		
5.0	10^{-4}	10^{-4} / 886
7.5	10^{-3}	10^{-3} / 936
10.0	10^{-2}	10^{-2} / 986

For the purpose of comparison, each simulation is executed twice: once where the wave forcing is independent on the oil layer presence ('reference simulation'), and once where the wave forcing is dependent on the oil layer presence ('reduction simulation'). Moreover, two sets of active processes are used. Once only oil entrainment and Stokes drift are activate ('idealized case'), and once simple wind drift and vertical turbulence is activated ('realistic case'). The total count of OSM simulations thus comes at 102.

Simulation results

In Appendix E, the results of all simulation cases are collected. Notable findings are discussed here. Four aspects of the oil spill evolution are investigated: the location of the center of mass, the standard deviation and the skewness of the oil mass spreading, and the oil mass distribution between surface and subsurface.

First, the idealized cases are discussed. The forward speed of the oil mass center is lowered in some reduction simulations. The effect is absent for a thin layer of light oil in an energetic wave climate, whereas the effect is significant (up to 39%) for a thick layer of heavy oil in a calm wave climate.

Diffusion, expressed in terms of the standard deviation the distribution of oil mass, is not lower in the reduction simulations compared to the reference simulations. Actually, the opposite is true. Reduction of the diffusion was expected, because the reduction of Stokes drift and of whitecap agitation together would lead to less shear diffusion. Instead, the diffusion is accelerated.

There is an important difference between the diffusion shape for oil spill development in the reduction simulations when compared to the reference simulations. This can be recognized if the skewness (see Figure 26) of the mass distribution along the propagation direction is considered. The characteristic shape of an oil slick is elongated in the direction of waves and wind, and with a thicker slick at the downwind side than at the upwind side shape, i.e. negative skewness. This was observed in the field (Elliott et al., 1986) and modeled in some of the reference simulations. For the low wind reduction simulations, actually a reversal of the characteristic shear diffusion mass distribution is found. For the medium and high wind cases, the reversal is not always found, but the skewness is increased. This effect can be explained by trailing edge convergence and leading edge convergence (see Figure 27). Oil that lags behind the main oil slick because it was entrained to depth in an earlier stage, catches up with the main oil slick once it resurfaces. Some loose oil is hardly subjected to the Stokes drift reduction, whereas the slick is affected by it. This causes convergence at the slick trailing edge. At the leading edge, a positive feedback mechanism arises: the layer thickness decreases because oil is entrained, which causes increased forward flow and increased entrainment, which leads to dilution of the oil. This causes divergence at the slick leading edge.

The intensity of the convergence and divergence in these simulations is likely an overestimation of the actual effect, because the wave attenuation is assumed to happen instantaneously in the model. The forward advection abruptly decreases when waves enter the oil slick and abruptly increases when waves exit the oil slick. In reality, this change is expected to take some distance. The approach was justified because the wave adjustment happened within short distance in the wave modeling, except for the cases with the thickest and heaviest oil. However, it appears that precisely for these cases, with thick and heavy oil, excessive convergence is found. The shortcoming could be resolved by incorporating a decay length.

Regarding the distribution of oil between the surface slick or subsurface droplets, no significant change is found.

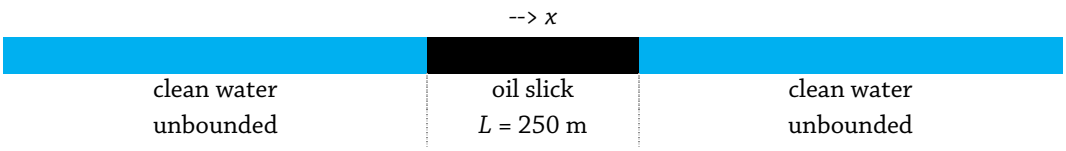

Figure 25. *Top view of the spatial model domain.*

(a) *negative skewness* (b) *positive skewness*

Figure 26. *Illustration of skewness.*[13]

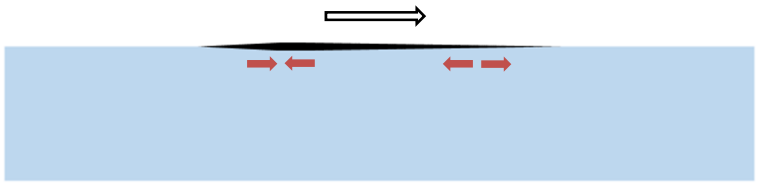

Figure 27. *Trailing edge convergence and leading edge divergence. Side view of the upper part of the water column, not to scale.*

[13] Image by Rodolfo Herman, retrieved from https://commons.wikimedia.org/wiki/File:Negative_and_positive_skew_diagrams_(English).svg

Second, the realistic cases are discussed. In general, the same processes are identified, but to a lesser extent. For instance, where the forward speed of the oil mass center was lowered up to 39% in the idealized cases, it is lowered only up to 12% in the realistic cases. In some (seemingly unrelated) cases, less horizontal mass diffusion is found in the reduction simulation compared to the corresponding reference simulation. This is attributed to a better, more pronounced representation of the shear diffusion process in the reference simulation of the realistic case, rather than an important effect in the reduction simulation. The difference mainly shows that, in the realistic cases, the differences between the reference simulation and the reduction simulation is more subtle.

5.4. Conclusions

The OpenDrift model was extended with an equation for sea surface agitation rate for low wind speeds, a Stokes drift equation specifically derived for the PM spectrum, and a more suitable method for determining the oil layer thickness. Finally, the reduction functions belonging to the *ST6* wind/whitecap formulation were added.

The difference between two oil spill evolution cases was investigated: one where the wave forcing was independent on the oil layer presence ('reference simulation'), and one where the wave forcing was dependent on the oil layer presence ('reduction simulation').

The reduction of Stokes drift appears to have a larger effect on the oil spill evolution than the reduction of sea surface agitation. This conclusion is based on the observation that the forward speed of the oil in some cases is lower for the reduction simulations than for the reference simulations, but no difference is found in the surface-subsurface oil distribution between the reduction simulations than for the reference simulations.

Besides the forward displacement and the surface-subsurface distribution of the oil, the diffusion of the oil is of interest. It is found that the oil slick diffusion in the reduction simulation is generally larger than in the reference simulation. Shear diffusion is not the cause of this, but trailing edge convergence and leading edge divergence are. This can be recognized if the skewness of the mass distribution is considered. Whereas shear diffusion leads to negative skewness, the convergence and divergence patterns lead to positive skewness.

If simple wind drift and ambient vertical turbulence are activated, then the same general observations are made (smaller mean forward transport, less negative oil slick skewness), but the effects are less pronounced.

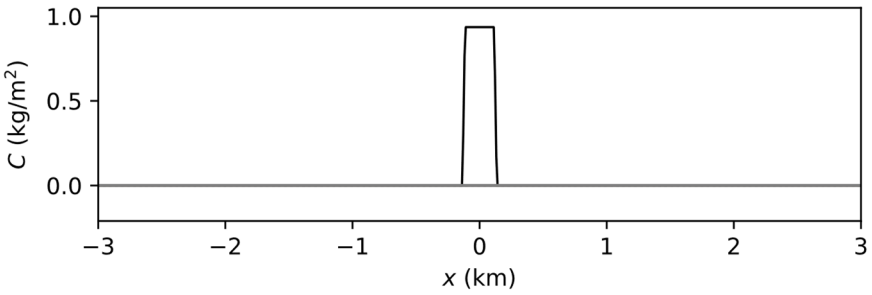

(a) *initial condition, all cases*

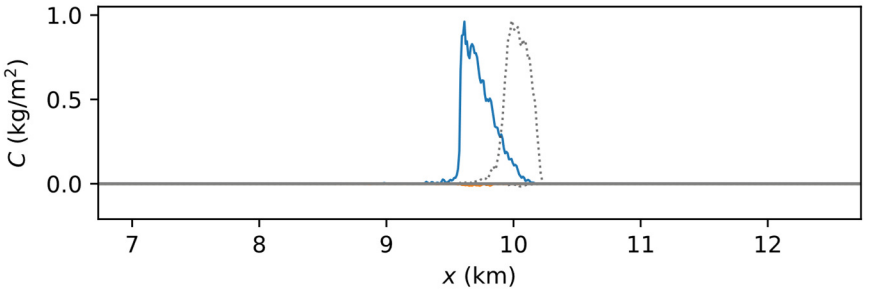

(b) *evolution after 24 hours, idealized case*

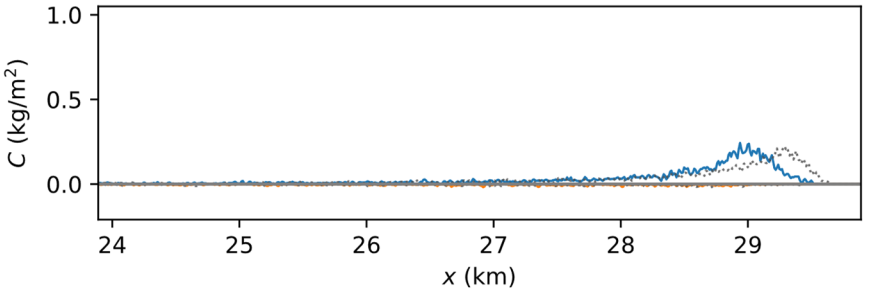

(c) *evolution after 24 hours, realistic case*

Figure 28. *Typical oil spill evolution, centered to the oil mass center. A black, drawn line indicates the initial condition. A blue, drawn line indicates the result of the reduction simulation. A grey, dashed line indicates the result of the reference simulation. The oil spill evolution is shown for* $U_{10} = 7.5$ *m/s,* $h_+ = 10^{-3}$ *m,* $\nu_+ = 10^{-3}$ m^2/s, $t = 24$ *h.*

6. Discussion

In this chapter, the individual results of this research are discussed. A critical view is given on the relevance of the results, the correspondence of the results to existing research, and the limitations of the applicability of the results.

6.1. Relevance

To mitigate the possible negative effects of a mineral oil spill, being able to accurately forecast its evolution is essential. In this respect, any contribution that is made to the understanding of oil spill transport (and weathering) processes can be considered relevant.

One must consider that an oil spill in the marine environment is part of a complex and chaotic system. On the one hand, this aspect implies that relatively small changes of one transport mechanism can cause relatively large changes to the overall fate of the oil slick. So, even though the researched feedback between oil and waves is small in magnitude, it still may cause quite a different development of the oil slick. This probably holds even stronger for the 3D case than for the 2DV case. On the other hand, one must be aware that the researched attenuation effect of the oil on the waves is only one process out of many interacting processes. Each of these processes can have cascading consequences, which is exemplary for chaotic systems. A better understanding of the phenomenon under investigation in this research can improve the accuracy of oil slick models in forecasting oil slick transport. But, to decrease uncertainty in oil spill model in general, a better understanding of the other transport processes and interactions is required as well. In the end, for each oil spill modeling purpose, the potential benefits of added insight must be weighed against the drawbacks of the added complexity. In oil spill response, pragmatism and quick response can be more important than accuracy, whereas for preventive purposes, oil spill modeling is likely allowed to take more time, so more processes can be included and more cases can be studied.

This thesis has explored a way to model the transformation of waves within an oil slick using a SWM, has introduced reduction functions as a way to use information from a wave model in an oil spill simulation, and has qualitatively investigated the significance of oil-induced wave attenuation for the evolution of an oil spill. Further development of the findings from this thesis may contribute especially to the separation of wave-driven and wind-driven processes in oil spill modeling. A challenging task, but with many possible benefits, especially when it comes to improving the calibration of models.

6.2. Conformity

As the results of this thesis are the product of many model simulations, the results should be used with care. Proper interpretation and validation of the results is necessary. In this paragraph, the results are compared to existing research and some thoughts about possible validation are shared.

Wave modeling

While the wave attenuating effect of surface layers has been studied theoretically and experimentally, most of the attention has gone to organic oil films of molecular-scale thickness. Less attention has been paid to mineral oils. Regarding the wave simulations of mineral oil slicks in this thesis, results are obtained that qualitatively match expectations and previous research. Validation of the results is still needed.

For instance, it must be determined whether the kinematic behavior of a surface mineral oil slick actually corresponds to the theory for the case of a continuous viscous floating fluid layer, and if the expected theoretical values for wave decay are found. This can best be done in a controlled environment, e.g. a wave tank, where the waves are generated externally. Similar experiments have been performed already, only with different surface layer fluids. Particle image velocimetry can aid in the investigation of the exact wave kinematics. Wave gauges with sufficient high sampling frequency and accuracy, placed along the wave propagation direction, can be used to determine the viscous energy dissipation.

Knowing about the viscous dissipation is not enough. As discussed in § 3.3, the explicit and implicit effects of a (mineral) oil slick on the remaining terms of the wave balance are known with low certainty. In this thesis, the SWM incorporates the implicit effects, but not the explicit effects. Next to that, wind/whitecap formulations are calibrated such that they give good results when used with the DIA algorithm for quadruplets (Van Vledder, Herbers, Jensen, Resio, and Tracy, 2000). In this thesis, the XNL algorithm is used to solve the quadruplet source term, because in principle it is more accurate than the DIA algorithm. The downside is that the accuracy of the wind/whitecap source terms may be (further) compromised. If more certainty is found on the individual terms of the wave energy balance, and especially their validity in the short gravity wave range, then more thorough numerical simulations of the wave energy balance can be made. An example of such research can be found in Benetazzo et al. (2019), which investigates the wind-wave interaction in case of a contaminated surface.

In general, for numerical modeling, much attention should be paid to the selection of the wave model. Conventional SWMs run into trouble for the considered short waves, because very small grid cells and very small time steps are required for convergence.

Oil spill modeling

The wave attenuation effect that is modeled in the SWM is transferred to the OSM by applying a correction to two wave parameters: the wave breaking frequency and the surface Stokes drift velocity. The reduction of whitecapping energy dissipation as modeled with SWAN is directly and linearly translated to a reduction of wave breaking frequency. As an engineering approach, it is simple to implement and understand. Yet, a more direct method may be found to link the (change of) wave energy dissipation in the SWM to the entrainment equations in the OSM. For example, the absolute wave parameters from the SWM could be transferred to the OSM, rather than the relative reduction.

Stokes drift velocities are calculated on the basis of linear wave theory, which assumes inviscid fluid. However, viscosity and boundary processes play a role. That is what causes the wave energy dissipation of interest, after all. Streaming effects are associated with the bottom and surface boundary layer, so a more complete analysis of the flow pattern might be necessary. This point is closely related to the remark on wave kinematics made previously. Also, a recommendation is given on this point in Chapter 7.

The modeled convergence and divergence of the Stokes drift velocity field cannot exist without vertical flow (upwelling and downwelling). This will probably contribute to the oil mass transport at the boundaries of the oil slick, but it was not covered in this research. Weber (1987) discusses a similar effect for a sea covered with ice.

While the expectation was that an oil slick would be thickest at the front and thinnest at the rear due to lagging of entrained oil mass, the contrary was found in some of the idealized oil spill simulations. The realistic model simulations, that include basic wind drift and oceanic turbulence, show this effect to a much lesser extent. Because this result has not been observed in the field (yet), care should be taken when using a model that produces these results. The effect may be present in the field, though, but have remained undetected so far.

6.3. Generalization and limitations

The assumptions that were made in this thesis constrain the applicability of the results. The most important limitations are listed below, and some thoughts about their impact and validity are shared.

Deep water

Oil spills have negative consequences in general, but their potential impact is largest in coastal areas. There, water is shallow. The applied wave theory is valid for deep water only, which is defined as the water at least as deep as one half wavelength. The primary consequence of waves entering shallow water, is that the wave dispersion relation becomes depth-dependent. For waves with frequencies of 1 to 5 Hz, this effect is hardly relevant. Water of approximately 1 meter depth and deeper, appears to such waves as deep water. One could therefore be inclined to think that, in coastal zones, long waves will behave just like regular shallow water waves unaffected by oil, and short waves will behave like deep water waves affected by oil. For both types of waves individually, the behavior is known. However, the net effect on the spectrum is more complex than that, because in shallow water, several secondary effects arise, like set-up, return currents, triad interactions, depth-induced breaking, and infra-gravity waves. They are not considered in this thesis.

Spectral shape

In this thesis, only fully developed wind waves were considered. By doing so, the wind wave spectrum under consideration was limited to the PM spectrum. It should be relatively easy to repeat the wave simulations of this thesis with different spectral shapes. The expectation is that the oil effect will be relatively larger. This can be explained by the fact that the PM spectrum represents a fully developed sea wave state, and thus resembles the most energetic wind sea possible at some wind speed. For less energetic sea states, less long waves are present whereas approximately the same amount of short waves are present. Because a viscous surface layer mainly affects the latter, the viscous effect relatively becomes larger.

The effect of the presence of swell waves in addition to the wind waves is probably small. Swell waves contribute relatively little to the near-surface Stokes drift (because of their low frequency and long wave length) and to whitecapping. Therefore, the reduction functions derived in this thesis will be only mildly sensitive to the contribution of swell waves.

Slick configuration

Only the simplest possible initial oil slick configuration was modeled: a single, straight, continuous surface layer. Observations of mineral oil spills show that the surface slick is usually discontinuous, and multiple 'patches' or 'strokes' are recognized. Langmuir turbulence is one of the explanations for the observed convergence and divergence patterns.

It is questionable if loose patches of oil have a comparable (dissipative) effect on the waves as a continuous slick. The fact that a mineral oil slick only partially covers the sea surface could be taken into account in modeling methods by introducing a patchiness factor, which reduces the 'fetch' over which floating oil slick dissipates wave energy.

Probabilistic character of particle tracking model

Making the oil spill transport dependent on oil layer thickness breaks the probabilistic character of the PTM. Originally, the fate of each LE was dependent on the environmental forcing(s) it met on its path. The evolution of the LEs could thus be considered as mutually independent. The mean and standard deviation of such simulations could be used to describe the oil spill evolution.

General developments in oil spill modeling, which have made the entrainment process dependent on layer thickness, and the model adaptation of this thesis, which has made the wave forcing dependent on layer thickness, break the probabilistic character of the PTM. Now, the fate of an LE is dependent on the fate of neighboring LEs. To perform a true probabilistic simulation, the results of multiple, individual PTM simulations should be combined.

7. General conclusions and recommendations

In this chapter, the general answers to the research question are given. Before answering the main research question, it is elaborated on the sub-questions. Also, recommendations for future research are given.

7.1. Conclusions

First, the three sub questions are answered. Then, the main research question is answered.

By which mechanisms and at what rate is an oil slick transported by the waves?

Wave forcing causes shear diffusion of an oil slick. First, breaking waves cause entrainment of surface oil and subsequent break-up of the oil mass into droplets. The rate of entrainment is dependent on the wave height and the amount of wave breaking. The depth of entrainment is dependent on the wave height, as is the diameter of the formed droplets.

Second, propagating waves cause mass transport in the wave propagation direction (Stokes drift). The velocity of this drift is, per Fourier wave component, dependent on the wave frequency, wave number and wave amplitude. For irregular waves, the contributions of the individual Fourier wave components can be added together. If the spectral shape is known, the Stokes drift profile can be determined efficiently using the surface Stokes drift velocity (which equals the third spectral moment) and the peak wave number.

The wave height, wave breaking frequency, surface Stokes drift and peak wave number are identified as key wave parameters to model the shear diffusion of an oil slick.

What is the effect of an oil slick on the wave properties that determine the oil slick transport?

Literature shows that a floating fluid layer causes wave attenuation because of interfacial and viscous effects. The interfacial effects are neglected in this thesis. The wave dispersion equation by Jenkins and Jacobs (1997) can be used to calculate the wave energy dissipation of a each Fourier wave component, but the net effect on the key wave properties depends on the change of the entire wave spectrum. This requires a numerical simulation, since several source terms are active in the deep water wave energy balance and a wide range of frequencies must be included.

Numerical simulations in this research show that, for fully-developed wind waves, the net result of all deep water processes (i.e., wind input, whitecapping dissipation, quadruplet redistribution, and viscous dissipation) is a wave spectrum with lower energy levels in the spectral tail, where viscous damping is most active.

No significant effect is found for the total wave energy (significant wave height) or the peak wave number. However, because of the strong dependence of the surface Stokes drift velocity on the short waves, a reduction of surface Stokes drift is found in the presence of a surface oil slick. In addition, the presence of fewer short waves appears to lower the overall input and dissipation of wave energy. Therefore, a reduction of whitecapping energy dissipation is found in the presence of a surface oil slick. For both surface Stokes drift and for whitecapping energy dissipation, the relative reduction grows for greater oil layer thickness, higher oil viscosity, and lower wind speed.

The reduction of whitecapping energy dissipation is found to be, roughly speaking, proportional to oil layer thickness and oil viscosity for the *ST6* wind/whitecap formulation, but proportional to the square root of oil layer thickness and oil viscosity for the *Westhuysen* wind/whitecap formulation. The reduction of surface Stokes drift is found to be, roughly speaking, proportional to the square root of oil layer thickness and oil viscosity, irrespective of the wind/whitecap formulation used.

What is the difference between oil spill evolution with and without taking into account the effect of oil on the waves?

Taking into account the reduction effect of oil presence on the Stokes drift, slower modeled forward movement of the oil slick is found. At the leading edge of the oil slick divergence of the Stokes drift velocity field is found, whereas at the trailing edge convergence is found. If only wave-forced processes are activated in the model, this leads to a shape of the oil slick which is opposite to common observations from the field and models (positive skewness instead of negative skewness). This is due to the instantaneous nature of the reduction function. If a decay length for the wave attenuation would be used in the model, the divergence and convergence would probably be smaller. It was found that, if next to wave-forced processes also basic wind drift and ambient vertical turbulence was active, the same general effects are found, but they are of less relative importance.

The overall distribution of surface and subsurface oil was hardly changed by incorporating the reduction functions.

How is the wave-driven evolution of a marine mineral oil spill affected by oil-induced viscous wave attenuation?

The presence of oil at sea affects its own transport. For sufficiently thick layers ($h_+ \geq \mathcal{O}\{10^{-3}\}$ m) of sufficiently viscous ($\nu_+ \geq \mathcal{O}\{10^{-3}\}$ m^2/s) oil, model simulations show slower net forward movement of a marine mineral oil spill, if the Stokes drift and sea surface agitation rate are reduced to account for the attenuation of (short) waves caused by to the oil-induced viscous damping, compared to reference simulations without these reductions. The convergence and divergence of Stokes drift velocities leads to change of oil mass distribution along the propagation direction, generally increasing the distribution skewness, and having mixed effects on the diffusion (in terms of standard deviation). The distribution of the oil mass over the surface and subsurface appears to be unaffected.

It must be noted that most wave-oil interaction is found for those combinations of oil properties and wave properties that are unfavorable for clear shear diffusion of the oil slick in the first place.

7.2. Recommendations

There are two aspects to this thesis: a scientific one and an engineering one. Both will profit from validation of the results presented in this thesis, because the results are largely based on numerical simulations so far. Definitely, validation is given as a recommendation. Depending whether the scientific aspect is more important or the engineering aspect is more important, different further recommendations should be given.

Regarding the engineering aspect, it probably suffices to keep it short and advise developers and users of oil spill models not to directly start implementing the wave-attenuation process in their models. The consequences of the wave attenuation on the final oil spill evolution as derived in this thesis are simply not important nor accurate enough for use in practical applications.

The subject is not uninteresting nor fully explored, however. This is where the scientific aspect comes in. Since the wave-driven and wind-driven aspects of oil slick transport are hard to distinguish in the field, many oil spill models have come up with a linear factor that is supposed to cover all of them and make simulation results match observations. The detailed processes that play in the surface boundary layer are key to a better scientific understanding of oil spill transport. For example, the presence of a surface layer will cause different wave kinematics, yielding different orbital paths and thus different Stokes drift. Also, attenuation of waves will cause a spatial gradient of radiation stress, yielding Eulerian flow. A thorough derivation (theoretical and experimental) of these flows might contribute to the ability to separate wave- and wind-driven effects, in observations and in models. It is recommended to explore the possibility of incorporating this in an oil spill model. As a starting point, it is referred to Weber and Saetra (1995); Xu and Bowen (1994).

In this thesis, the link between the SWM and the OSM was through reduction functions. It is advised to study the reduction more in-depth. Maybe, a fundamental physical relationship between the independent and dependent parameters can be found. Also, it is strongly advised to make the reduction functions 'fetch'-dependent. By doing so, the trailing edge convergence and leading edge divergence of the oil mass will be modeled with more precision. This is desirable, because exactly this process is what causes the remarkable change of the oil slick skewness. The transfer between SWM and OSM could be taken to a higher level by directly linking the output of SWMs to input for OSMs. For instance, SWMs output includes the amount of wave energy dissipated in breaking events. The energy dissipation rate could be used directly in OSMs, instead of via a reduction function that reduces the whitecapping rate.

Repeating the wave simulations in 2D, and performing full 3D simulation of the oil spill evolution is recommended. Different oil slick sizes and configurations, non-uniform oil slick initializations, will probably lead to results which are better applicable to real-life situations.

To finish off with an individual recommendation on the use of oil spill models. It would be useful to investigate the a reliable yet efficient method of transforming the masses of the LEs into a layer thickness. Equations for oil spill transport over the years have become more comprehensive. Dependency of the transport equations on oil layer thickness has been incorporated relatively recently, which also has increased the need for modeling the oil layer thickness. The effect of employing different gridding, kernel and Voronoi methods on model prestation remains to be investigated.

References

Alpers, W., and Hühnerfuss, H. (1989). The damping of ocean waves by surface films: A new look at an old problem. *Journal of Geophysical Research*, *94*(C5), 6251–6265. https://doi.org/10.1029/JC094iC05p06251

Behroozi, F. (2004). Fluid viscosity and the attenuation of surface waves: A derivation based on conservation of energy. *European Journal of Physics*, *25*(1), 115–122. https://doi.org/10.1088/0143-0807/25/1/014

Benetazzo, A., Cavaleri, L., Ma, H., Jiang, S., Bergamasco, F., Jiang, W., … Qiao, F. (2019). Analysis of the effect of fish oil on wind waves and implications for air-water interaction studies. *Ocean Science*, *15*(3), 725–743. https://doi.org/10.5194/os-15-725-2019

Boufadel, M. C., Bechtel, R. D., and Weaver, J. (2006). The movement of oil under non-breaking waves. *Marine Pollution Bulletin*, *52*(9), 1056–1065. https://doi.org/10.1016/j.marpolbul.2006.01.012

Breivik, Ø., Bidlot, J. R., and Janssen, P. A. E. M. (2016). A Stokes drift approximation based on the Phillips spectrum. *Ocean Modelling*, *100*, 49–56. https://doi.org/10.1016/j.ocemod.2016.01.005

Breivik, Ø., Janssen, P. A. E. M., and Bidlot, J.-R. (2014). Approximate Stokes drift profiles in deep water. *Journal of Physical Oceanography*, *44*(9), 2433–2445. https://doi.org/10.1175/JPO-D-14-0020.1

Christensen, K. H., and Terrile, E. (2009). Drift and deformation of oil slicks due to surface waves. *Journal of Fluid Mechanics*, *620*, 313–332. https://doi.org/10.1017/S0022112008004606

Dagestad, K.-F., Röhrs, J., Breivik, O., and Ådlandsvik, B. (2018). OpenDrift v1.0: A generic framework for trajectory modelling. *Geoscientific Model Development*, *11*(4), 1405–1420. https://doi.org/10.5194/gmd-11-1405-2018

De Carolis, G., and Desiderio, D. (2002). Dispersion and attenuation of gravity waves in ice: A two-layer viscous fluid model with experimental data validation. *Physics Letters, Section A: General, Atomic and Solid State Physics*, *305*(6), 399–412. https://doi.org/10.1016/S0375-9601(02)01503-7

Deltares. (2014). *D-Waq PART: User Manual*.

Delvigne, G. A. L., and Sweeney, C. E. (1988). Natural dispersion of oil. *Oil and Chemical Pollution*, *4*, 281–310. https://doi.org/10.1016/S0269-8579(88)80003-0

DHI. (2015). *MIKE 21 & MIKE 3 Flow Model FM Oil Spill Module*.

Einstein, A. (1906). Eine neue Bestimmung der Moleküldimensionen. *Annalen Der Physik*, *19*, 289–306. https://doi.org/10.1002/andp.19063240204

Einstein, A. (1911). Berichtigung zu meiner Arbeit: "Eine neue Bestimmung der Moleküldimensionen." *Annalen Der Physik*, *34*, 591–592. https://doi.org/10.1002/andp.200590031

Elliott, A. J. (1986). Shear diffusion and the spread of oil in the surface layers of the North Sea. *Deutsche Hydrographische Zeitschrift*, *39*(3), 113–137. https://doi.org/10.1007/BF02408134

Elliott, A. J., Hurford, N., and Penn, C. J. (1986). Shear diffusion and the spreading of oil slicks. *Marine Pollution Bulletin*, *17*(7), 308–313. https://doi.org/10.1016/0025-326X(86)90216-X

Ermakov, S. A., Sergievskaya, I. A., and Gushchin, L. A. (2012). Damping of gravity-capillary waves in the presence of oil slicks according to data from laboratory and numerical experiments. *Izvestiya, Atmospheric and Oceanic Physics*, *48*(5), 565–572. https://doi.org/10.1134/S000143381204007X

ExxonMobil. (2014). *Oil spill response field manual*.

Fingas, M. (2016). *Introduction to Spill Modeling*. *Oil Spill Science and Technology: Second Edition*. Elsevier Inc. https://doi.org/10.1016/B978-0-12-809413-6.00008-4

Fingas, M. (2018). The challenges of remotely measuring oil slick thickness. *Remote Sensing*, *10*(2). https://doi.org/10.3390/rs10020319

Franklin, B. (1774). Of the stilling of waves by means of oil. Extracted from sundry letters between Benjamin Franklin, LL. D. F. R. S. William Brownrigg, M. D. F. R. S. and the Reverend Mr. Farish. *Philosophical Transactions*, *64*, 445–460.

Holthuijsen, L. H. (2007). *Waves in oceanic and coastal waters*. Cambridge university press.

Holthuijsen, L. H., and Herbers, T. H. C. (1986). Statistics of breaking waves observed as whitecaps in the open sea. *Journal of Physical Oceanography*, *13*(2), 192–207. https://doi.org/10.1175/1520-0485(1986)016<0290:SOBWOA>2.0.CO;2

Hühnerfuss, H., Walter, W., Lange, P. A., and Alpers, W. (1987). Attenuation of wind waves by monomolecular sea slicks and the Marangoni effect. *Journal of Geophysical Research*, *92*(C4), 3961–3963. https://doi.org/10.1029/JC092iC04p03961

Janssen, P. A. E. M. (1989). Wave-induced stress and the drag of air flow over sea waves. *Journal of Physical Oceanography*, *19*(6), 745–754. https://doi.org/10.1175/1520-0485(1989)019<0745:WISATD>2.0.CO;2

Janssen, P. A. E. M. (1991). Quasi-linear theory of wind-wave generation applied to wave forecasting. *Journal of Physical Oceanography*, *21*(11), 1631–1642. https://doi.org/10.1175/1520-0485(1991)021<1631:QLTOWW>2.0.CO;2

Jenkins, A. D., and Dysthe, K. B. (1997). The effective film viscosity coefficients of a thin floating fluid layer. *Journal of Fluid Mechanics*, *344*, 335–337. https://doi.org/10.1017/S0022112097006125

Jenkins, A. D., and Jacobs, S. J. (1997). Wave damping by a thin layer of viscous fluid. *Physics of Fluids*, *9*(5), 1256–1264. https://doi.org/10.1063/1.869240

Johansen, Ø., Reed, M., and Bodsberg, N. R. (2015). Natural dispersion revisited. *Marine Pollution Bulletin*, *93*(1–2), 20–26. https://doi.org/10.1016/j.marpolbul.2015.02.026

Komen, G. J., Hasselmann, S., and Hasselmann, K. (1984). On the existence of a fully developed wind-sea spectrum. *Journal of Physical Oceanography*, *14*(8), 1271–1285. https://doi.org/10.1175/1520-0485(1984)014<1271:OTEOAF>2.0.CO;2

Lamb, H. (1932). *Hydrodynamics* (6th ed.). Cambridge university press.

Laxague, N. J. M., Özgökmen, T. M., Haus, B. K., Novelli, G., Shcherbina, A., Sutherland, P., … Molemaker, J. (2018). Observations of near-surface current shear help describe oceanic oil and plastic transport. *Geophysical Research Letters*, *45*(1), 245–249. https://doi.org/10.1002/2017GL075891

Li, Z., Spaulding, M. L., and French-McCay, D. (2017). An algorithm for modeling entrainment and naturally and chemically dispersed oil droplet size distribution under surface breaking wave conditions. *Marine Pollution Bulletin*, *119*(1), 145–152. https://doi.org/10.1016/j.marpolbul.2017.03.048

Li, Z., Spaulding, M. L., French-McCay, D., Crowley, D., and Payne, J. R. (2017). Development of a unified oil droplet size distribution model with application to surface breaking waves and subsea blowout releases considering dispersant effects. *Marine Pollution Bulletin*, *114*(1), 247–257. https://doi.org/10.1016/j.marpolbul.2016.09.008

Miche, M. (1944). Mouvements ondulatoires de la mer en profondeur constante ou décroissante. *Annales Des Ponts et Chaussées*, *114*, 369–406.

Milgram, J. H. (1998). Short wave damping in the simultaneous presence of a surface film and turbulence. *Journal of Geophysical Research*, *103*(C8), 15717–15727. https://doi.org/10.1029/98JC01191

National Oceanic and Atmospheric Administration. (n.d.). Exxon Valdez oil spill. Retrieved March 7, 2019, from https://response.restoration.noaa.gov/oil-and-chemical-spills/significant-incidents/exxon-valdez-oil-spill

National Oceanic and Atmospheric Administration. (2012). *General NOAA Operational Modeling Environment (GNOME) Technical Documentation*.

National Oceanic and Atmospheric Administration. (2018). Oil Library. Retrieved from anaconda.org/noaa-orr-erd/oil_library, accessed 24 June 2019

Ng, C.-O. (2000). Water waves over a muddy bed: a two-layer Stokes' boundary layer model. *Coastal Engineering*, *40*(3), 221–242. https://doi.org/10.1016/S0378-3839(00)00012-0

Paquier, A., Moisy, F., and Rabaud, M. (2016). Viscosity effects in wind wave generation. *Physical Review Fluids*, *1*(8), 1–15. https://doi.org/10.1103/PhysRevFluids.1.083901

Pierson, W. J., and Moskowitz, L. A. (1964). Proposed spectral form for fully developed wind seas based on the similarity theory of S. A. Kitaigorodskii. *Journal of Geophysical Research*, *69*, 5181–5190.

Reed, M., Leirvik, F., Johansen, Ø., and Brørs, B. (2009). *Numerical algorithm to compute the effects of breaking waves on surface oil spilled at sea*. Retrieved from https://crrc.unh.edu/sites/crrc.unh.edu/files/final_report_sintef_natural_dispersion_october-2009.pdf

Rogers, W. E., Babanin, A. V., and Wang, D. W. (2012). Observation-consistent input and whitecapping dissipation in a model for wind-generated surface waves: Description and simple calculations. *Journal of Atmospheric and Oceanic Technology*, *29*(9), 1329–1346. https://doi.org/10.1175/JTECH-D-11-00092.1

Röhrs, J., Dagestad, K. F., Asbjørnsen, H., Nordam, T., Skancke, J., Jones, E., … Brekke, C. (2018). The effect of vertical mixing on the horizontal drift of oil spills. *Ocean Science*, *14*, 1581–1601. https://doi.org/10.5194/os-14-1581-2018

Salisbury, D. J., Anguelova, M. D., and Brooks, I. M. (2013). On the variability of whitecap fraction using satellite-based observations. *Journal of Geophysical Research: Oceans*, *118*(11), 6201–6222. https://doi.org/10.1002/2013JC008797

Salisbury, D. J., Anguelova, M. D., and Brooks, I. M. (2014). Global distribution and seasonal dependence of satellite-based whitecap fraction. *Geophysical Research Letters*, *41*(5), 1616–1623. https://doi.org/10.1002/2014GL059246

Sergievskaya, I. A., and Ermakov, S. A. (2017). Damping of gravity–capillary waves on water surface covered with a visco-elastic film of finite thickness. *Izvestiya, Atmospheric and Oceanic Physics*, *53*(6), 650–658. https://doi.org/10.1134/S000143381706010X

Stokes, G. G. (1847). On the theory of oscillatory waves. *Transactions of the Cambridge Philosophical Society*, *8*, 441–455.

Sutherland, G., Halsne, T., Rabault, J., and Jensen, A. (2017). The attenuation of monochromatic surface waves due to the presence of an inextensible cover. *Wave Motion*, *68*, 88–96. https://doi.org/10.1016/j.wavemoti.2016.09.004

The SWAN team. (2019a). *SWAN: Scientific and technical documentation*.

The SWAN team. (2019b). *SWAN: User manual*.

Tkalich, P., and Chan, E. S. (2002). Vertical mixing of oil droplets by breaking waves. *Marine Pollution Bulletin*, *44*(11), 1219–1229. https://doi.org/10.1016/S0025-326X(02)00178-9

United States Coast Guard. (2011). *On scene coordinator report Deepwater Horizon oil spill*.

van der Westhuysen, A. J., Zijlema, M., and Battjes, J. A. (2007). Nonlinear saturation-based whitecapping dissipation in SWAN for deep and shallow water. *Coastal Engineering*, *54*(2), 151–170. https://doi.org/10.1016/j.coastaleng.2006.08.006

Van Vledder, G. P., Herbers, T. H. C., Jensen, R. J., Resio, D. T., and Tracy, B. (2000). Modelling of non-linear quadruplet wave-wave interactions in operational wave models. In *Proceedings of the 27th International Conference on Coastal Engineering* (Vol. 276, pp. 797–811). https://doi.org/10.1061/40549(276)62

Visser, A. W. (1997). Using random walk models to simulate the vertical distribution of particles in a turbulent water column. *Marine Ecology Progress Series*, *158*(1), 275–281. https://doi.org/10.3354/meps158275

Weber, J. E. (1987). Wave attenuation and wave drift in the marginal ice zone. *Journal of Physical Oceanography*, *17*(12), 2351–2361. https://doi.org/10.1175/1520-0485(1987)017<2351:WAAWDI>2.0.CO;2

Weber, J. E., and Saetra, Ø. (1995). Effect of film elasticity on the drift velocity of capillary-gravity waves. *Physics of Fluids*, *7*(2), 307–314. https://doi.org/10.1063/1.868629

Xu, Z., and Bowen, A. J. (1994). Wave- and wind-driven flow in water of finite depth. *Journal of Physical Oceanography*.

Zeinstra-Helfrich, M., Koops, W., and Murk, A. J. (2016). How oil properties and layer thickness determine the entrainment of spilled surface oil. *Marine Pollution Bulletin*, *110*(1), 184–193. https://doi.org/10.1016/j.marpolbul.2016.06.063

Zeinstra-Helfrich, M., Koops, W., and Murk, A. J. (2017). Predicting the consequence of natural and chemical dispersion for oil slick size over time. *Journal of Geophysical Research: Oceans*, *122*(9), 7312–7324. https://doi.org/10.1002/2017JC012789

Zhang, Y., Zhang, J., Wang, Y., Meng, J., and Zhang, X. (2015). The damping model for sea waves covered by oil films of a finite thickness. *Acta Oceanologica Sinica*, *34*(9), 71–77. https://doi.org/10.1007/s13131-015-0729-1

Appendices

A. Overview of oil spill models

	GNOME, ADIOS	OpenDrift, OpenOil	OILMAP	D-WAQ	MIKE OSM
Developer	NOAA, noaa.gov	In use at, but not formally developed by NMI, met.no	RPS, asascience.com	Deltares, deltares.nl	DHI, dhi.dk
Documentation	National Oceanic and Atmospheric Administration (2012)	Dagestad, Röhrs, Breivik, and Ådlandsvik (2018)	not available	Deltares (2014)	DHI (2015)
Description	GNOME is a particle tracking environment. ADIOS is a database with oil weathering properties. Primarily developed for responsive purpose. Much empiricism and ad-hoc changes of parameters are allowed for. Open-source code, C++ and Python.	OpenDrift consists of a basic modeling class that calculates particle trajectories. OpenOil is a subclass, that adds specific oil processes to the transport. OpenOil uses the ADIOS oil weathering database. Open-source code, Python.	OILMAP is in operational use at Rijkswaterstaat. The Rijkswaterstaat *Matroos* data portal offers a direct customized download of hydrodynamical and wind data from their operational models, for use with OILMAP.	D-WAQ is part of the Delft3D modeling suite. D-WAQ is a package for water quality, it can solve concentrations, and it also has particle tracking functionality including oil weathering equations.	MIKE oil spill module is part of the MIKE modeling suite.
Handling of Stokes drift	Implicitly incorporated in wind drift	Surface Stokes drift obtained from external source, scaled to other depths.	unknown	Implicitly incorporated in wind drift	From hydrodynamical model
Handling of wind drift	Wind drift of surface particles only. Drift coefficient between 1 and 4 per cent, redrawn every time step. No wind drift angle.	Wind drift of surface particles only, or linear decay with depth. Drift coefficient determined by user. No wind drift angle.	unknown	*with 3D flow field:* Wind drift of surface particles only. Drift coefficient and angle determined by user. *with 2DH flow field:* Parabolic profile superimposed on flow (3% of the wind speed at surface, no net flow over the vertical). Wind drift of surface and subsurface particles.	*with 3D flow field:* Multiple options; either use bed shear profile, surface wind acceleration, both, or none. Drift angle can be included. *with 2DH flow field:* Same options as for 3D flow field, with possibility of additionally including parabolic profile (no net flow over the vertical).

B. Scales and properties of oil spills

One aspect that makes oil spill modeling challenging, is the fact that the properties of the spilled oil can vary by several orders of magnitude. Therefore, some data on oil spills and oil properties is collected in this paragraph.

Volume, slick area, slick thickness

Oil spills can arise in any size. Two well-known large oil spills are taken as examples. The first one is the 1989 *Exxon Valdez* oil spill, the second one is the 2010 *Deepwater Horizon* oil spill. In the *Exxon Valdez* case, 11 million gallons (42.000 m^3) of Prudhoe Bay crude oil was spilled from an oil tanker directly to the sea surface in a nearshore area (National Oceanic and Atmospheric Administration, n.d.). The spilt oil amounts to roughly one fifth of the total capacity of the ship. In the *Deepwater Horizon* case, approximately 4.9 million barrels (780.000 m^3) of crude oil was spilled from a blown-out well at the sea bottom over a period of 87 days, at approximately 65 kilometers from the coast (United States Coast Guard, 2011).

The location (at surface or at bottom) and duration of the spill affect the size and location of the oil slick that forms. Thus, only knowing the volume of an oil spill gives no information about the affected area nor about the oil thickness of the surface oil slick. As a rough indication of what oil slick area and thickness may be expected, Figure 29 shows the possible relations between oil spill volume, slick area, and slick thickness (provided that all the oil is at the surface), and Figure 30 shows an estimate for the surface slick thickness development for a 10.000 m^3 oil spill. The actual oil layer thickness proves to be a parameter that is hard to obtain in practice (Fingas, 2018). In this research, however, it is assumed that the oil layer thickness at every location in the oil slick is known.

Viscosity and mass density

The viscosity of different oil types varies over several orders of magnitude. Moreover, the viscosity of mineral oils is dependent on temperature and weathering state. The NOAA provides an Oil Library (National Oceanic and Atmospheric Administration, 2018) that contains properties of many oil types. In Figure 31, the viscosity and mass density combinations of all oil types in the NOAA Oil Library is shown. It should be noted that unweathered oils are considered. Evaporation of the lighter oil fractions and emulsification of the oil slick can increase the oil slick viscosity up to three orders of magnitude (Fingas, 2016).

The viscosity change of the water due to the presence of dispersed oil droplets is deemed negligible, considering Einstein's viscosity equation (Einstein, 1906, 1911), and assuming the oil-in-water emulsion behaves as a dilute suspension of solid particles.

Parameter domain

In this thesis, the gravitational acceleration g, the water viscosity ν_-, and the water density ρ_- are taken to be fixed. Their values are set equal to the standard parameter settings of the SWM-software SWAN (The SWAN team, 2019b).

The oil layer thickness h_+, the oil viscosity ν_+, and the oil density ρ_+ are of main interest in this research. For these parameters, a range of interest is taken, based on observations and measurements (ExxonMobil, 2014; National Oceanic and Atmospheric Administration, 2018; Zeinstra-Helfrich et al., 2017), see Figure 29, Figure 30 and Figure 31. In principle, the oil layer can have a thickness from monomolecular scale up to any thickness. As a lower bound, 10^{-4} m is chosen, so only situations are considered where the effect of the layer thickness becomes noticeable (Jenkins and Jacobs, 1997). As an upper bound, 10^{-2} m is chosen, because thicker oil slicks do not occur for longer periods of time: because of buoyancy, an oil slick will spread out. For oil viscosity, 10^{-4} m^2/s is chosen as a lower bound, so only situations are considered where the oil is more viscous than water by two orders of magnitude, and 10^{-2} m^2/s is chosen as an upper bound, because more viscous oil hardly occurs in the form of a continuous layer, which is a requirement for the damping theory to apply. For oil density, values in between approximately 800 and 1000 kg/m^3 are to be expected.

The remaining parameters in the equation are all surface/interface properties. An estimate of the order of magnitude of these properties is taken from various sources (Alpers and Hühnerfuss, 1989; Sergievskaya and Ermakov, 2017; Zeinstra-Helfrich et al., 2016). The final parameter domain is shown in the table below.

Parameter	Magnitude	Unit
g	9.81	m/s^2
ν_-	$1.30 \cdot 10^{-6}$	m^2/s
ρ_-	1025	kg/m^3
h_+	$10^{-4} – 10^{-2}$	m
ν_+	$10^{-4} – 10^{-2}$	m^2/s
ρ_+	800 – 1000	kg/m^3
γ_-	10^{-2}	N/m
γ_+	10^{-2}	N/m
χ_-	10^{-2}	N/m
χ_+	10^{-3}	N/m
ψ_-	10^{-3}	Ns/m
ψ_+	10^{-4}	Ns/m

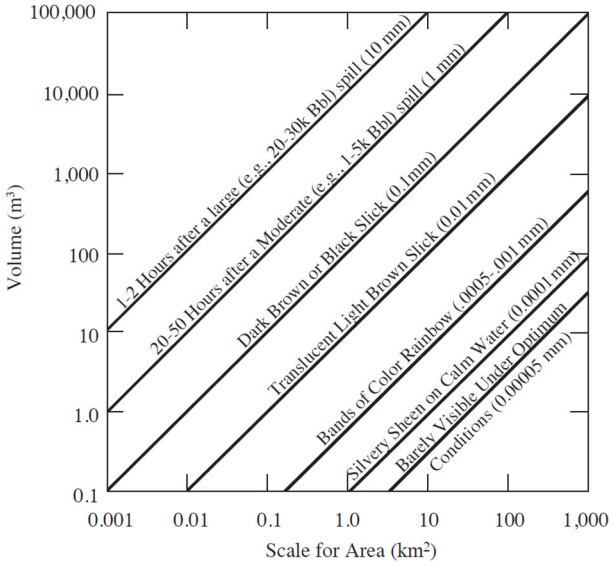

Figure 29. *The relation between oil spill volume, slick area, and slick thickness.*[14]

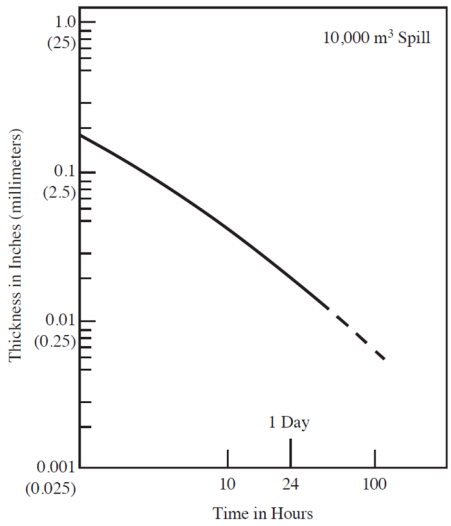

Figure 30. *Estimate of oil slick thickness through time for a 10.000 m³ spill of medium crude oil under calm seas and low winds.*[15]

[14] Image retrieved from: (ExxonMobil, 2014), their figure 1–10

[15] Image retrieved from: (ExxonMobil, 2014), their figure 1–9

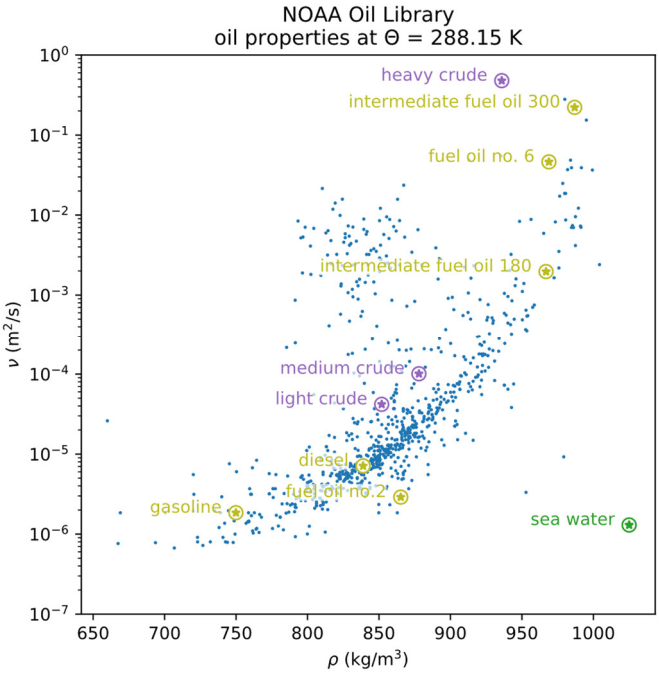

Figure 31. *Kinematic viscosity and mass density combinations of the unweathered mineral oils from the NOAA Oil Library (blue). Some generic crude and fuel oil types are marked (purple resp. khaki). Also, sea water mass density and kinematic viscosity is indicated (green).*

C. Wave dispersion relation by Jenkins and Jacobs (1997)

Jenkins and Jacobs (1997) derived an approximate wave dispersion relation for the case of a Newtonian fluid of infinite depth with a thin layer of viscous Newtonian fluid on top.

Full dispersion relation

The full wave dispersion relation equals

$$N^* = \sqrt{G} - i\delta \,,$$

where

$$\delta = \frac{2\nu_-^* + \frac{1}{2}\varsigma_\mathrm{T}^* + i\frac{(\gamma_\mathrm{T}^*(1-\rho_+^*) - \gamma_-^*)h_+^*}{G^{1/2}} + \frac{1}{2\sqrt{i}}\frac{\rho_+^* h_+^* G^{1/4}\varsigma_\mathrm{T}^*}{\sqrt{\nu_-^*}} + \frac{\sqrt{i}}{2}\frac{{\rho_+^*}^2 {h_+^*}^2 G^{3/4}(R^2-1)}{\sqrt{\nu_-^*}}}{1 + \sqrt{i}\frac{\varsigma_\mathrm{T}^*}{G^{1/4}\sqrt{\nu_-^*}} + \frac{1}{\sqrt{i}}\frac{\rho_+^* h_+^* G^{1/4}}{\sqrt{\nu_-^*}}},$$

$$\gamma_\mathrm{T}^* = \gamma_-^* + \gamma_+^* \,, \qquad G = 1 + \gamma_\mathrm{T}^*, \qquad R = \frac{\rho_+^* + \gamma_+^*}{G\rho_+^*},$$

$$\varsigma_\mathrm{T}^* = \varsigma_+^* + \varsigma_-^* + 4\rho_+^*\nu_+^* h_+^* + \frac{\varsigma_+^*\varsigma_-^* h_+^*}{\rho_+^*\nu_+^*} \,, \qquad \varsigma_\pm^* = \psi_\pm^* - \frac{\chi_\pm^*}{i\omega^*},$$

where all variables have been made dimensionless, indicated by an asterisk,

$$\nu_\pm^* = \sqrt{\frac{k^3}{g}}\nu_\pm \,, \qquad \rho_\pm^* = \frac{1}{\rho_-}\rho_\pm \,, \qquad h_\pm^* = kh_\pm \,, \qquad N^* = \frac{1}{\sqrt{gk}}N \,,$$

$$\gamma_\pm^* = \frac{k^2}{g\rho_-}\gamma_\pm \,, \qquad \chi_\pm^* = \frac{k^2}{g\rho_-}\chi_\pm \,, \qquad \psi_\pm^* = \sqrt{\frac{k^3}{g^3\rho_-^2}}\psi_\pm \,,$$

where ν is the kinematic viscosity, ρ is the mass density, h is the layer thickness, γ is the surface/interfacial tension, χ is the surface/interfacial elasticity, ψ is the surface/interfacial viscosity, ω is the angular wave frequency, i is the imaginary unit, the plus index indicates upper layer properties (oil) or surface properties (air-oil interface), and the minus index indicates lower layer properties (water) or interface properties (oil-water interface).

The given wave dispersion relation is subject to restrictions. It only holds if the viscous layer thickness is sufficiently thin compared to the wave length, which is reflected in the inequality $kh_+ \ll 1$, and sufficiently thin compared to the viscous layer oscillatory boundary layer thickness, which is reflected in the inequality $\sqrt{\omega/\nu_+}\, h_+ \ll 1$. The wave amplitude should be small with respect to the wave length, $a \ll L$, but it may be larger than the viscous surface layer thickness, so $a > h_+$ is valid.

Since the wave dispersion relation has wave number k as independent variable, a domain has to be chosen for this parameter. However, it is preferred to work in terms of wave frequency, for which a parameter domain of interest between 0.1 and 5.0 Hz is chosen. Using the regular deep water wave dispersion relation, this wave frequency domain is transformed

into a wave number domain, yielding a domain approximately between 0.04 and 100 rad/m. It will be proven a posteriori that using the regular deep water wave dispersion relation for relating wave number to wave frequency is valid.

Satisfaction of the first requirement is visualized in Figure 32. The value of kh_+ is indicated with colors: green indicates that the value is lower than 0.1, so the requirement is fulfilled. Yellow colors indicate a value of kh_+ between 0.1 and 1.0. Red colors indicate a value of kh_+ larger than 1.0, so the wave dispersion relation is probably inaccurate for those cases. It can be seen that, for the shortest waves, the requirement is not fully met for the case of a 1 cm upper layer thickness.

Satisfaction of the second requirement is visualized in Figure 33, for three different kinematic viscosities of the upper layer fluid. The same color scheme is employed as in Figure 32. It can be seen that, for highly viscous fluids, the requirement is always met. However, for low viscosity fluids in combination with large upper layer thicknesses or short waves, the requirement is not always met.

Simplified dispersion relation: neglecting surface/interfacial properties

It is desired to decrease the complexity of the wave dispersion relation. Therefore, it is investigated if surface/interfacial properties can be neglected. To do so, the wave frequency (real part and imaginary part independently) is calculated for various combinations of k, h_+ and ν_+. This is done twice: once including and once excluding the contribution of the six surface/interface parameters. From the difference, the relative error is calculated. A wave number domain of 0.1 to 100 rad/m is used. Other parameters are taken from the parameter domain of interest as defined in Appendix B.

In Figure 34, it is shown that the real part of the wave number (relating wave frequency to wave length), when neglecting the surface/interface parameters, is always within 10% of its actual value when surface/interface parameters are included in the calculation.

In Figure 35, it is shown that the imaginary part of the wave number (relating wave frequency to wave attenuation rate) mostly has a relative error of less than 10%. However, for cases where the surface layer is not so viscous and not so thick, the error is relatively large. This can be attributed to the fact that surface/interface properties are relatively more dominant in those cases. Neglecting the surface/interface parameters leads to an underestimation of the wave damping, but in general the error is negligibly small.

Concluding, the surface/interface properties (γ, χ and ψ) can be neglected with respect to the viscous properties for the purposes of this thesis. Then, the wave dispersion relation equals

$$N = \underbrace{\sqrt{gk} + 2\nu_- k^2 \Im\{\mathcal{Y}\}}_{\text{real}} - \underbrace{i\, 2\nu_- k^2 \Re\{\mathcal{Y}\}}_{\text{imaginary}},$$

$$\mathcal{Y} = \frac{1 + Y + \frac{\sqrt{\nu_-^*}}{\nu_+^* \sqrt{i}} Y^2}{1 + \left(4\sqrt{i}\sqrt{\nu_-^*} + \frac{\sqrt{\nu_-^*}}{\nu_+^* \sqrt{i}}\right) Y},$$

$$Y = \frac{\rho_+ \nu_+}{\rho_- \nu_-} k h_+ .$$

Validity of using the regular deep water wave dispersion relationship

For various purposes, it is necessary to convert wave frequency into wave number and vice versa. This requires a complicated calculation and iteration. Therefore, it is investigated if surface/interfacial *and* viscous properties can be neglected. To do so, the wave frequency (real part only) is calculated for various combinations of k, h_+ and ν_+. This is done twice: once using the wave dispersion relation by Jenkins and Jacobs (1997) and once using the regular deep water wave dispersion relation. From the difference, the relative error is calculated. A wave number domain of 0.1 to 100 rad/m is used. Other parameters are taken from the parameter domain of interest as defined in Appendix B.

In Figure 36, it is shown that the real part of the wave number, when neglecting the surface/interface and viscous parameters, is always very close to its actual value, except for the short gravity waves in the single case of a thick (10^{-2} m) and viscous oil layer (10^{-2} m^2/s). Concluding, the regular deep water wave dispersion relation can be used for the purpose of this thesis.

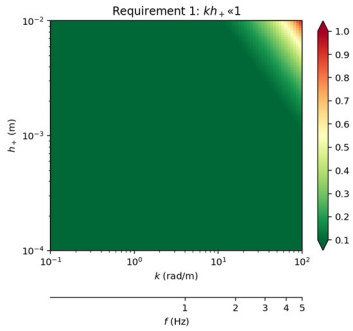

Figure 32. *Value of kh_+ for various combinations of k and h_+. Linear wave frequency f is indicated for reference (based on the regular deep water wave dispersion relation).*

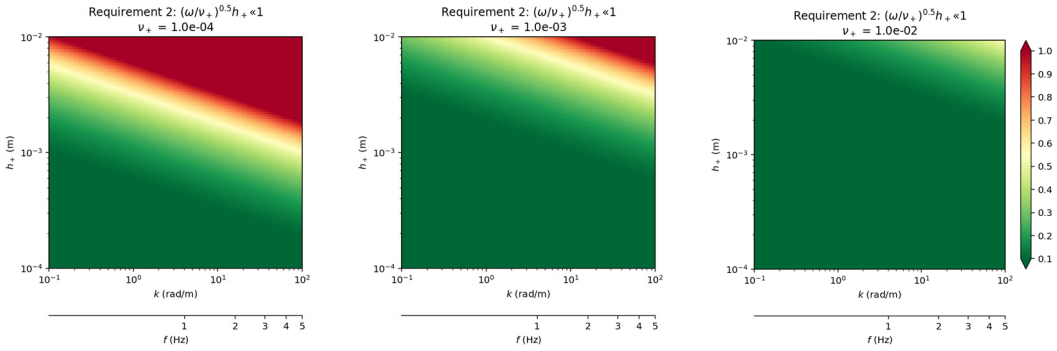

(a) $\nu_+ = 10^{-4}$ m^2/s (b) $\nu_+ = 10^{-3}$ m^2/s (c) $\nu_+ = 10^{-2}$ m^2/s

Figure 33. *Value of $\sqrt{\omega/\nu_+}\ h_+$ for various combinations of k, h_+ and ν_+. Linear wave frequency f is indicated for reference (based on the regular deep water wave dispersion relation).*

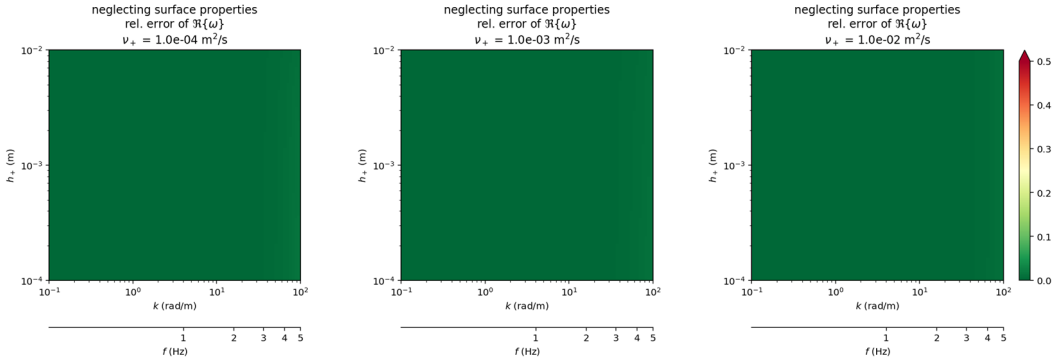

(a) $\nu_+ = 10^{-4}$ m^2/s (b) $\nu_+ = 10^{-3}$ m^2/s (c) $\nu_+ = 10^{-2}$ m^2/s

Figure 34. *The relative error in the calculation of the real part of the wave frequency by neglecting the surface/interface parameters, for various combinations of k, h_+ and ν_+. Linear wave frequency f is also indicated (based on the regular deep water wave dispersion relation).*

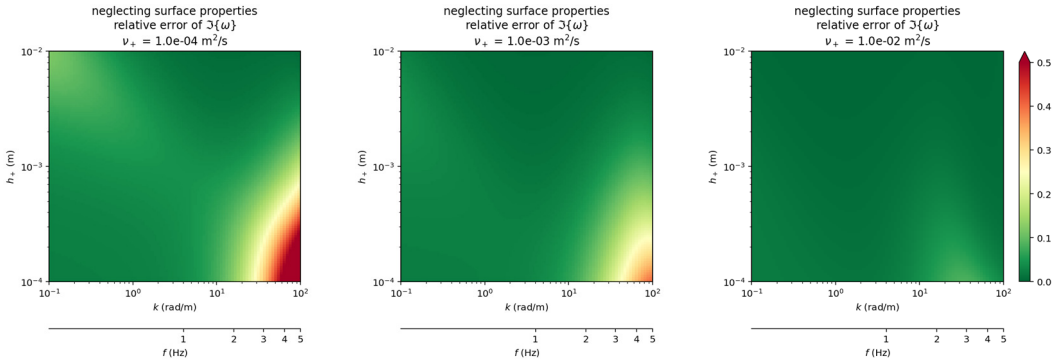

(a) $\nu_+ = 10^{-4}$ m^2/s (b) $\nu_+ = 10^{-3}$ m^2/s (c) $\nu_+ = 10^{-2}$ m^2/s

Figure 35. *The relative error in the calculation of the imaginary part of the wave frequency by neglecting the surface/interface parameters, for various combinations of k, h_+ and ν_+. Linear wave frequency f is also indicated (based on the regular deep water wave dispersion relation).*

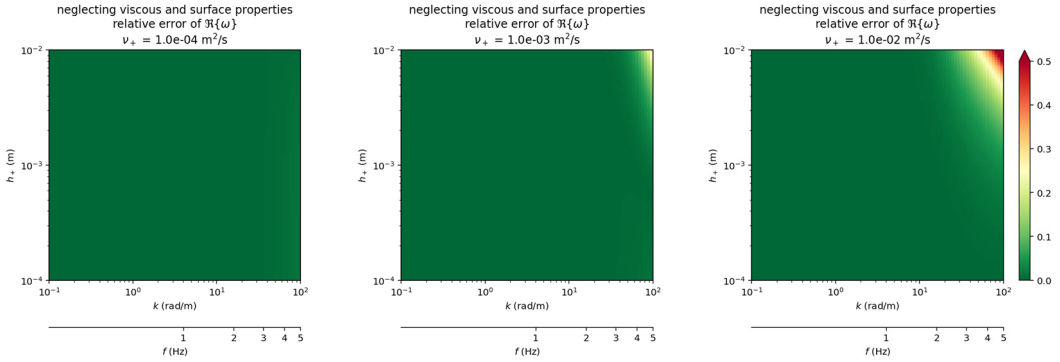

(a) $\nu_+ = 10^{-4}$ m^2/s (b) $\nu_+ = 10^{-3}$ m^2/s (c) $\nu_+ = 10^{-2}$ m^2/s

Figure 36. *The relative error in the calculation of the real part of the wave frequency by neglecting the surface/interface AND viscous parameters, for various combinations of k, h_+ and ν_+. Linear wave frequency f is also indicated (based on the regular deep water wave dispersion relation).*

D. Definition of the Pierson-Moskowitz wave spectrum

In this thesis, only fully developed, stationary sea states are considered. Holthuijsen (2007) gives the following characteristic properties for fully developed significant wave height and peak wave period, based on Pierson and Moskowitz (1964),

$$H_{\mathrm{s}} = 0.24\,\frac{U_{10}^2}{g},$$

$$T_{\mathrm{p}} = 7.69\,\frac{U_{10}}{g},$$

where U_{10} is the wind speed at 10 meter height, and g is the gravitational acceleration. The PM spectrum is the classic definition of a fully developed wind wave spectrum. It is defined by

$$E_f = 0.0081\frac{g^2}{(2\pi)^4} f^{-5} \exp\left(-\frac{5}{4}\left(\frac{f_{\mathrm{p}}}{f}\right)^4\right),$$

where the peak frequency f_{p} can be obtained by inverting the peak period,

$$f_{\mathrm{p}} = \frac{1}{T_{\mathrm{p}}} = 0.13\frac{g}{U_{10}}.$$

E. Full results of the oil spill modeling

The results of all OSM simulations are collected in this appendix. Each OSM simulation produces the paths through time for all LEs. At the end of the simulation, after 24 hours, the LEs might be distributed like in Figure 37a. To give better insight into the oil mass distribution at the end of the simulation, and of the development of the oil spill trough time, graphs are made like in Figure 37b.

The plots show (i) the location and distribution of the oil mass after 24 hours, and the development through time of (ii) the center of mass, (iii) the standard deviation, (iv) the skewness, and (v) the distribution of oil mass between the surface slick and subsurface droplets.

The simulation visualizations are ordered according to the following table.

U_{10}	Idealized case	Realistic case
5.0 m/s	Figure 38	Figure 39
7.5 m/s	Figure 40	Figure 41
10.0 m/s	Figure 42	Figure 43

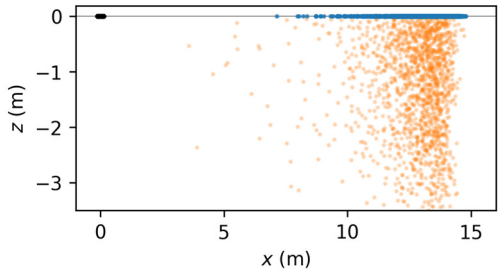

(a) *LE locations in the x,z-plane at the start (black) and at the end (blue, orange) of a simulation*

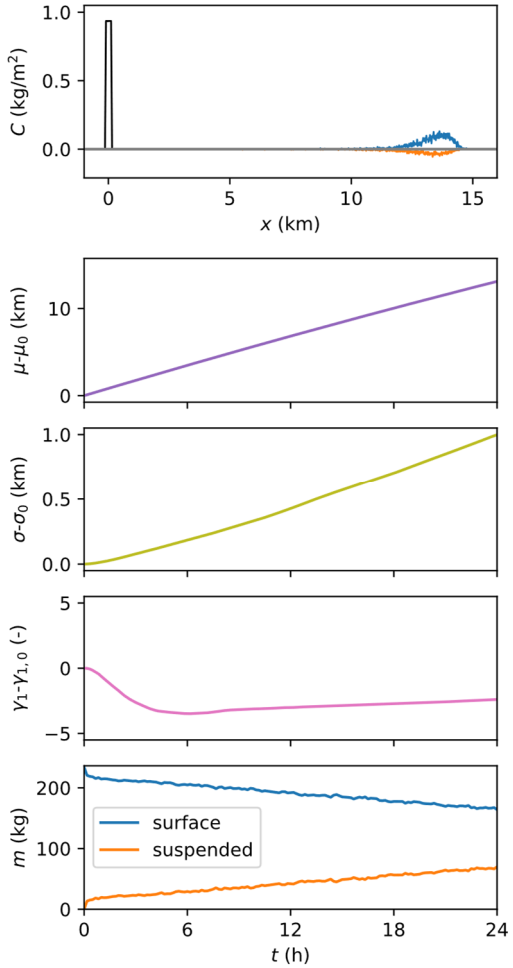

(b) *Statistics of the displayed oil spill evolution: mass distribution in space, and development through time of mass center, mass diffusion, mass skewness, surface-subsurface mass distribution*

Figure 37. *Results of an arbitrary oil spill simulation, and the associated graphs as displayed in Appendix E.*

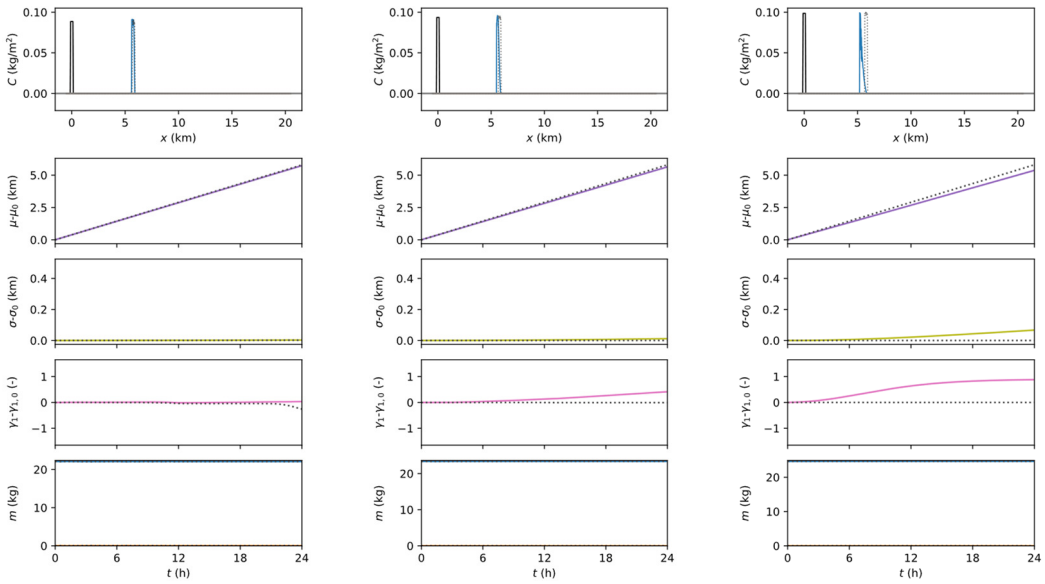

(a) $h_+ = 10^{-4}$ m, $\nu_+ = 10^{-4}$ m^2/s (b) $h_+ = 10^{-4}$ m, $\nu_+ = 10^{-3}$ m^2/s (c) $h_+ = 10^{-4}$ m, $\nu_+ = 10^{-2}$ m^2/s

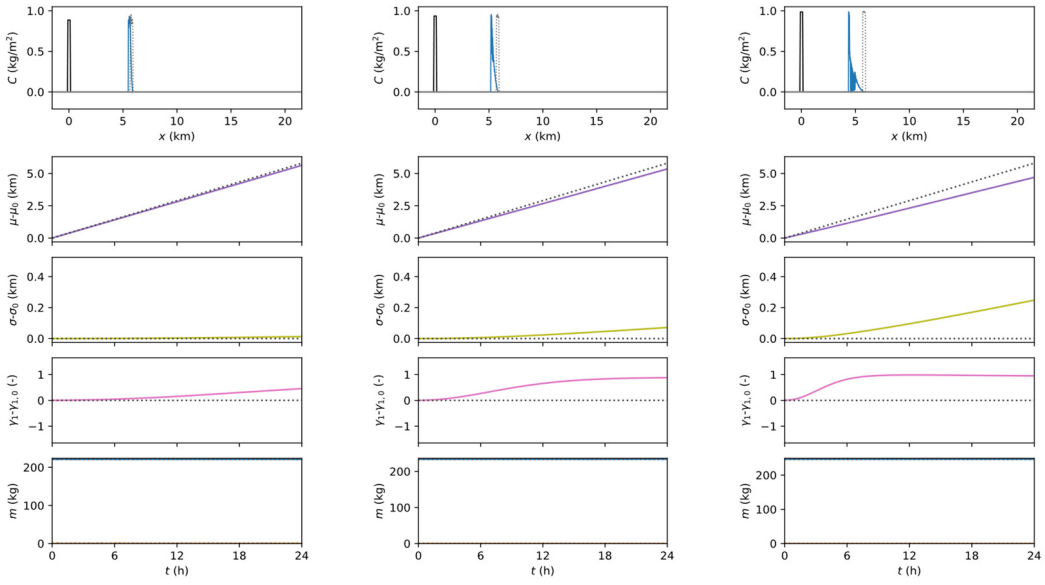

(d) $h_+ = 10^{-3}$ m, $\nu_+ = 10^{-4}$ m^2/s (e) $h_+ = 10^{-3}$ m, $\nu_+ = 10^{-3}$ m^2/s (f) $h_+ = 10^{-3}$ m, $\nu_+ = 10^{-2}$ m^2/s

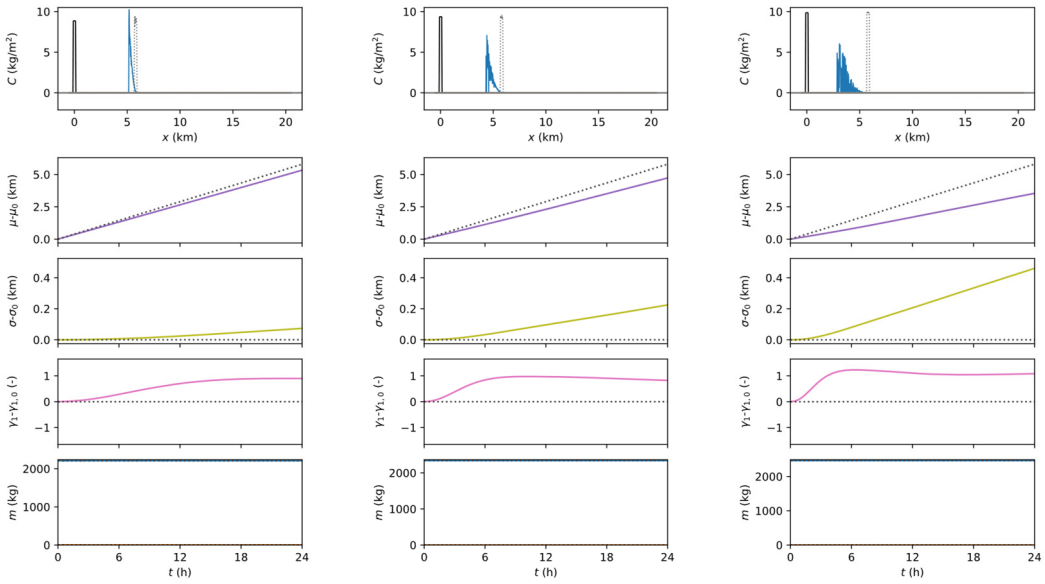

(g) $h_+ = 10^{-2}$ m, $\nu_+ = 10^{-4}$ m^2/s (h) $h_+ = 10^{-2}$ m, $\nu_+ = 10^{-3}$ m^2/s (i) $h_+ = 10^{-2}$ m, $\nu_+ = 10^{-2}$ m^2/s

Figure 38

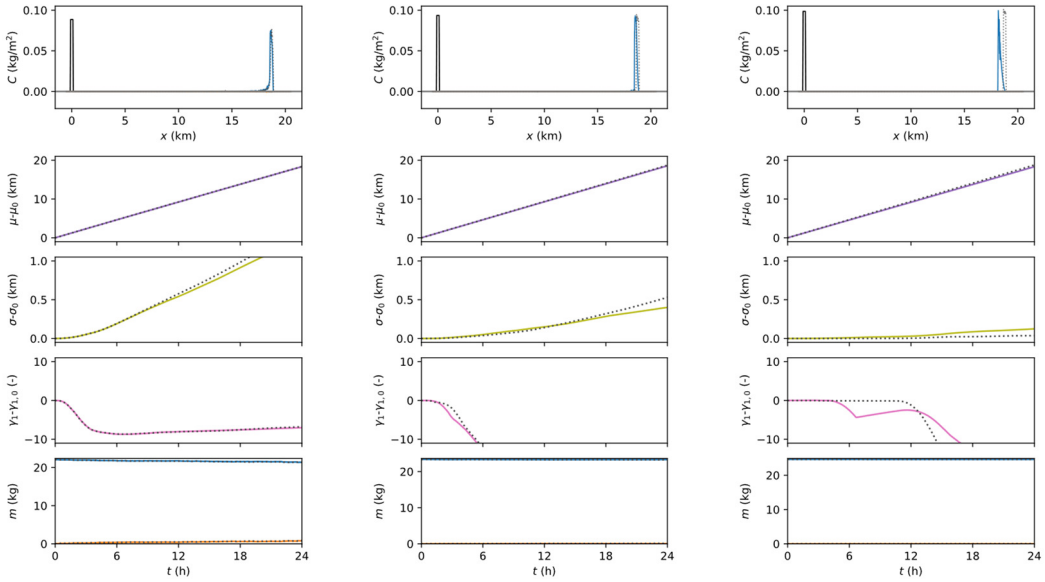

(a) $h_+ = 10^{-4}$ m, $\nu_+ = 10^{-4}$ m^2/s (b) $h_+ = 10^{-4}$ m, $\nu_+ = 10^{-3}$ m^2/s (c) $h_+ = 10^{-4}$ m, $\nu_+ = 10^{-2}$ m^2/s

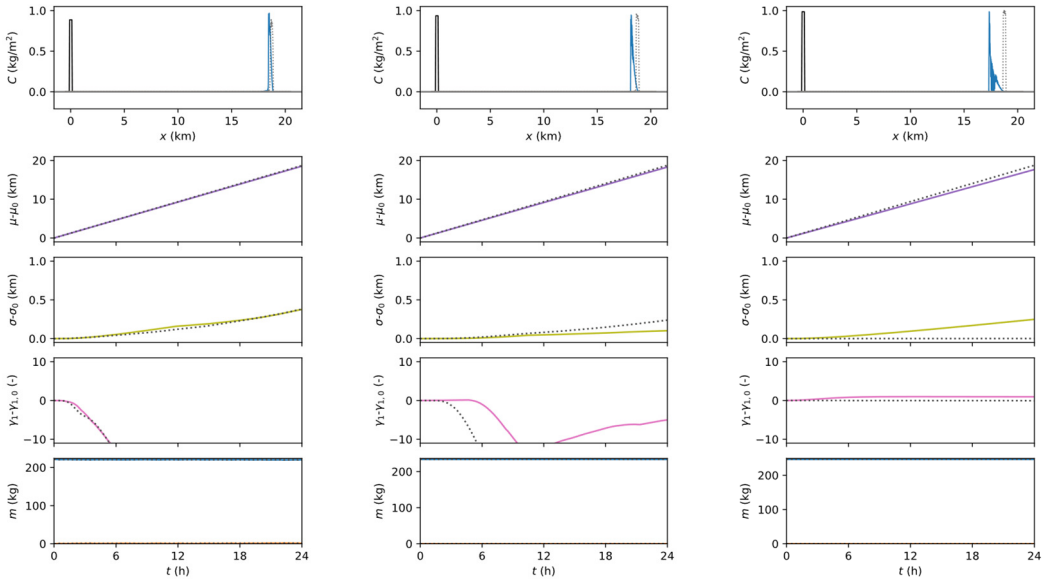

(d) $h_+ = 10^{-3}$ m, $\nu_+ = 10^{-4}$ m^2/s (e) $h_+ = 10^{-3}$ m, $\nu_+ = 10^{-3}$ m^2/s (f) $h_+ = 10^{-3}$ m, $\nu_+ = 10^{-2}$ m^2/s

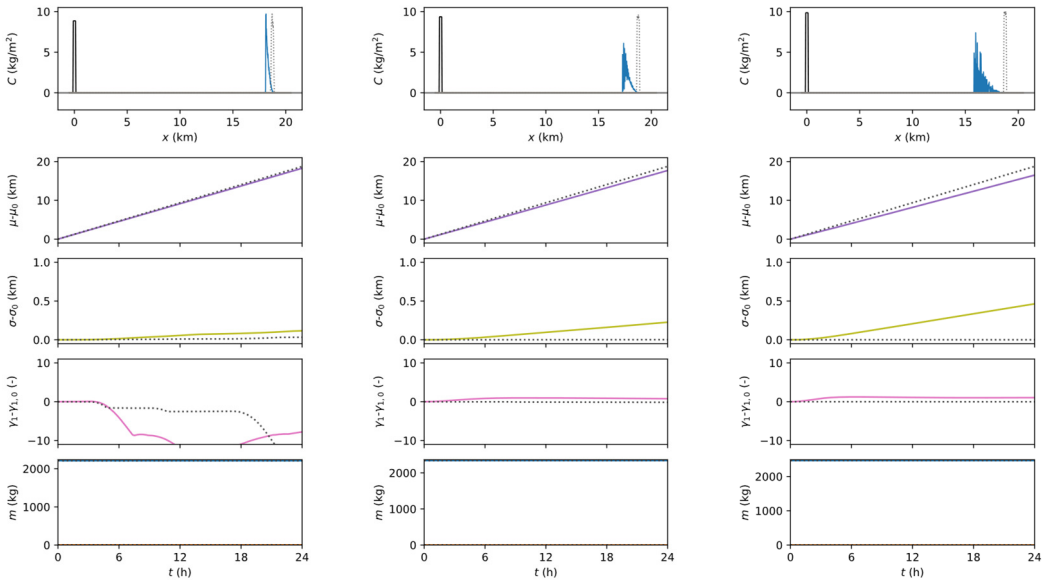

(g) $h_+ = 10^{-2}$ m, $\nu_+ = 10^{-4}$ m^2/s (h) $h_+ = 10^{-2}$ m, $\nu_+ = 10^{-3}$ m^2/s (i) $h_+ = 10^{-2}$ m, $\nu_+ = 10^{-2}$ m^2/s

Figure 39

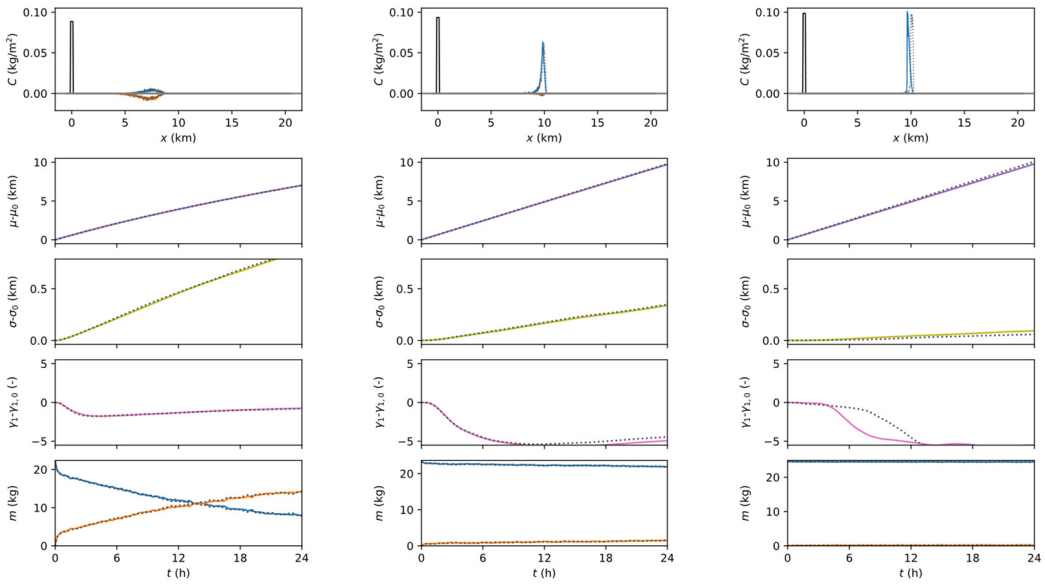

(a) $h_+ = 10^{-4}$ m, $\nu_+ = 10^{-4}$ m^2/s (b) $h_+ = 10^{-4}$ m, $\nu_+ = 10^{-3}$ m^2/s (c) $h_+ = 10^{-4}$ m, $\nu_+ = 10^{-2}$ m^2/s

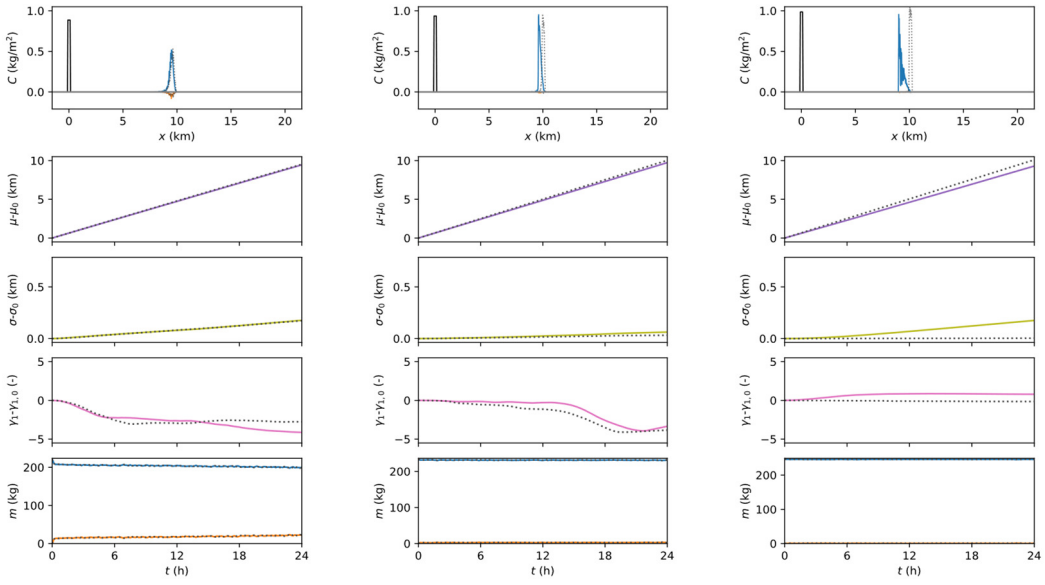

(d) $h_+ = 10^{-3}$ m, $\nu_+ = 10^{-4}$ m^2/s (e) $h_+ = 10^{-3}$ m, $\nu_+ = 10^{-3}$ m^2/s (f) $h_+ = 10^{-3}$ m, $\nu_+ = 10^{-2}$ m^2/s

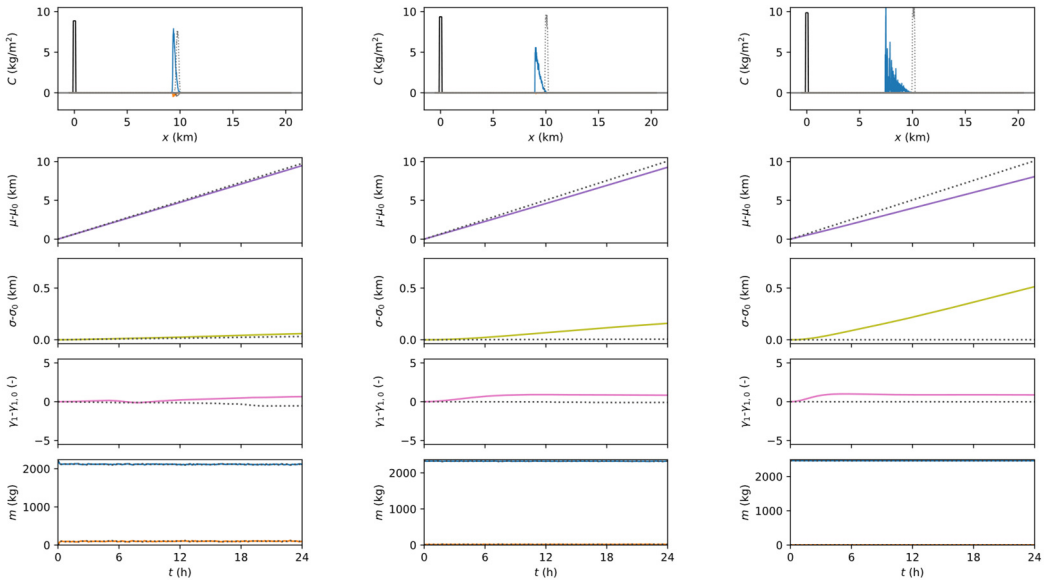

(g) $h_+ = 10^{-2}$ m, $\nu_+ = 10^{-4}$ m^2/s (h) $h_+ = 10^{-2}$ m, $\nu_+ = 10^{-3}$ m^2/s (i) $h_+ = 10^{-2}$ m, $\nu_+ = 10^{-2}$ m^2/s

Figure 40

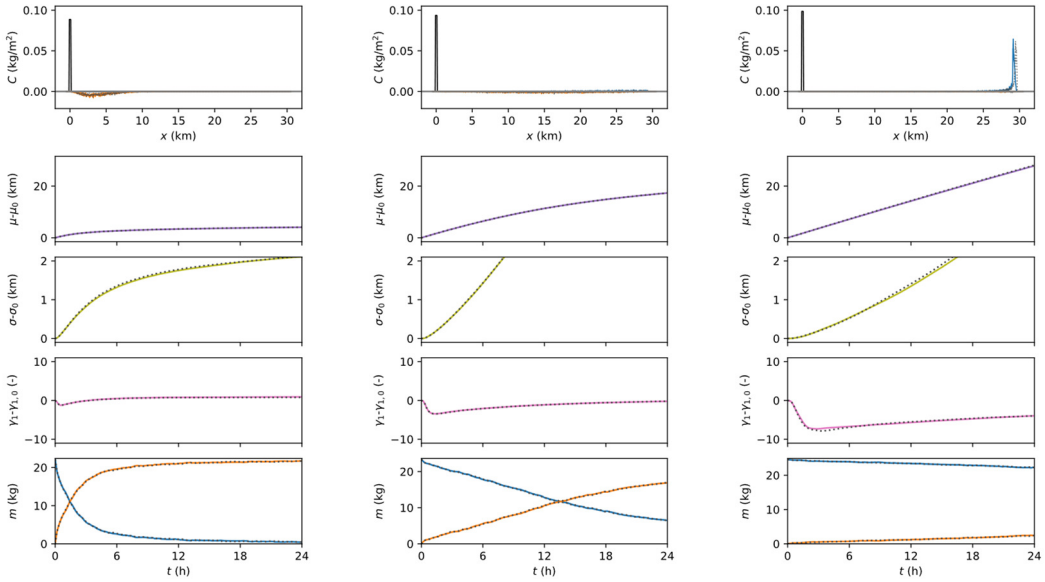

(a) $h_+ = 10^{-4}$ m, $\nu_+ = 10^{-4}$ m^2/s (b) $h_+ = 10^{-4}$ m, $\nu_+ = 10^{-3}$ m^2/s (c) $h_+ = 10^{-4}$ m, $\nu_+ = 10^{-2}$ m^2/s

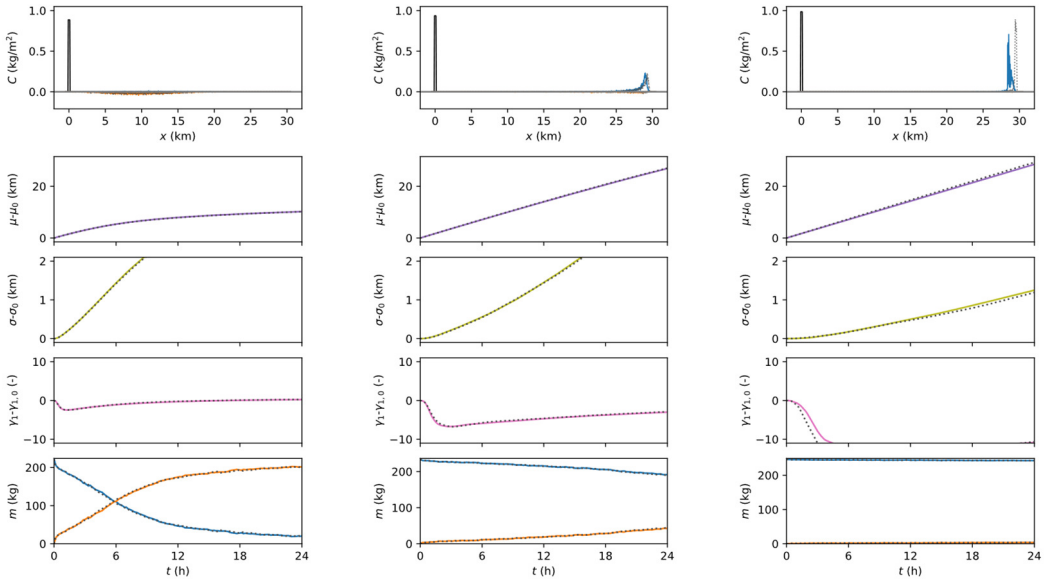

(d) $h_+ = 10^{-3}$ m, $\nu_+ = 10^{-4}$ m^2/s (e) $h_+ = 10^{-3}$ m, $\nu_+ = 10^{-3}$ m^2/s (f) $h_+ = 10^{-3}$ m, $\nu_+ = 10^{-2}$ m^2/s

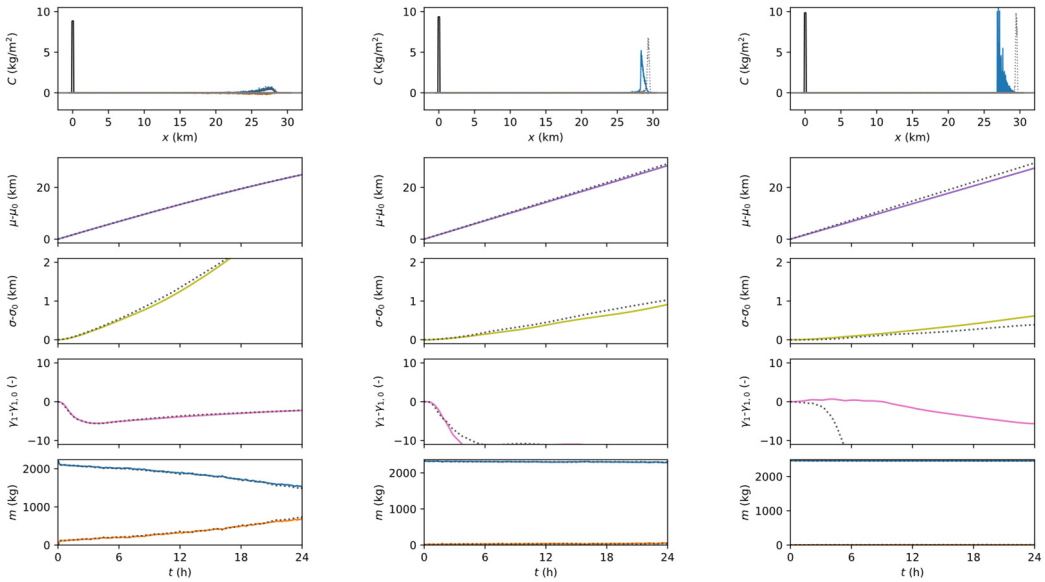

(g) $h_+ = 10^{-2}$ m, $\nu_+ = 10^{-4}$ m^2/s (h) $h_+ = 10^{-2}$ m, $\nu_+ = 10^{-3}$ m^2/s (i) $h_+ = 10^{-2}$ m, $\nu_+ = 10^{-2}$ m^2/s

Figure 41

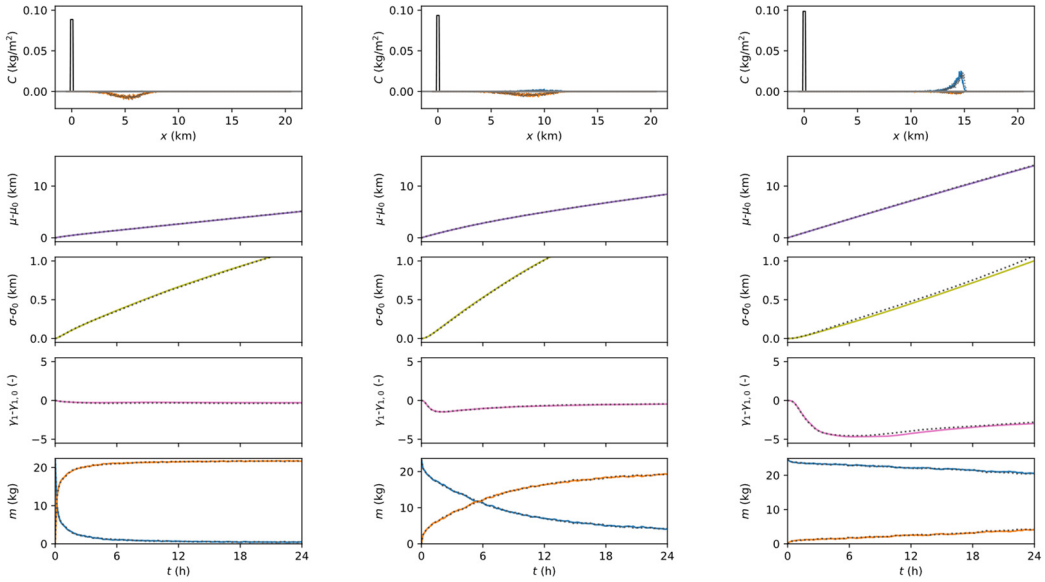

(a) $h_+ = 10^{-4}$ m, $\nu_+ = 10^{-4}$ m^2/s (b) $h_+ = 10^{-4}$ m, $\nu_+ = 10^{-3}$ m^2/s (c) $h_+ = 10^{-4}$ m, $\nu_+ = 10^{-2}$ m^2/s

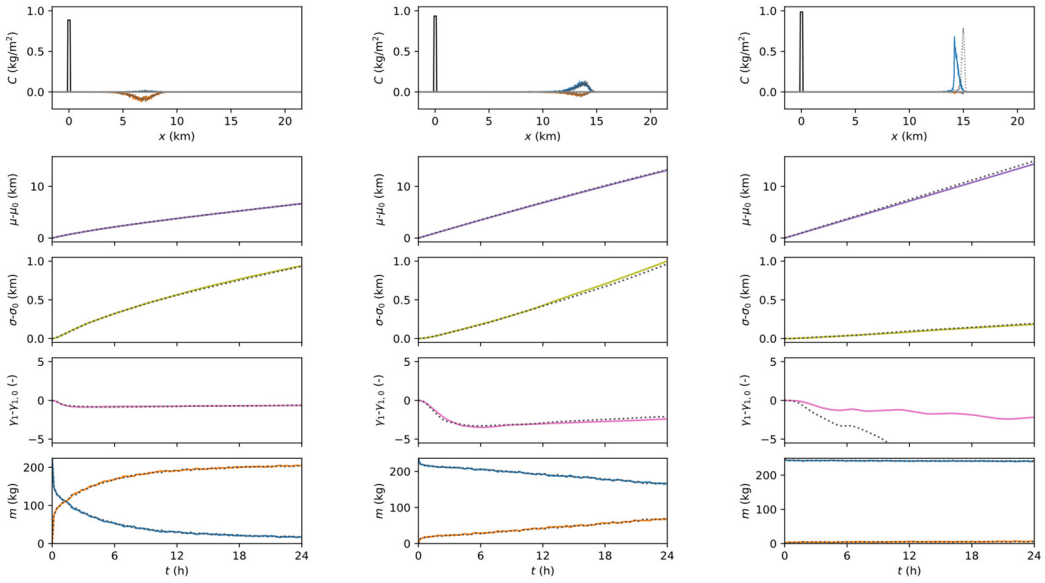

(d) $h_+ = 10^{-3}$ m, $\nu_+ = 10^{-4}$ m^2/s (e) $h_+ = 10^{-3}$ m, $\nu_+ = 10^{-3}$ m^2/s (f) $h_+ = 10^{-3}$ m, $\nu_+ = 10^{-2}$ m^2/s

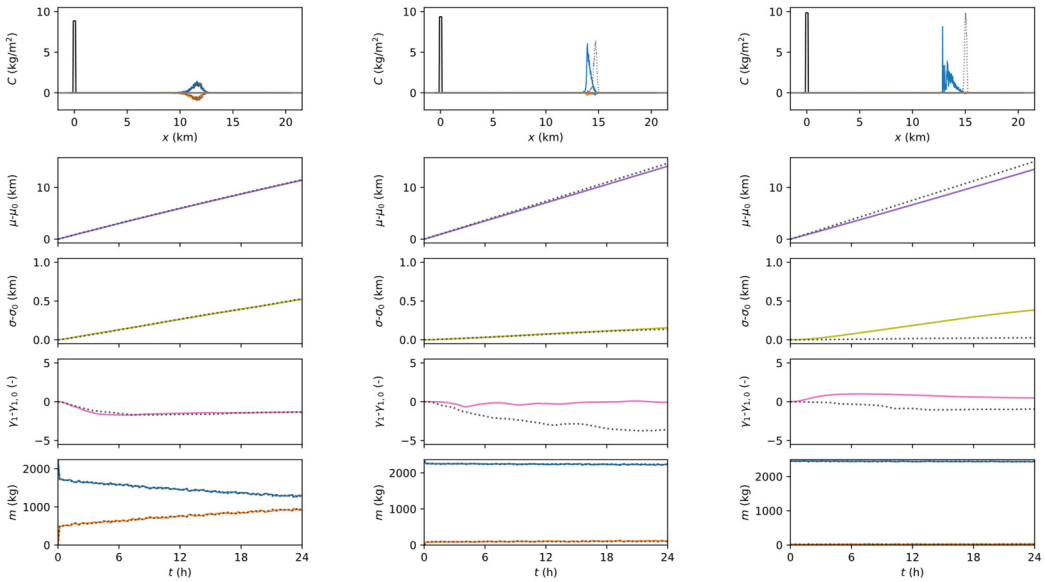

(g) $h_+ = 10^{-2}$ m, $\nu_+ = 10^{-4}$ m^2/s (h) $h_+ = 10^{-2}$ m, $\nu_+ = 10^{-3}$ m^2/s (i) $h_+ = 10^{-2}$ m, $\nu_+ = 10^{-2}$ m^2/s

Figure 42

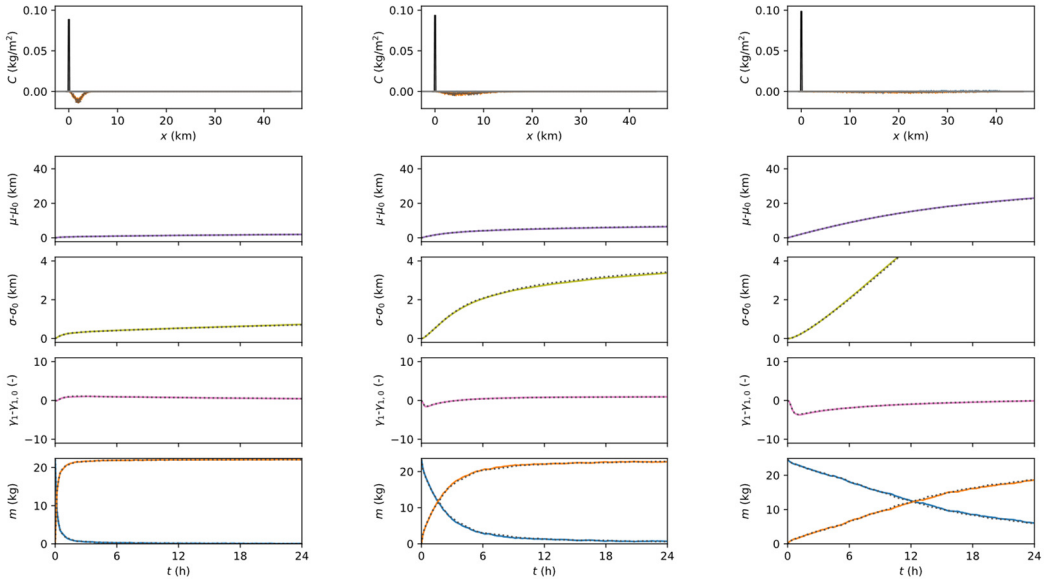

(a) $h_+ = 10^{-4}$ m, $\nu_+ = 10^{-4}$ m^2/s (b) $h_+ = 10^{-4}$ m, $\nu_+ = 10^{-3}$ m^2/s (c) $h_+ = 10^{-4}$ m, $\nu_+ = 10^{-2}$ m^2/s

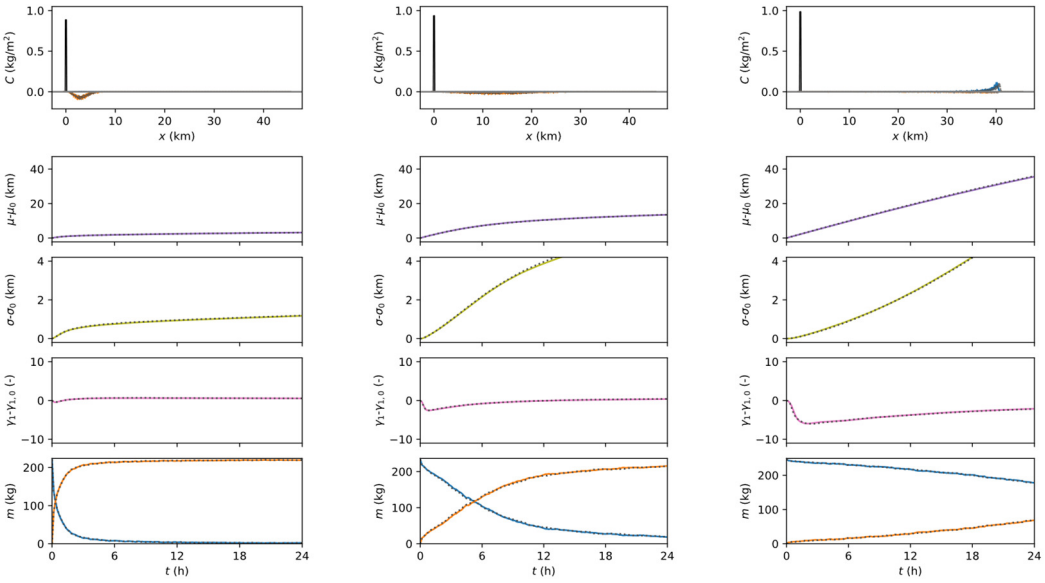

(d) $h_+ = 10^{-3}$ m, $\nu_+ = 10^{-4}$ m^2/s (e) $h_+ = 10^{-3}$ m, $\nu_+ = 10^{-3}$ m^2/s (f) $h_+ = 10^{-3}$ m, $\nu_+ = 10^{-2}$ m^2/s

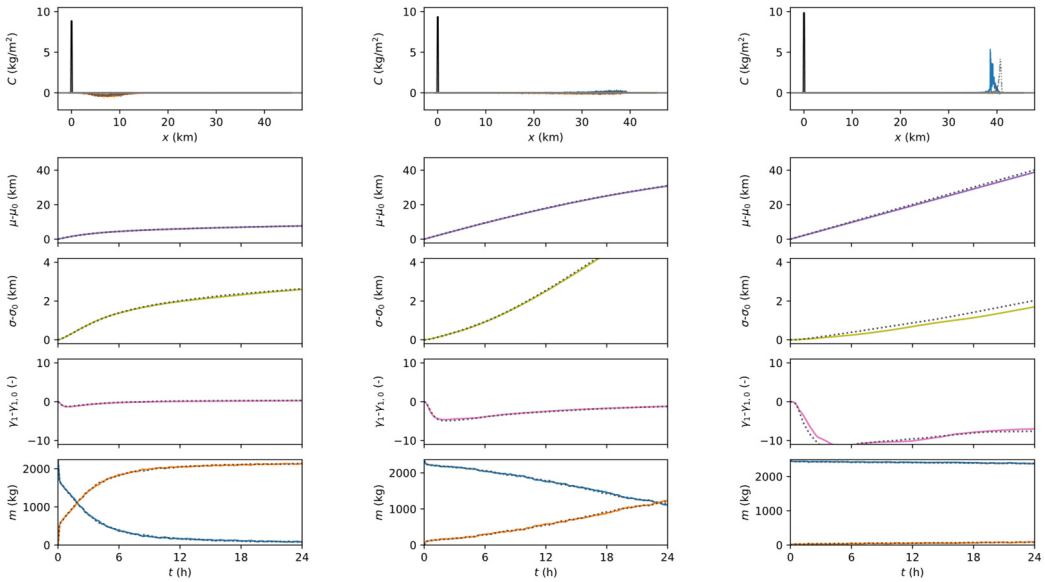

(g) $h_+ = 10^{-2}$ m, $\nu_+ = 10^{-4}$ m^2/s (h) $h_+ = 10^{-2}$ m, $\nu_+ = 10^{-3}$ m^2/s (i) $h_+ = 10^{-2}$ m, $\nu_+ = 10^{-2}$ m^2/s

Figure 43